ELLIPSOMETRIC STUDIES OF PROTEIN ADSORPTION ONTO HARD SURFACES IN A FLOW CELL

.

Unilever Research Vlaardingen is gratefully acknowledged for their co-operation in and financial support of the work described in this thesis.

This thesis was written on an Apple Macintosh using *Textures* a LaTeX 2_ε implementation and *EndNote* to add and format references. *Excel* was used for the graphs.

Omslag: de ellipsometrie opstelling
inzet: de onderdelen van de parallelle plaat flowcel
Foto's: G.S. Vos

Cover: ellipsometric setup
insert: individual parts of the parallel plate flow cell
Fotos: G.S. Vos

CIP-GEGEVENS KONINKLIJKE BIBLIOTHEEK, DEN HAAG

Rekveld, Sander

Titel/Sander Rekveld;[ill. van de auteur].:[S.L.:S.N]. Ill.
Proefschrift Enschede.-Met lit. opg.-Met samenvatting in het Nederlands.

ISBN 90-9010946-3

Trefw.: eiwitten, adsorptie, ellipsometrie

ELLIPSOMETRIC STUDIES OF PROTEIN ADSORPTION ONTO HARD SURFACES IN A FLOW CELL

Proefschrift

ter verkrijging van
de graad van doctor aan de Universiteit Twente,
op gezag van de rector magnificus,
prof.dr. F.A. van Vught,
volgens besluit van het College voor Promoties
in het openbaar te verdedigen
op donderdag 9 oktober 1997 te 16:45 uur.

door

Sander Rekveld

geboren op 12 oktober 1967
te Emmen

oktober 1997

Dit proefschrift is goedgekeurd door de promotoren Prof.dr.ir. T. Reith en Prof.dr.ing. H. Strathmann en de assistentpromotor Dr.ir. I.G. Rácz.

promotiecommissie:
Prof.dr. F.A. van Vught (Rector Magnificus Universiteit Twente)
Prof.dr. W.E. van der Linden (Dekaan Faculteit Chemische Technologie)

Prof.dr. G.J. Vancso (Universiteit Twente, Faculteit Chemische Technologie)
Prof.dr.ir. M.M.C.G. Warmoeskerken (Universiteit Twente, Faculteit Chemische Technologie)

Prof.dr. H. Elwing (Universiteit van Göteborg, Göteborg, Zweden)
Dr.ir. W. Norde (Landbouw Universiteit Wageningen)
Prof.dr. C.J. van Oss (Staatsuniversiteit van New York, Buffalo, Verenigde Staten van Amerika)

Dr.ir. H. Wormeester (Universiteit Twente, Faculteit Technische Natuurkunde)

"Many a protein changes its song after it has been caught, and it turns out to be a mockingbird"
Leo Vroman in Blood, Garden City, New York: The Natural History Press; 1968

aan mijn ouders
aan Daniëlle

Voorwoord

Bij het voltooien van dit proefschrift wil ik graag iedereen bedanken die direct en indirect hebben bijgedragen aan mijn opleiding en werk.

Allereerst wil ik daarom graag mijn promotor prof. Tom Reith bedanken voor de leerzame tijd de afgelopen jaren, ook prof. Heiner Strathmann wil ik bedanken voor zijn optreden als co-promotor. Mijn begeleider Imre Rácz ben ik veel dank verschuldigd voor de zelfstandige wijze waarop ik het onderzoek heb kunnen inrichten en voor het inzicht en de mensenkennis op beslissende momenten. Ook prof. Groot Wassink die als adviserend professor optrad wil ik hierbij bedanken.

Cindy, zonder jouw doorzettingsvermogen en nauwkeurigheid als super-technicus tijdens bijna de gehele AIO-periode zou ik niet weten hoe het proefschrift er nu uit zou hebben gezien. Ook zonder de begeleiding en expertise van Herbert Wormeester en in een eerder stadium Derk Jan Wenting uit de groep van Prof. Poelsema (TN) zou het onderzoek onmogelijk zijn geweest.

De afgelopen jaren in de onderzoekgroep Fysische Scheidingen heb ik als erg prettig ervaren en het is dan ook nooit voorgekomen dat ik niet met plezier naar het werk ging. Ik wil daarom ook iedereen bedanken. Alfons Rooks en Bert Vos en in de eerste jaren John Meinema en Karsten Lüdemann voor de technische ondersteuning en Karsten later als persoonlijke leverancier van vervoersmiddelen. Frank Foeth voor zijn hulp bij initiële pogingen met het numeriek oplossen van het model, het binnenhalen van een bepaalde afstudeerder en voor het bij mij introduceren van LaTeX. De twee studiereizen met de groep naar het buitenland, naar Zweden en Groot-Brittanië heb ik zeer gewaardeerd en zijn het wat mij betreft waard om een traditie te worden.

Dank ben ik ook verschuldigd aan Unilever Research, in het bijzonder Robert-Jan Uhlhorn voor de begeleiding in de eerste paar jaar van de promotieopdracht en Mike Garvey (URPS) voor de nuttige bijeenkomsten over hard surface cleaning in Port Sunlight en Colworth House (UK) en voor de *grand* die het mogelijk maakte om een presentatie te geven in Edgewater (USA).

Verder wil ik graag nog de namen noemen van Jaap Dijt (LUW), Mirjam Oldenzeel (AKZO Nobel) en Theo Jeurnink (NIZO) die in het beginstadium hebben geholpen met (toen nog) reflectometrie en de stroomcel.

I also thank Prof. Hans Elwing and Agneta Askendal (Linköping Institute of Technology, Sweden) for their hospitality and first introduction to ellipsometry during two visits to Sweden and for the answers to many experimental questions.

Hans Visser (NIZO) wil ik bedanken voor het bij mij introduceren van het werk van Prof. Van Oss en medewerkers en voor de (telefoon)gesprekken die we in de loop der jaren hebben gevoerd als we vaak toevallig tegen dezelfde problemen aanliepen.

Ook wil ik Emile Cornelissen bedanken voor de leuke tijd die we samen hebben gehad eerst als collega's en daarna ook als huisgenoten en voor het feit dat ik via jou ook stiekem nog een beetje feeling kon houden met de membraantechnologiegroep.

Wie ook niet onvermeld kunnen blijven zijn de drie MTS stagiaires die allen zes maanden hebben geholpen, Roeland Duikersloot (zelfs acht maanden), Rianne Vos en Ronnie Busschers. Mijn (helaas) enige afstudeerder Marcel de Boer die later ook nog als KIP'er aan het onderzoek heeft meegeholpen net als ex-collega Bert Bosch, Christine van Rees en Menno Kremers met wiens hulp, en het ADIN

programma en de vele onmisbare aanwijzigen van Hans Kuipers van Proceskunde, het convectie-diffussie-interactie model numeriek is opgelost.

Als laatste wil ik de mensen bedanken die 'op afstand' het promotieproces hebben geholpen. Enrico Westenberg die mij vanuit de Verenigde Staten de nodige boeken, software en computer-apparatuur heeft doen toekomen, vaak sneller dan wanneer het hier in Europa zou zijn besteld en natuurlijk goedkoper. Mijn ouders voor hun interesse en stimulering.

Als allerlaatste wil ik Daniëlle bedanken voor het feit dat ze het ook de laatste anderhalf jaar bij mij heeft uitgehouden toen ik vrijwel altijd mijn gedachten bij 'De Wetenschap' had.

Contents

List of Figures

List of Tables

List of Symbols

Symbol	Quantity	Units
M	molecular mass	[g mol^{-1}]
N_{Av}	Avogadro's number	[mol^{-1}]
S_c	contactable surface area	[m^2]
ϕ^{total}	total interaction energy	[mJ]
ΔG_{132}	free energy of interaction between material 1 and 2 in medium 3	[mJ m^{-2}]
y_0	Distance between liquid and solid in contact angle measurements	[m]
γ_i	surface energy/tension of component i	[mJ m^{-2}]
$\gamma_i^{\oplus}$	electron acceptor parameter of the surface energy of component i	[mJ m^{-2}]
$\gamma_i^{\ominus}$	electron donor parameter of the surface energy of component i	[mJ m^{-2}]
γ_{ij}	interfacial energy/tension between components i and j	[mJ m^{-2}]
T	Absolute temperature	[K]
λ	decay length of water	[nm]
a_p	Particle radius	[m]
y	Coordinate perpendicular to the wall. With the origin at the wall in chapter 3, and in the middle of the channel in chapter 5	[m]
k	Boltzmann's constant ($1.38{\cdot}10^{-23}$)	[J K^{-1}]
θ	contact angle	[°]
c	bulk concentration	[kg m^{-3}]
c_w	bulk concentration at the wall (y = a)	[kg m^{-3}]
t	time	[s]
∇	nabla operator	[–]
u	particle velocity	[m s$^-$1]
F_{1-4}	universal correction factors for hydrodynamic interaction	[–]
v	fluid velocity	[m s^{-1}]
δ_{IFBL}	Interfacial force boundary layer	[m]
Pe	Peclet number	[–]
$\bar{v}$	average fluid velocity	[m s^{-1}]
H	height of channel	[mm]
a	half height of channel	[mm]
ϕ_v	volumetric flow rate	[m^3 s^{-1}]
$\dot{\gamma}$	shear rate	[s^{-1}]
Re	Reynolds number	[–]
L_e	hydrodynamic entrance length	[m]
η	dynamic viscosity	[N s m^{-2}]
τ	shear stress	[N m^{-2}]
a	half height of channel	[m]
$\mathbb{D}$	diffusion coefficient	[m^2 s^{-1}]

Γ_i	surface concentration in state i	[mg m^{-2}]
k_a	rate constant of adsorption from IFBL approach	[m s^{-1}]
k_{ai}	rate constant of adsorption in state i	[m^3 mg^{-1} s^{-1}]
k_{di}	rate constant of desorption in state i	[s^{-1}]
k_{t12}	rate constant of transformation from state 1 to state 2	[m^2 mg^{-1} s^{-1}]
Γ_{max}	maximum surface concentration in state 1	[mg m^{-2}]
α	the ration of the occupied area between state 2 and state 1	[–]
$\delta_{diffusion}$	boundary layer for diffusive mass transport	[m]
n	refractive index	[–]
N	complex index of refraction	[–]
i	$i^2 = -1$	[–]
ϕ_x	(complex) angle in layer x	[°]
δ	phase	[–]
ψ	amplitude ratio	[°]
Δ	phase difference	[°]
ρ	ratio complex reflection coefficients	[–]
r_p	reflection coefficient parallel to the plane of incidence	[–]
r_{123}	overall reflection coefficient in a n-layer system	[–]
t_p, t_s	transmission coefficient parallel to the plane of incidence	[–]
β	phase difference	[–]
$\frac{dn}{dc}$	refractive index increment	[ml g^{-1}]
λ	wavelength in vacuo	[nm]
J	flux	[mg m^{-2} s^{-1}]

Chapter 1

Introduction

The adsorption of soluble proteins at solid-liquid interfaces is of fundamental importance in nature. A common example is the role played by proteins in blood clotting. Understanding of protein adsorption is also important in many industrial areas. Fouling by protein adsorption, or by cell adhesion to a precursor layer of protein, presents a major problem in, e.g., membrane separations and the design of biocompatible implants in the human body. The liquid medium of interest in this study, if not explicitly stated otherwise, is water.

Protein adsorption and desorption can occur simultaneously, and the determination of the individual or overall rate of both processes has been the aim of many previous studies.

Despite the large interest, experimental methods suitable for studying protein adsorption kinetics are few (Ivarsson, Hegg, *et al.* 1985; Ramsden 1993). An intuitive direct way of observing is by means of microscopy. Their dimension, usually between 5 and 50 nanometers, makes protein molecules adsorbed at surfaces to small to detect by light microscopes. Electron microscopy which does have enough resolving power cannot be used for *in situ* kinetic measurements.

A number of review articles on protein adsorption have appeared in the literature (Brash and Horbett 1995; Haynes and Norde 1994; Ramsden 1995). From these reviews it is clear that despite the large interest in protein adsorption in the past decades, understanding of protein adsorption is still poor at this time. Even more puzzling is, that although most studies use the same type of protein (usually albumin or fibrinogen), there are many contradictions between those studies. Apart from the nature of the protein, the reason for the differences in results are usually described to be due to differences in:

- the measurement technique
- the surface characteristics
- the solution properties
- the hydrodynamic conditions

Frequently, experimental techniques involve the passage of the adsorbed proteins through the solution-air interface. This alone, but also drying or rinsing the surface containing the protein layer can change the structure of the layer or even the amount adsorbed considerably (Vroman 1994). Another example of possible influences of some of the measurement techniques used, is the use of radioactive labelling in earlier studies of protein adsorption. It has been shown that labelled human albumin adsorbs preferential onto polystyrene compared to unlabelled human albumin (Van der Scheer 1978). Unreproducible surfaces are another common source of large differences between measurements. A very strict protocol for preparing or cleaning of the surfaces is necessary in order to be able to perform

reproducibly adsorption studies, preferentially followed by some form of characterisation. Examples of solution properties are pH and type of buffer, ionic strength, and very important, flow conditions like shear velocity. Protein adsorption under mass transport limited conditions will, for instance, obscure information about adsorption and desorption kinetics (Brash and Horbett 1995).

Both rate and amount of protein have been shown to be affected by flow conditions (Lee and Kim 1974). Nevertheless, experiments under well defined hydrodynamic conditions are very rare indeed (Cha and Beissinger 1996a; Cha and Beissinger 1996b; Cheng, Darst, *et al.* 1987; Dejardin, Le, *et al.* 1994; Lok, Cheng, *et al.* 1983a; Shibata and Lenhoff 1992b).

1.1 Proteins

Proteins are biological macromolecules that make up living organisms and are essential to their functioning. Proteins are large molecules, ranging in molecular mass from a few thousand g mol^{-1} to more than a million g mol^{-1}. First discovered in 1838, proteins are now recognised as the predominant ingredients of cells, and they represent more than fifty percent of the dry mass of animals. The word *protein* comes from the Greek *proteios* (primary). Proteins are specific for each species. Humans consist of an estimated 30 thousand different proteins, of which only about 2 percent have been adequately described. Protein molecules range from long insoluble fibres which make up tissue and hair, to compact soluble globules which can pass through cell membranes and initiate metabolic reactions.

Structure of Proteins

The most basic level of protein structure, the primary structure, consists of a sequence of amino acids. Forces between these amino acids, such as hydrogen bonds, disulfide bridges, electrostatic interaction between positive and negative charges, cause a protein molecule to coil or fold into a secondary structure. Examples of such structures are α-helix and β-sheet. Forces between these secondary structures result in the structure of a protein which determines it's final macroscopic dimension and so-called tertiary structure. The model protein that have been used in this study will be discussed in the next sections.

Fibrinogen

Fibrinogen is a blood plasma protein responsible for blood clotting. It is an example of a fibrous protein. Other examples of fibrous proteins are collagen (which makes up bone), keratin (which makes up the outermost layer of skin and hair). The typical mammalian fibrinogen has a molecular mass of 340,000 g mol^{-1}. The best characterised fibrinogen so far is that isolated from human blood plasma, although many early and some present day workers use bovine material. Under normal conditions, human fibrinogen exists in blood plasma at a level of 2 to 4 g ℓ^{-1}. Fibrinogen is the least soluble of the major proteins in blood plasma. Human fibrinogen contains 29 disulfide bonds, three are used to bind the dimeric parts of the molecule together, the remaining 26 bonds exist in two identical sets of 13 each in the two halves of the molecule (Doolittle 1980). Fibrinogen has been a model protein in many other studies because of its function in blood coagulation.

In Table 1.1 some properties of fibrinogen are given. Extinction is the specific extinction at a wavelength of 280 nm. Because fibrinogen is an ellipsoidal molecule it can be adsorbed in two orientations with respect to the surface, i.e., end-on or side-on, with a low and high adsorbed amount respectively

Table 1.1: Overview of some of the properties of Fibrinogen

Molecular mass [g mol^{-1}]	340,000
Iso Electric Point [pH]	5.8
Diffusion coefficient [m^2 s^{-1}]	$1.98 \cdot 10^{-11}$
Dimensions [nm^3]	$45 \times 6 \times 6$
Extinction$_{\lambda=280nm}$ [g^{-1} ℓ cm^{-1}]	1.55
Adsorbed amount in a hypothetical monolayer*	
side-on [mg m^{-2}]	2
end-on [mg m^{-2}]	16

1.2 Surfaces

The material and morphology of the surface used in an adsorption study has a large influence on the adsorption. Careful preparation of the surfaces and characterisation of the surfaces used is essential in order to be able to compare the different adsorption studies.

Surface materials that have been used in protein adsorption studies include metals, oxides and a multitude of synthetic polymers. The morphology of the surface and the surface roughness can nowadays be determined not only by scanning electron microscopy but also by scanning tunnelling and atomic force microscopy to resolutions of a few Ångstroms. Characterisation of the surface free energy which is an important factor determining the interaction between a protein and the surface can be measured directly with a force balance. However, surface force measurements are cumbersome and the apparatus is expensive. An easy, commonly used technique for surface characterisation, is the determination of the contact angles of drops of high energy liquids on the surface material.

1.3 Kinetics of Adsorption and Desorption

1.3.1 Adsorption

Although a great number of proteins readily dissolve in water, they usually also have a high affinity for interfaces. Proteins do not only adsorb at solid-liquid interfaces but also, and usually even more, at air-liquid interfaces. The concentration in the adsorbed layer at interfaces is often many times the concentration of the protein in bulk solution. For example a 10 mg ℓ^{-1} solution of fibrinogen has been shown to deposit a layer of 5 mg m^{-2}. Depending on the thickness of the layer the equivalent concentration in the layer can easily reach a 100,000 mg ℓ^{-1} (Welin-Klintström 1992). It is this behaviour of proteins that makes them very useful for a number of applications, yet presents a major problem in a number of industrial applications where fouling should be avoided.

A priori knowledge of interaction forces between surfaces and proteins would greatly enhance the prediction of adsorption phenomena. Unfortunately, these interaction forces are still far from being fully understood. The results from a direct measurement technique, the force balance (Israelachvili 1992) are now becoming available. Without the availability of direct measurements of the interaction forces, a model that predicts these forces between the protein and surface must be used. Derjaguin and Landau (Derjaguin and Landau 1941) and Verwey and Overbeek (Verwey and Overbeek 1948) developed a model (now called the DLVO theory) to calculate these forces. However, for systems encountered in practice for example proteins, DLVO theory, which describes the total interaction force

*Calculated by dividing the molecular mass by Avogadro's Number and by the contactable surface area for the two orientations, $\frac{M}{N_{Av} S_c}$.

as the summation of the Van der Waals (VdW) and Electrostatic (EL) force, can only predict trends. The difference between calculations of adsorption rates of model colloids using the DLVO theory and actual measurements is an order of magnitude even in highly idealised experiments (Elimelech, Gregory, *et al.* 1995). Two different explanations for this shortcoming of the DLVO theory can be found in the literature. One describes the differences to the effects of surface roughness, and chemical heterogeneity of the surfaces. The second stresses the effects of additional forces, becoming important especially when hydrogen bonding is possible (Elimelech, Gregory, *et al.* 1995; Swanton 1995; van Oss 1993). Acid Base (AB) interaction forces are such forces and can play an important role when there is either strong or weak interaction between the surface and water. In this study the effects of surface roughness and chemical heterogeneity have been minimalised and the Van Oss, Chaudhury and Good (VCG) theory is used to extend the DLVO model to include AB interaction forces.

1.3.2 Reorientation, Reconformation and Crystallisation

Proteins are not simply hard spherical colloidal particles. Because of this several authors have considered changes in orientation, conformation and formation of two dimensional structures to explain observed adsorption phenomena.

Most proteins have a tertiary structure that is spheroidal with a major and minor axis, rather then spherical. Hence, initial adsorption to a surface can occur in more then one orientation with respect to the surface. Subsequent transition in time from one orientation to the other is likely if a favourable higher contact area is created. When the concentration of bulk protein is high, overshoots in the adsorbed amount, have been reported in the literature, e.g., (De Feijter, Benjamins, *et al.* 1978). This could be a further indication of a change in orientation, but also an indication of structural changes within a protein molecule.

Structural changes (also called conformational rearrangements) in which the secondary and/or tertiary structure of the protein changes as a result of adsorption or desorption have also been observed. These changes could even be a substantial driving force for adsorption (Norde and Anusiem 1992).

Crystallisation or the formation of supramolecular structures upon adsorption of proteins is another phenomenon reported in the literature, e.g., (Nygren, Stenberg, *et al.* 1992).

Up to date, no conclusive a priori knowledge exists to predict which of the discussed processes is dominant or are dominant in a given system.

1.3.3 Desorption

Literature about desorption, i.e., the detachment of proteins from a surface is puzzling. Many studies assume desorption to be absent in the case of proteins. Other studies show substantial desorption when replacing the solution in contact with the surface with pure buffer or by rinsing at low to moderate shear rates. It has been argued in the literature that desorption is a slow process. Desorption of colloidal particles is due to tangential forces exerted on the particles by shear stress (Van de Ven 1989). If the same holds for proteins, then studies at high shear velocities could be helpful in understanding desorption properties of proteins.

1.3.4 Exchange

Exchange is a process by which one protein is removed by a second protein and is different from desorption, in that desorption involves only one protein molecule that is replaced by solvent molecules.

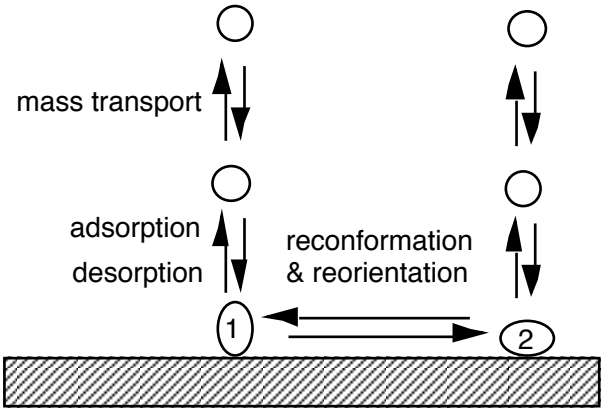

Figure 1.1: Schematic drawing illustrating the kinetics of processes occurring during protein adsorption. The numbers refer to different orientations or conformations.

Exchange of adsorbed protein layers by proteins of a different kind is called competitive adsorption or 'The Vroman Effect' (Vroman 1994). Exchange by 'other' proteins of the same kind in a single protein solution (Brash and Samak 1978) have been also been reported in the literature. For exchange by low molecular weight molecules, like surfactants, the term *elution* is sometimes used. Desorption and exchange studies of fibrinogen on several surfaces and with a number of surfactants have been reported in the literature (Retzinger, Cook, *et al.* 1994; Wahlgren, Welin-Klintström, *et al.* 1995; Wahlgren, Arnebrant, *et al.* 1993; Wahlgren, Paulsson, *et al.* 1993). From these studies it becomes clear that usually only a certain fraction of the adsorbed fibrinogen can be removed.

1.3.5 Kinetics

The kinetics of protein adsorption are determined by the adsorption rate at the surface, changes in conformation and/or surface diffusion or even crystallisation phenomena. Furthermore, the kinetics of protein adsorption can be (and often are in the literature) obscured by mass transport limitations in either adsorption or desorption steps.

Mass transport and the adsorption processes are presented schematically in Figure 1.1. Most phenomena observed in protein adsorption can be modelled using phenomenological rate coefficients depicted by the arrows in Figure 1.1. Mass transport to and from the surface is strongly influenced by the hydrodynamic conditions (Elimelech, Gregory, *et al.* 1995; Levich 1962; Probstein 1989; van de Ven 1989). At static, i.e., non flowing conditions mass transport may be the rate controlling step (De Feijter, Benjamins, *et al.* 1978). More commonly though, the rate of adsorption is less than expected from calculation assuming mass transfer limited adsorption (Norde, Arai, *et al.* 1991).

1.4 Experimental Techniques

1.4.1 Ellipsometry

Ellipsometry is an optical technique in which the changes in polarisation after reflection are determined. By determining the state of polarisation on both the bare surface and on this surface covered by a protein layer, it is possible to convert the change in polarisation into a refractive index and a thickness of the adsorbed layer by using an optical model of the surface, protein layer and solution.

Principles of the method can be found in the literature (Azzam and Bashara 1977; Tompkins 1993), as well as many protein adsorption studies (Arnebrant 1987; Baeckström 1987; Cuypers 1976;

De Feijter, Benjamins, *et al.* 1978; Lassen and Malmsten 1996; Malmsten 1994; Van der Scheer 1978; Wahlgren 1992; Welin-Klintström 1992).

1.4.2 Contact Angles

Contact angle data gain more and more importance in protein adsorption studies. It has been found that contact angles on adsorbed proteins have relevance to protein adsorption (van der Vegt, Norde, *et al.* 1996). Contact angle data on surface materials, surfactants and protein layers are used to determine the kinetics of protein adsorption, desorption and exchange.

1.5 Aim

The aim of this study was to gain more insight into the kinetics of adsorption of proteins onto flat, solid, impermeable surface materials by:

- measurering the adsorbed amount as a function of time under defined hydrodynamic conditions at different bulk concentrations
- formulating and validate mathematical models of protein adsorption
- relating the results of contact angle measurements on surfaces and proteins to the observed adsorption kinetics

Chapter 2

Experimental methods for Investigating Protein Adsorption Kinetics

2.1 Introduction

Protein adsorption has been the object of many experimental studies in the past decades. Many studies have considered the 'equilibrium' amount of protein that adsorbs at a solid liquid interface after a given period of time. From these experiments many conflicting conclusions where drawn.

Therefore, in order to study protein adsorption, dynamic rather than 'equilibrium' measurements should be the main focus in order to elucidate the underlaying mechanisms. Furthermore, in the literature, the effect of mass transfer on the rate of adsorption is often impossible to determine because of the poorly characterised or controlled hydrodynamic conditions under which many studies have been conducted.

Conformational changes of protein molecules during adsorption are a further complication when studying the kinetics of protein adsorption and desorption. Hence, detection of only the amount of protein on the surface is not enough to fully understand the processes behind protein adsorption.

It is the aim of this chapter to firstly review flow cells and experimental techniques that have been described in the literature and to discuss some problems that have been identified using these techniques. Secondly, the technique used in the present study is described in more detail.

In order to assess the effect of mass transfer from adsorption and desorption kinetics, well defined hydrodynamic conditions during an experiment are a first requirement. So before looking at the actual experimental techniques a few, often employed, flow cell designs are discussed.

2.2 Flow Cells

The type of flow cell that is used to study the dynamics of protein adsorption is a critical factor, as it not only limits the number of techniques that can be chosen, but also determines the flow pattern directly near the surface that influences the magnitude and direction of the movement of protein to the surface. In the flow cells that will be discussed the flow pattern is either a simple shear flow tangential to the surface, a stagnation point flow perpendicular to the surface, or a combination of these two (van de Ven 1989).

Desorption of colloidal particles is primarily coupled to the shear stress (van de Ven 1989). For proteins, the same principles should apply. This important aspect has been neglected in many protein adsorption desorption studies. For example, a flow geometry without shear forces, e.g., stagnation point flow, is not very well suited to study *de*sorption kinetics of proteins.

In most flow cells it is tried to establish a flow pattern for which the Navier-Stokes equations can be easily solved. However, this is the case only for a handful of geometries (Schlichting 1979). Hence, the variety of flow cells used in studies in the literature is not very diverse.

In reviewing a number of flow cells employed frequently in the literature special attention is given to advantages and disadvantages of the flow cells, in particular:

- what is the dominant direction of flow, i.e., parallel or perpendicular to the surface, i.e., is the flow tangential or does it have a more stagnation flow character
- how well defined are the hydrodynamics in the cell
- what is the flow strength (Reynolds number, shear rate etc.) that can be attained
- how must the surface that can be studied be, i.e., flat, curved, rotating or stationary

2.2.1 Stirred Cuvettes

A flow cell that is employed frequently is a cuvette, see Figure 2.1a. The cuvette is usually stirred. The surface at which adsorption takes place can be flat or curved and is either immersed into the cuvette or forms one of the cuvette walls. The surface is stationary. However, the flow pattern is difficult to characterise. Both shear and stagnation flow occur although shear is dominant. Some studies have reported on the effects of mass transfer by determining the diffusion boundary layer by means of film theory (Wahlgren 1992). Air bubbles present in the solution form a problem, when present close to the surface. Deaeration and filtering through a hydrophobic filter overcomes most of this problem. The flow velocities that can be obtained are low even when stirrer speeds are high.

2.2.2 Stagnation Point Flow

In Figure 2.1b stagnation point flow is depicted. This type of flow geometry can be either a pseudo two dimensional (and is then also referred to as Hiemenz flow) or a three dimensional axisymmetrical flow (sometimes called wall jet or impinging jet). This type of flow is well defined if the dimensions of the flow cell are properly chosen (Dabros and van de Ven 1983). The studied surface can be placed horizontally (Dabros and van de Ven 1983) or vertically (Dijt, Cohen Stuart, *et al.* 1990).

The flow velocities that can be used is low to moderate, because at high flow velocity unwanted vortices are formed that disturb the defined flow pattern. To reduce this problem a different geometry has sometimes been employed in the literature. In this geometry a second wall is positioned facing the surface of interest, see Figure 2.1b. dashed lines.

Only in or near the stagnation point the flow is well defined, the size of the area depending on flow velocity, but it is usually in the order of a few square micrometers. Well defined turbulent flow is not possible with this geometry. Furthermore, the surface of interest must be flat and stationary.

2.2.3 Rotating Disk

The flow pattern that is created when a disk rotates in free solution, Figure 2.1c has some similarities with the flow described in the last section.

Higher flow strenghts are possible without affecting the flow pattern. Well defined turbulent flow is possible. The flow velocity increases with radial distance from the centre of the disk, thus a range of shear rates at one fixed angular speed is present. This flow is a three dimensional flow, with mixed shear and stagnation point character, although near the surface the flow can be approximated by

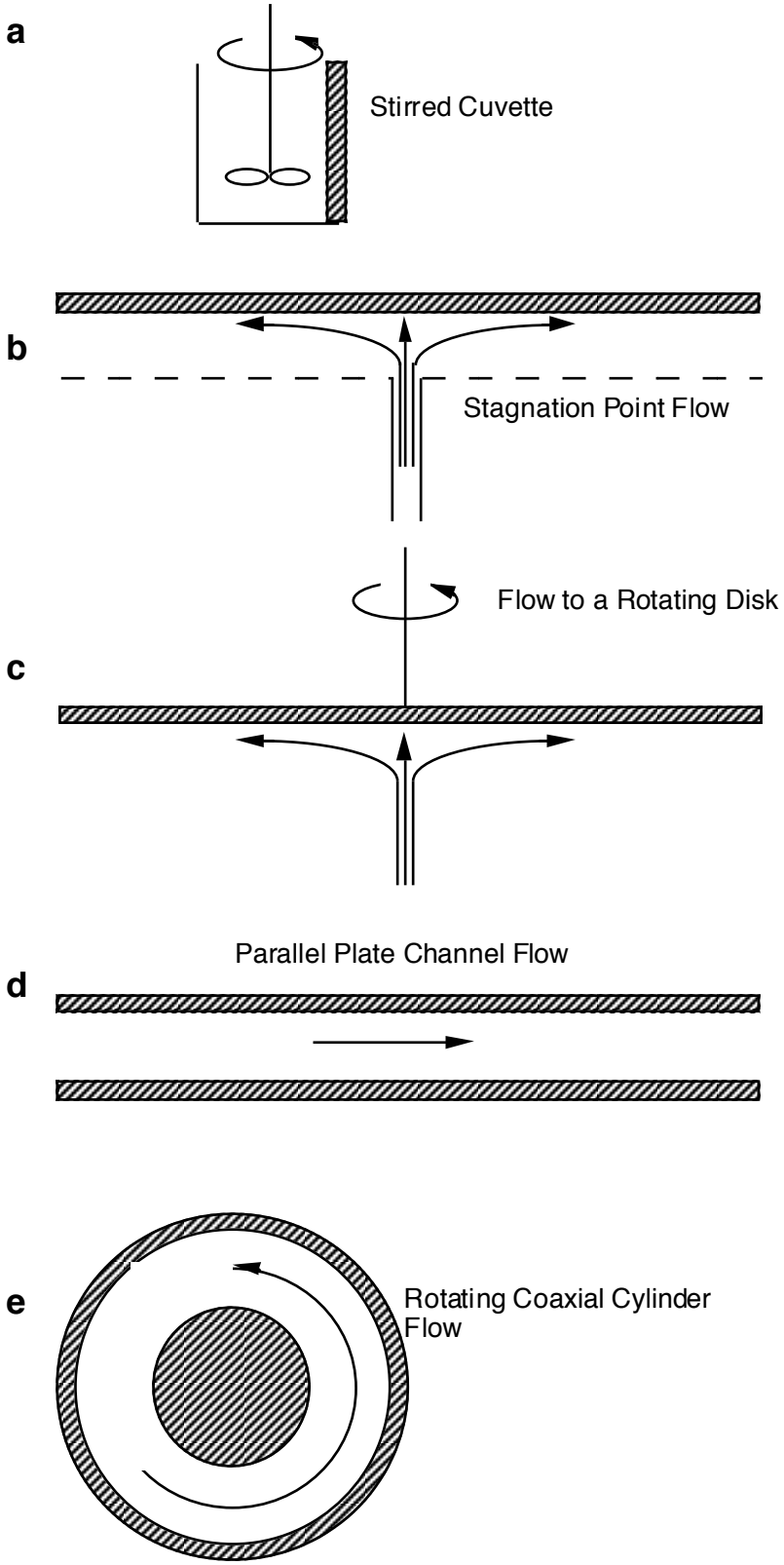

Figure 2.1: Schematic drawing illustrating the various flow cells. The arrows represent the stream lines. Adsorption can take place at the shaded areas, see also text for explanation.

a two-dimensional flow with only shear flow away from the centre and stagnation point flow in the centre of the disk. The surface of interest is rotating and must be flat.

2.2.4 Parallel Plate Channel

A flow cell that enables very high flow velocities is the parallel plate flow cell, see Figure 2.1d. Flow can either be laminar or turbulent and is well defined when the flow is fully developed. The length of the channel required to develop well defined flow is called the hydrodynamic entrance length. Laminar flow at very high flow strenghts are possible in flow cells with a high aspect ratio. In the laminar region only simple shear flow is present. The surface of interest must be studied at least one hydrodynamic entrance length downstream of the inlet of the flow cell. The surface must be flat and is stationary.

2.2.5 Rotating Coaxial Cylinders

In this flow geometry two cylinders, with liquid in between, of which at least one is rotated, form the flow channel as depicted in Figure 2.1e. High flow velocities are possible although above a certain flow velocity secondary flows develop, i.e., so called Taylor vortices. In the laminar region a simple shear flow is present, in the turbulent region stagnation flows develop. The surface of interest is always curved and can be either rotating or stationary.

2.2.6 Discussion

In this study the combined effect of adsorption and desorption on the total rate is studied. Therefore, the stagnation point flow was not used, as no desorption is expected to occur. The parallel plate, rotating disk and coaxial cylinder flow cells combine defined laminar or turbulent flow with a high shear rate. The parallel plate flow cell is the only flow geometry discussed where a stationary flat surface can be used as the surface of interest, combined with a high flow velocity with shear. Therefore, a parallel plate flow cell was developed in the present study.

2.3 Experimental Techniques

2.3.1 Introduction

In the literature techniques that are able of providing the adsorbed amount of protein on a surface have been reviewed (Ivarsson and Lundström 1986; Ramsden 1993). These techniques are further discussed here and are divided in four categories according to the quantity which is probed:

- labelling techniques like fluorescence and radio labelling.
- acoustic vibration techniques like the quartz micro balance and surface acoustic wave devices
- electrical methods like impedance or electrokinetic methods
- optical techniques like light scattering, surface plasmon resonance, raman spectroscopy, infrared reflectance spectroscopy, integrated optics and ellipsometry

In the next sections the above techniques will be reviewed according to the following requirements:

1. the technique should not influence the protein, the surface or the hydrodynamic conditions in any way
2. with the technique it should be possible to determine the amount of adsorbed protein *in situ* with a high enough sample frequency
3. the technique should be able to determine the amount of protein on a number of different surface materials
4. the technique should preferably give information on conformation and/or orientation in the adsorbed layer

2.3.2 Labelling Techniques

With labelling techniques protein molecules are tagged with a radio active or fluorescent label. This label is then detected and the number of protein molecules on the surface can be calculated. Especially radioactive labelling has become less popular nowadays for obvious reasons of safety. For some protein molecules fluorescence is intrinsic, i.e., the protein molecule itself has fluorescent properties.

ad. 1. Labelling techniques that were favourite in the early literature have been shown to sometimes greatly influence the adsorption properties of labelled proteins compared to their unlabelled counterparts (van der Scheer 1978).

ad. 2. Furthermore, when deposition rates are low, it is necessary to periodically flush out the cell before counting. This means that it is not possible to obtain continuous data, and that in this case the properties of the flush solution should be similar, and the flush rate much smaller then the recirculating flow, making the experimental setup complex (Elimelech, Gregory, *et al.* 1995). Detachment of labels over time is also a common pitfall of these techniques, as well as change of fluorescence upon adsorption.

ad. 3. A great advantage of labelling is that the geometry of the surface or surface material do not influence the ability to measure protein adsorption.

ad. 4. Radioactive or fluorescent labelling have the drawback that no information on conformation and/or orientation in the adsorbed layer can be obtained.

2.3.3 Acoustic Vibration Techniques

These techniques relay on the change in resonance frequency with adsorbed mass on the surface of flat piezo electric material. In air calculations are straight forward, immersed in protein solution there is a coupling between the oscillation properties of the liquid and the oscillations in the crystal.

ad. 1. Recently, the vibrations of a quartz micro balance have been shown to influence the adsorption properties of proteins (Lacour, Torresi, *et al.* 1992).

ad. 2. Measurements *in situ* with high sample frequency are possible.

ad. 3. The surface material is limited to piezo electric materials.

ad. 4. No information on conformation and/or orientation in the adsorbed layer can be obtained using this technique.

2.3.4 Electrical Techniques

A dissolved protein will become charged as the result of their ionisable amino acid groups. With electrical techniques the change in electrostatic charge at the surface is detected. If the charge on an individual protein molecule is known then the total number of protein molecules can be calculated.

ad. 1. Electrical techniques do not influence the system under study.

ad. 2. Measurements *in situ* with high sample frequency are possible.

ad. 3. Some metals are covered by isolating oxide layers, making their interfacial characteristics similar to glasses, but metal oxide layers may also be conducting, see for example (Jacobs 1995), making it more difficult to use these methods.

ad. 4. information on conformation and/or orientation in the adsorbed layer cannot be obtained by these methods.

2.3.5 Optical Techniques

Optical techniques make use of the fact that upon reflection, refraction or scattering of a light beam the properties of this light beam change. Most techniques determine changes in amplitude, phase or wavelength. From these changes, optical parameters, and even bonding states of molecules, of the protein layer may be obtained.

ad. 1. All optical techniques are essentially non perturbing techniques.

ad. 2. Optical techniques are suited for *in situ* measurements with a high sample frequency, in the order of seconds to a minute, depending on the individual techniques. Small air bubbles present in the protein solution present a problem in optical techniques, because they scatter light and therefore deteriorated the signal. Therefore, air bubbles should be removed by deaeration of the protein solution or eliminated by other means.

ad. 3. For optical techniques the light beam must be able to interact with the protein layer by either penetrating through the surface material or by reflecting from it. By coating the surface of interest an even wider range of surface materials can be studied.

ad. 4. Optical techniques can give information on conformation and/or orientation in the adsorbed layer.

Ellipsometry, and similar other techniques like reflectometry, scanning angle reflectometry and surface plasmon resonance determine the change in polarisation of a light beam after interaction with the protein layer. All of these optical techniques can be understood using the Fresnel equations. In Appendix A the use of the Fresnel equations for these techniques is discussed. In Appendix B the experimental setup specifically used in this study is discussed.

2.3.6 Discussion & Conclusion

As stated in the introduction of this section, four criteria for choosing a method where given. Only optical techniques meet all these criteria. The choice between several optical techniques is somehow arbitrary, because similar information is obtained. In this study ellipsometry has been chosen. Ellipsometry has also been the method of choice in many other studies, facilitating comparison between those studies and the present. Usually ellipsometry is used in external reflection mode. In this study ellipsometry in attenuated total internal reflection mode has been used to study a protein layer at a wall of a parallel plate flow cell.

Chapter 3

Characterisation of the Interfacial Interaction between Proteins and Surfaces

Summary

Adsorption of proteins onto surface materials is highly influenced by interfacial forces. Using contact angle measurements and the Acid-Base or VCG theory the protein and the surface materials are characterised and total interaction energies calculated.

The surface properties of oxidised silicon wafers both untreated and silanised, gold, chromium oxide, and titanium dioxide surfaces are determined. All surface materials are polar to some extend.

The interaction between fibrinogen and the five surface materials are calculated in water and air. The medium in which adsorption takes place has a large influence on the interaction energy. In air fibrinogen has a large interaction with all surface materials and itself. In water the interaction between silicon dioxide, chromium oxide and titanium dioxide is greatly modified. By using the surface properties of fibrinogen and the surface materials, interaction energy versus distance curves are calculated and show quantitatively the energy barriers in the interactions in the systems.

The interaction energy curves are used together with the interfacial force boundary layer theory in the system fibrinogen titanium dioxide to determine the rate constant of adsorption. A value of $4.8 \cdot 10^{-8}$ m^3 mg^{-1} s^{-1} ($1.6 \cdot 10^4$ ℓ mol^{-1} s^{-1}) is found for the adsorption rate constant and is used in Chapter 5.

3.1 Introduction

The interaction potential that exists between a surface and a protein, see Figure 3.1, determines whether this protein will adsorb to a surface or not, and at what rate. Direct measurements of the forces between layers of protein and surface materials have become possible by means of the force balance (Israelachvili 1992). However, experiments require much skill and equipment is expensive.

Recent theory has made calculations of the total interaction energy between a protein and surface materials in aqueous media from contact angle measurements both easy and versatile. In short the theory of surface tension components as pioneered by Fowkes has been extended by Van Oss, Chaudhury and Good. They propose a separation of the polar surface tension component into two separate surface tension parameters, the electron donor and electron acceptor term. These parameters are the Lewis acid and base properties respectively. In aqueous media these polar interactions are able to explain many experiments in polar media. The theory has been very successful in determining the adsorption, solubility and osmotic pressure of polar materials in aqueous media, for example, the

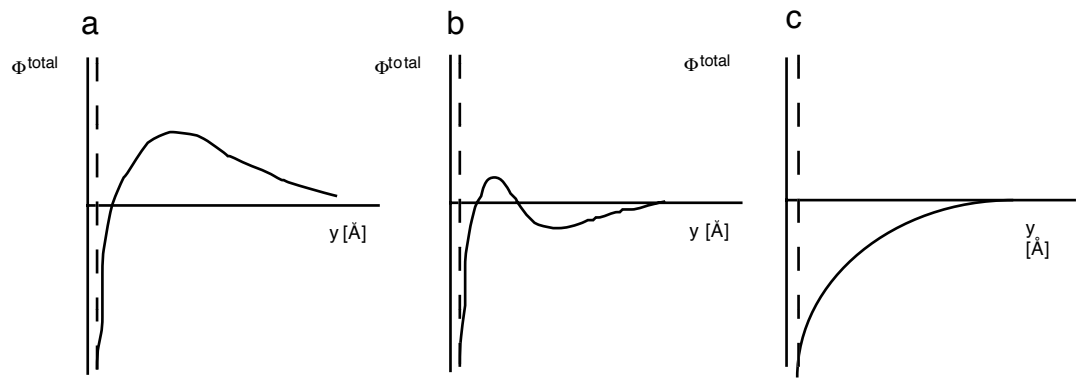

Figure 3.1: Schematic illustration of a typical total interaction energy curve against separation distance y, i.e., a DLVO-plot. a, b and c correspond to situations with high, small and no energy barrier for adsorption. The dashed vertical line is located at $y = y_0$ the distance at which contact angle measurements are performed.

dependence of the flux through a membrane limited by osmotic pressure (Bhattacharjee, Sharma, *et al.* 1994), the adsorption of bio-molecules to different membrane materials (Gourley, Britten, *et al.* 1994) and the critical micelle concentration of surfactants (van Oss 1994).

In this chapter extended-DLVO plots are calculated from contact angle measurements. The extended-DLVO plots are used to calculate the rate contstant of adsorption. Contact angle measurements yield surface tension components of the surface materials that in turn are used to calculate the total free energy change at the equilibrium distance y_0. This gives a single point of the extended-DLVO plots, the complete decay with distance is calculated.

3.2 Theory

3.2.1 Total Interaction Energy between Protein and Surface Material

DLVO theory

To calculate the non-covalent interactions between colloidal particles and a surface material the Derjaguin, Landau, Verwey and Overbeek (DLVO) theory has been used for many years and considers the total interaction energy to be the summation of two interactions, the Lifshitz-Van der Waals interaction (LW) and electrostatic (EL) interaction:

$$\phi^{\text{total}}(y) = \phi^{\text{LW}}(y) + \phi^{\text{EL}}(y) \tag{3.1}$$

With $\phi(y)$ the interaction energy as a function of the distance y between the adsorption surface and the surface of the protein, see also Figure 3.1. This theory has proven fruitful in studying the rate of many adsorption processes, providing quantitative or semi quantitative predictions in some experimental systems. For other systems predictions are not even qualitatively correct, see for example (Elimelech, Gregory, *et al.* 1995). One way to explain the discrepancy is to consider microscopic surface characteristics like heterogeneity and surface roughness, another is to include additional or non-DLVO interactions. These can play, especially in aqueous media, an important role (Elimelech, Gregory, *et al.* 1995; Swanton 1995).

Extended-DLVO

The Van Oss, Chaudhury and Good theory (VCG) (van Oss 1993; van Oss 1994), also referred to as the (Lewis) Acid-Base theory includes non-DLVO polar interactions:

$$\phi^{\text{total}}(y) = \phi^{\text{LW}}(y) + \phi^{\text{EL}}(y) + \phi^{\text{AB}}(y) \tag{3.2}$$

Because of the additional polar, also called electron-donor/electron-acceptor or Lewis acid-base, interactions it is referred to as extended-DLVO.

The EL interaction energy component can be determined by streaming potential measurements for surfaces (Van Wagenen and Andrade 1980; Van Wagenen, Coleman, *et al.* 1981) and by electroosmosis for protein molecules.

3.2.2 Van Oss, Chaudhury Good or Acid-Base theory

Surface Tension

The surface tension γ, expressed in mJ m^{-2}, mN m^{-1} or dyne cm^{-1}, is defined as half the free energy change necessary to create unit surface area of a material *in vacuo*. The surface energy is the solid state analogon of the surface tension. In 1962, Fowkes proposed that surface tension/energy could be separated into apolar and polar components. This became what is now called the theory of surface tension components:

$$\gamma_1^{\text{total}} = \sum \gamma_1^{\text{i}} = \gamma_1^{\text{LW}} + \gamma_1^{\text{AB}} \tag{3.3}$$

Were LW and AB have been used rather than d (for dispersive) and p (for polar) used in Fowkes' original formulation. Fowkes has split up the total surface tension in two surface tension components LW and AB (Equation 3.3). Van Oss *et al.* have further subdivided the AB component into two surface tension parameters $\gamma^{\oplus}$ and $\gamma^{\ominus}$.

$$\gamma_1^{\text{AB}} = 2\sqrt{\gamma_1^{\oplus}\gamma_1^{\ominus}} \tag{3.4}$$

Where $\gamma^{\oplus}$ represents the electron acceptor parameter and $\gamma^{\ominus}$ the electron donor part. It is this separation of the AB component that allows the AB interaction to be either repulsive or attractive.

Interfacial Tension

According to (Dupré 1869) the change in free energy when creating unit area between material 1 and 2 in a medium 3 is given by:

$$\Delta G_{132} = \gamma_{12} - \gamma_{13} - \gamma_{23} \tag{3.5}$$

With γ_{ij} the interfacial tension between materials i and j. This is schematically illustrated in Figure 3.2. For the change in free energy when creating unit area by splitting a material 1 in a medium 3 this becomes:

$$\Delta G_{131} = 0 - \gamma_{13} - \gamma_{13} = -2\gamma_{13} \tag{3.6}$$

Using Equation 3.5 with known interfacial tensions γ_{12}, γ_{13} and γ_{23} between three materials 1, 2 and 3, allows direct calculation of the total interaction energy between those materials.

While the interfacial tension between immiscible liquids can be measured, the solid/liquid or solid/solid interfacial tensions are inaccessible to direct measurement. To overcome this problem a combining rule is necessary to calculate γ_{ij} from the individual surface tensions γ_i and γ_j of the respective materials (Van Oss 1993). Different combining rules must be used for LW and AB

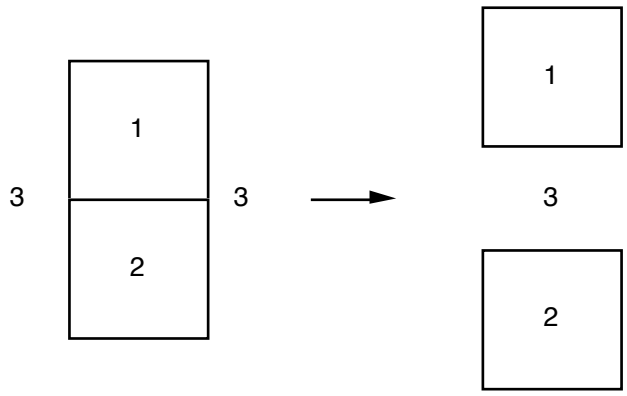

Figure 3.2: Schematic illustration of the Dupré equation

component, to calculated the interfacial tensions of the components. For apolar interactions the geometric mean can be used.

$$\gamma_{12}^{\mathrm{LW}} = \gamma_1^{\mathrm{LW}} + \gamma_2^{\mathrm{LW}} - 2\sqrt{\gamma_1^{\mathrm{LW}}\gamma_2^{\mathrm{LW}}} \tag{3.7}$$

or

$$\gamma_{12}^{\mathrm{LW}} = \left(\sqrt{\gamma_1^{\mathrm{LW}}} - \sqrt{\gamma_2^{\mathrm{LW}}}\right)^2 \tag{3.8}$$

For polar interactions the geometric combining rule only correctly predicts situations encountered in practice if it is formulated with separate contributions for electron acceptor and electron donor parameters:

$$\gamma_{12}^{\mathrm{AB}} = \gamma_1^{\mathrm{AB}} + \gamma_2^{\mathrm{AB}} - 2\sqrt{\gamma_1^{\oplus}\gamma_2^{\ominus}} - 2\sqrt{\gamma_1^{\ominus}\gamma_2^{\oplus}} \tag{3.9}$$

or

$$\gamma_{12}^{\mathrm{AB}} = 2\sqrt{\gamma_1^{\oplus}\gamma_1^{\ominus}} + 2\sqrt{\gamma_2^{\oplus}\gamma_2^{\ominus}} - 2\sqrt{\gamma_1^{\oplus}\gamma_2^{\ominus}} - 2\sqrt{\gamma_1^{\ominus}\gamma_2^{\oplus}} \tag{3.10}$$

or

$$\gamma_{12}^{\mathrm{AB}} = 2\left(\sqrt{\gamma_1^{\oplus}} - \sqrt{\gamma_2^{\oplus}}\right)\left(\sqrt{\gamma_1^{\ominus}} - \sqrt{\gamma_2^{\ominus}}\right) \tag{3.11}$$

3.2.3 Decay with Distance of the Total Interaction Energy

To determine the decay with distance of the interaction energy from contact angle measurements we write Equation 3.5 in the form

$$\Delta G_{132,y=y_0}^{\mathrm{total}} = \gamma_{12}^{\mathrm{total}} - \gamma_{13}^{\mathrm{total}} - \gamma_{23}^{\mathrm{total}} \tag{3.12}$$

With $\Delta G_{132,y=y_0}^{\mathrm{total}}$ the free energy change determined from contact angle measurements. The contact angle liquid is in contact with the surface in a geometry of semi-infinite parallel plates. The distance between liquid and solid has been determined to be $y_0 = 1.57$Å (Van Oss 1994). Hence, it is now possible to express the total interaction energy in a three phase system as a function of $\gamma^{\mathrm{LW}}, \gamma^{\oplus}$ and $\gamma^{\ominus}$ by substituting the Equations 3.8 & 3.11 and similar equations for $\gamma_{13}^{\mathrm{total}}$ and $\gamma_{23}^{\mathrm{total}}$ into Equation 3.12 to give:

$$\begin{aligned}\Delta G_{132,y=y_0}^{\mathrm{total}} = {} & 2\left(\sqrt{\gamma_3^{\mathrm{LW}}} - \sqrt{\gamma_1^{\mathrm{LW}}}\right)\left(\sqrt{\gamma_2^{\mathrm{LW}}} - \sqrt{\gamma_3^{\mathrm{LW}}}\right) \\ & +2\sqrt{\gamma_3^{\oplus}}\left(\sqrt{\gamma_1^{\ominus}} + \sqrt{\gamma_2^{\ominus}} - \sqrt{\gamma_3^{\ominus}}\right)\end{aligned}$$

$$+2\sqrt{\gamma_3^{\ominus}}\left(\sqrt{\gamma_1^{\oplus}}+\sqrt{\gamma_2^{\oplus}}-\sqrt{\gamma_3^{\oplus}}\right)$$
$$-2\sqrt{\gamma_1^{\oplus}\gamma_2^{\ominus}}-2\sqrt{\gamma_1^{\ominus}\gamma_2^{\oplus}} \tag{3.13}$$

Where the first two terms on the right hand side are equal to $\Delta G^{\mathrm{LW}}_{132,y=y_0}$ and the remaining four make up $\Delta G^{\mathrm{AB}}_{132,y=y_0}$.

Using the three interaction energy components from Equation 3.2 $\Delta G^{\mathrm{LW}}_{132,y=y_0}, \Delta G^{\mathrm{AB}}_{132,y=y_0}$, and $\Delta G^{\mathrm{EL}}_{132,y=y_0}$ it is possible to construct interaction energy versus distance diagrams like in Figure 3.1. For unretarded Lifshitz-Van der Waals interactions the rate of decay of the interaction for the sphere and a semi-infinite flat plate geometry is (Van Oss 1994):

$$\phi^{\mathrm{LW}}_{132}(y) = \frac{2\pi\Delta G^{\mathrm{LW}}_{132,y=y_0} y_0^2 a_{\mathrm{p}}}{y} \tag{3.14}$$

With $\Delta G^{\mathrm{LW}}_{132,y=y_0}$ the Lifshitz-Van der Waals interaction energy component in the semi-infinite thick plates in a parallel geometry, i.e., using contact angle measurements. a_{p} is the radius of the sphere.

For the acid-base component of the total interaction energy the equation for the rate of decay is:

$$\phi^{\mathrm{AB}}_{132}(y) = 2\pi\Delta G^{\mathrm{AB}}_{132,y=y_0}\lambda a_{\mathrm{p}} \mathrm{e}^{(y_0-y)/\lambda} \tag{3.15}$$

With $\Delta G^{\mathrm{AB}}_{132,y=y_0}$ the acid-base interaction energy component determined using contact angles, and λ the decay length of water. λ for water lies between 0.2 and 1.0 nm, when AB interactions are repulsive (Van Oss 1994).

3.2.4 Surface Tension Components from Contact Angle Measurements

To determine the surface tension parameters of a surface material via contact angle measurements the Young-Dupre equation is used:

$$(1+\cos\theta)\,\gamma_L^{\mathrm{total}} = -\Delta G_{SL}^{\mathrm{total}} = -\gamma_{SL}^{\mathrm{total}} + \gamma_S^{\mathrm{total}} + \gamma_L^{\mathrm{total}} \tag{3.16}$$

This equation is schematically depicted in Figure 3.3. Using the above equation with Equations 3.3, 3.7 & 3.10 gives:

$$(1+\cos\theta)\,\gamma_L^{\mathrm{total}} = 2\sqrt{\gamma_S^{\mathrm{LW}}\gamma_L^{\mathrm{LW}}} + 2\sqrt{\gamma_S^{\oplus}\gamma_L^{\ominus}} + 2\sqrt{\gamma_S^{\ominus}\gamma_L^{\oplus}} \tag{3.17}$$

Were S and L replace 1 and 2 and represent the solid and liquid respectively. This equation links the experimentally determined contact angles θ, and known values of $\gamma_L^{\mathrm{total}}, \gamma_L^{\mathrm{LW}}, \gamma_L^{\oplus}$ and $\gamma_L^{\ominus}$ of a contact angle liquid to three unknown values of $\gamma_S^{\mathrm{LW}}, \gamma_S^{\oplus}$, and $\gamma_S^{\ominus}$ of the surface. To solve for all three unknowns three different liquids have to be employed on the same surface material. This gives then three equations with three unknowns.

In general the exact solution of such a system of equations is possible, although occasionally small negative values for $\sqrt{\gamma_S^{\oplus}}$ arise and the system of equations has no exact solution. The negative roots are believed to arise because of errors in experimentally determined θ's. Therefore a method that minimises the total error in the system, is used in such cases. Furthermore, the best method is to first solve the equation with the θ for the completely apolar liquid and with this obtained value for γ_S^{LW} solve the remaining two equations, to give $\gamma_S^{\oplus}$ and $\gamma_S^{\ominus}$.

Hence, the LW and AB interaction energy components for the interaction between proteins and surface materials can be determined from contact angle measurements on a flat piece of surface material, if the surface roughness is less than 0.1 micron, and also on deposited layers of protein molecules.

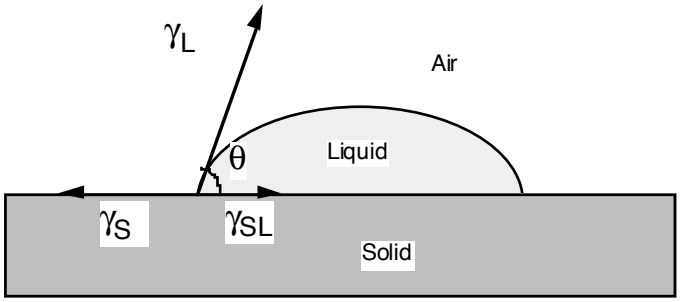

Figure 3.3: Schematic illustration of the Young-Dupré equation

3.2.5 Rate Constant of Adsorption

Convection–Diffusion–Interaction Equation

The transfer of colloidal particles from flowing solutions towards surfaces can be calculated by incorporating the total interaction energy versus distance curve in the mass balance for the system, as follows (Elimelech, Gregory, *et al.* 1995):

$$\frac{\partial c}{\partial t} = -\nabla \cdot \left(\mathbf{u}c + \mathbb{D} \cdot \nabla \phi^{\text{total}} c \right) + \nabla \cdot (\mathbb{D} \cdot \nabla c) \tag{3.18}$$

With c the particle concentration, $\mathbf{u}$ the particle velocity vector, ϕ^{total} the total interaction energy between surface and particle, and $\mathbb{D}$ the particle diffusion tensor. If the flow can be approximated by a two-dimensional flow, the interaction only has a component in the y-direction and the diffusivity is not a function of concentration, Equation 3.18 in the coordinate system given in Figure 3.4* is , becomes:

$$\frac{\partial c}{\partial t} = -u_{\parallel} \frac{\partial c}{\partial x} - u_{\perp} \frac{\partial c}{\partial y} - \frac{\partial}{\partial y} \left[\mathbb{D}_{\perp} \frac{\mathrm{d}\phi^{\text{total}}}{\mathrm{d}y} c \right] + \mathbb{D}_{\parallel} \frac{\partial^2 c}{\partial x^2} + \mathbb{D}_{\perp} \frac{\partial^2 c}{\partial y^2} \tag{3.19}$$

It states that the total flux to the surface, i.e., in the y-direction, is a function of the particle fluxes: due to *migration*, which is a result of the colloidal interactions with the surface:

$$J_{\text{migration}} = -\mathbb{D}_{\perp} \frac{\mathrm{d}\phi^{\text{total}}}{\mathrm{d}y} c \tag{3.20}$$

due to convection in the direction of the surface:

$$J_{\text{convection}} = -u_{\perp} c \tag{3.21}$$

due to Brownian diffusion:

$$J_{\text{diffusion}} = -\mathbb{D}_{\perp} \frac{\partial c}{\partial y} \tag{3.22}$$

The boundary conditions are chosen as follows:

$$c(y = \infty) = c_0 \tag{3.23}$$

and

$$c(y = 0) = 0 \tag{3.24}$$

Without approximations the above three dimensional Partial Differential Equation (PDE) Equation

*Note that the origin of the y-coordinate is located at the wall in this chapter for mathematical simplicity, whereas in Chapter 5 it is located in the center between the plates of the parallel plate flow cell

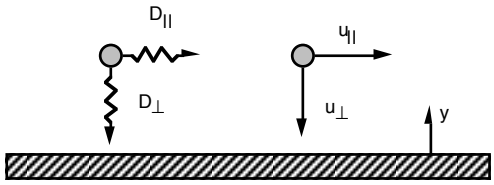

Figure 3.4: Overview of the coordinate system and the notation use in formulating the convection–diffusion–interaction equation.

3.18 with the given boundary conditions have no analytical solution, hence numerical solutions have to be found. However, to our knowledge, this rigorous treatment in either two or three dimensions has never been solved numerically.

An important approximation that leads to an analytical solution of Equation 3.18, is the Interaction Force Boundary Layer (IFBL) approximation that will be discussed after the hydrodynamics.

Hydrodynamics

The motion of the protein molecules near the surface differs from that of the fluid. The difference from the undisturbed flow field can be calculated using universal correction factors for hydrodynamic interaction (Elimelech 1994):

$$u_{\parallel} = F_3 v_{\parallel} \tag{3.25}$$
$$u_{\perp} = F_1 F_2 v_{\perp} \tag{3.26}$$
$$\mathbb{D}_{\parallel} = F_4 \mathbb{D}_{\infty} \tag{3.27}$$
$$\mathbb{D}_{\perp} = F_1 \mathbb{D}_{\infty} \tag{3.28}$$

Where $\mathbb{D}_{\infty}$ is the diffusion coefficient far from the wall, i.e., when $u = v$ and F_1 to F_4 are correction factors for particle motion and diffusion near a planar solid wall as function of the dimensionless separation distance H$= y/a_{\mathrm{p}}$. With a_{p} the particle radius.

For a protein of 50 nm in diameter like fibrinogen it is not a good assumption to take all correction factors equal to unity for all dimensionless separation distances as can be seen in Figure 3.5 after Elimelech (Elimelech 1994). In all results shown hereafter the universal correction factors for a spherical particle as solved by Brenner (Brenner 1961) are used.

Interaction Force Boundary Layer Approximation

The first to give a connection between the adsorption rate constant and the total interaction energy versus distance has been Von Smoluchowski (Von Smoluchowski 1917). His equations have been updated by Hammes (Hammes 1978) and (van Oss accepted for publication 26 June, 1997). An other frequently applied method of determining the adsorption rate constant is the Interaction Force Boundary Layer (IFBL) approximation as developed by Ruckenstein and Prieve (Ruckenstein and Prieve 1973) and Spielman and Friedlander (Spielman and Friedlander 1974). This model can predict adsorption rate constants when an energy barrier is present. The kinetic rate constant can be determined from the total energy of interaction ϕ^{total}.

The main idea behind the model is that the interaction forces act only over a very short distance. Hence, the flow in the cell is divided into two regions. A layer close to the wall where only diffusion and interfacial interactions play a role and a bulk region where the interfacial interactions do not play a significant role and transport is determined by convection and diffusion. The layer close to the wall is called the interfacial force boundary layer (IFBL) and has a thickness of δ_{IFBL}.

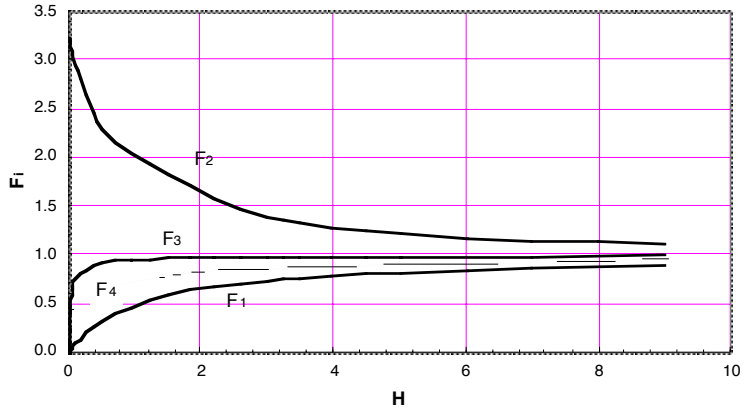

Figure 3.5: Universal correction factors for particle motion and diffusion near a planar solid wall as function of the dimensionless particle separation distance H= y/a_p.

An analytical solution to Equation 3.19 in the IFBL can be obtained if the non-stationary term is dropped and:

1. an energy barrier for deposition is present
2. the diffusion boundary layer is large compared to the IFBL
3. the total interaction energy acts only perpendicular to the surface
4. tangential diffusion is small compared to the diffusion perpendicular to the surface
5. the particles are irreversibly bound to the surface, i.e., the surface acts as a perfect sink, i.e., the concentration at the wall is zero

If the above holds, the convection–diffusion–interaction equation reduces to the convection diffusion equation ($u = v$ and $\phi^{\mathrm{total}} = 0$) outside the surface force boundary layer and an irreversible first order reaction as the boundary condition at the interface. The authors show that the adsorption rate can be approximated by the following expression:

$$\frac{\mathrm{d}\Gamma}{\mathrm{d}t} = \frac{\mathbb{D}_\infty}{\int\limits_{y=0}^{y=\delta_{\mathrm{diffusion}}} \left[\frac{1}{F_1}\mathrm{e}^{\phi^{\mathrm{total}}/kT} - 1\right] \mathrm{d}y} c_w \tag{3.29}$$

In which c_w is an effective wall concentration obtained by linear extrapolation of the bulk concentration profile at $y = 0$ as shown in Figure 3.6.

This is an important result since the this model allows us to treat the system as a convective diffusion problem with a pseudo-first-order reaction as boundary condtion[†]:

$$\frac{\mathrm{d}\Gamma_1}{\mathrm{d}t} = k_\mathrm{a} c_w \tag{3.30}$$

With c_w defined according to Figure 3.6. with an adsorption rate constant of:

[†]Note that in order to compare the results in this chapter with that in Chapter 5 the adsorption rate constant k_a should be divided by $\Gamma_{\max}$ to yield $k_{\mathrm{a}1}$

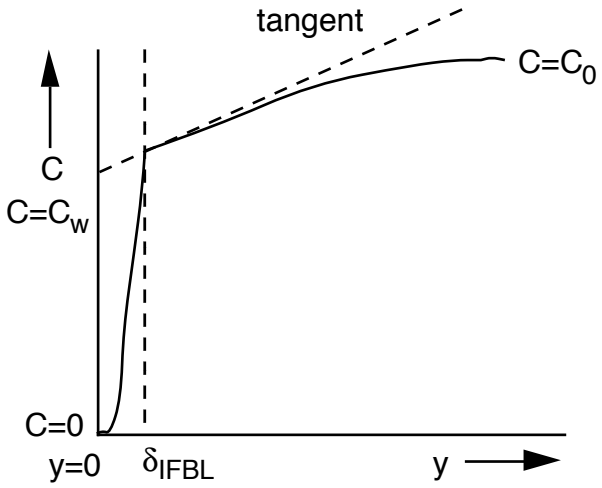

Figure 3.6: A qualitative description of the concentration profile as a function of the separation distance from the wall and the effective wall concentration c_w, as used in the IFBL approximation.

$$k_{\mathrm{a}} = \frac{\mathbb{D}_{\infty}}{\int\limits_{y=0}^{y=\delta_{\mathrm{diffusion}}} \left[\frac{1}{F_1} \mathrm{e}^{\phi^{\mathrm{total}}/kT} - 1\right] \mathrm{d}y} \tag{3.31}$$

With k_{a} the rate constant of adsorption, $\mathbb{D}_{\infty}$ the diffusion coefficient in the bulk, δ_{IFBL} the thickness of the interfacial force boundary layer, F_1 the perpendicular hydrodynamic correction factor for particle motion near a planar wall, y the surface to surface distance, k Boltzmann's constant and T the absolute temperature. F_1 can be approximated by (Elimelech 1994):

$$\frac{1}{F_1} = 1 + \frac{a_{\mathrm{p}}}{y} \tag{3.32}$$

This means that a direct comparison can be made with the adsorption rate constant k_{a1} used in Chapter 5.

3.3 Experimental

The contact angle liquids used for the determination of the surface tension parameters were ultra pure water from a Milli-Q+ unit (Millipore, USA), glycerol, and 1-bromonaphthalene grade p.a. (Merck GmbH, Germany).

It should be noted that contact angle liquids need to have a total surface tension higher than the surface energy of the surface material in order to obtain finite contact angles, i.e., non-spreading conditions. This limits the available number of liquids. Table 3.1 from (van Oss 1993) gives the surface tension properties in mJ m^{-2} for the contact angle liquids used in this study.

The metal surfaces were prepared by evaporation of the metal onto glass slides (Menzel-Gläser, Germany). The slides have dimensions 76 mm by 26 mm and have a thickness of $\approx$ 1 mm. The slides are cleaned and coated with a thin titanium layer or gold layer of $\approx$ 40.0 nm evaporated onto the slides. The metal layers are obtained by thermal evaporation onto the slides in a Varian 3117 (Varian, USA).

Polished silicon wafers are used as basis for the untreated and silanised silicon oxide surfaces. Hydrophobic wafers are obtained by treating the wafers for 90 minutes in a 7% solution of dichlorodimethylsilane p.a. grade (Merck GmbH, Germany) in toluene p.a. grade (Merck GmbH, Germany) as described by Welin-Klintstroem (Welin-Klintström 1992). The wafers are purchased from Aurel GmbH,

Table 3.1: Surface tension components of the contact angle liquids at 20°C in mJ m^{-2} from (van Oss 1993).

	γ_L^{total}	γ_L^{LW}	γ_L^{AB}	$\gamma_L^{\oplus}$	$\gamma_L^{\ominus}$
1-Bromonaphthalene	44.4	44.4	≈0	≈0	≈0
Water‡	72.8	21.8	51.0	25.5	25.5
Glycerol	64.0	34.0	30.0	3.92	57.4

Germany, diameter 2 and 3 inch, thickness ≈ 381 μm, resistivity ≤ 0.015 Ω cm, orientation ⟨100⟩, type P, Boron doped.

Contact Angle Measurements

Contact angle measurements are performed on a G1-Goniometer (Krüss GmbH, Germany). Three drops of 0.05 mℓ were subsequently placed on a surface and the contact angle was determined by the direct method, i.e., by reading the angle between the tangent of the contact point and the horizontal line of the solid surface using a protractor at each side of the drop by manually placing the tangent. 'Equilibrium' contact angles have been determined. The tabulated values are the average of three liquid droplets, i.e., six measurements. The measuring chamber could be sealed with a lid to prevent evaporation.

3.4 Results

3.4.1 Surface Tension Components from Contact Angles

Table 3.2: Measured contact angles in °, on untreated and silanised silicon dioxide, titanium dioxide, chromium oxide and gold, with water, glycerol and 1-bromonaphthalene. Average values (N = 6).

	θ_{Water}	θ_{Glycerol}	$\theta_{1-\text{Bromonaphthalene}}$
SiO_2-'OH'	14	16	19
SiO_2-'CH_3'	72	59	36
TiO_2	60	51	22
Au	78	65	19
Cr_xO_y	70	58	30

From the contact angle data in Table 3.2 the surface tension components of untreated oxidised silicon (SiO_2-'OH'), silanised oxidised silicon (SiO_2-'CH_3'), titanium dioxide, chromium oxide and gold have been determined. The results are summarised in Table 3.3. It should be noted that in a very recent publication Van Oss (van Oss 1997) shows that the above solid substrata were most probably not completely dry as manifested by the non-neglible $\gamma^{\oplus}$ values.

Contact angle measurements can also give information about a protein layer (van Oss 1994). The results for fibrinogen from this reference is used and given in Table 3.4.

‡Note that water was selected as the reference polar liquid, and should always be included as one of the polar liquids. Note also that the ratio of $\gamma_L^{\oplus}$ and $\gamma_L^{\ominus}$ for water are *chosen* unity.

Table 3.3: Surface tension components of the untreated and silanised SiO_2, titanium dioxide, chromium oxide, and gold surfaces from contact angle measurements at 20°C in mJ m^{-2}.

	γ_S^{total}	γ_S^{LW}	γ_S^{AB}	$\gamma_S^{\oplus}$	$\gamma_S^{\ominus}$
SiO_2-'OH'	62.8	42.1	20.7	2.43	44.4
SiO_2-'CH_3'	42.3	36.5	5.8	1.01	8.36
TiO_2	48.4	41.3	7.08	0.802	15.6
Au	44.0	42.1	1.88	0.160	5.64
Cr_xO_y	43.9	38.5	5.36	0.740	9.70

Table 3.4: Surface tension components in mJ m^{-2}, for fibrinogen reported in the literature from contact angle measurements at 20°C (van Oss 1994).

	γ_S^{total}	γ_S^{LW}	γ_S^{AB}	$\gamma_S^{\oplus}$	$\gamma_S^{\ominus}$
Fibrinogen	40.6	40.6	0	0	54.9

3.4.2 Total Interaction Energy between Protein and Surface Material

The total energy of interaction between a protein and a surface material in water can be determined from Table 3.3 using Equation 3.13 and the properties of water and air from Table 3.5.

Except for the apolar (LW) and the polar (AB) interactions, electrostatic (EL) interactions may also be important. Normally, the electrostatic interaction that arises from a net charge has to be taken into account. However, for fibrinogen the ζ-potential is -3.6 mV at pH 7 (van Oss 1990), this is less than the 10 mV limit above which these effects cannot be neglected. Hence, the EL interaction are not taken into account when studying the total interaction energy.

The results of the total interaction energy calculations are summarised in Table 3.6 and Table 3.7.

3.4.3 Decay with Distance of the Total Interaction Energy

In Figures 3.7-3.11 Equations 3.14 and 3.15 have been used to calculated extended-DLVO curve using the properties of fibrinogen and the five different surface materials from Table 3.3.

3.4.4 Surface Tension Components from Contact Angle Measurements

In Table 3.3 the surface tension parameters of three surfaces often used as model surfaces for protein adsorption were given. SiO_2-'OH' and SiO_2-'CH_3' refer to clean untreated silicon dioxide and silanised silicon dioxide respectively. The data given in the table shows that the untreated silicon dioxide has a large electron donor part, that is reduced dramatically by silanising. Earlier reports on physicochemical properties of untreated and silanised silicon oxide (Jönsson, Ivarsson, *et al.* 1982), using Zisman plots, gave values of γ_S^{total} of 39 mJ m^{-2} for untreated and 21 mJ m^{-2} for silanised silicon dioxide. The values determined in this chapter are 63 mJ m^{-2} and 42 mJ m^{-2} respectively. Joensson, already discussed that the value for the untreated silicon oxide was questionable, because of it's polar nature. However, table 3.3 shows that also the value for silanised silicon dioxide must be questioned, because of the still sizable value of the electron donor part of the surface energy. The table further shows that titanium dioxide is more polar than silanised silicon and that gold is less

Table 3.5: Surface tension components in mJ m^{-2}, of water and air at 20°C .

	γ_S^{total}	γ_S^{LW}	γ_S^{AB}	$\gamma_S^{\oplus}$	$\gamma_S^{\ominus}$
Water	72.8	21.8	51.0	25.5	25.5
Air	0	0	0	0	0

Table 3.6: Total interaction energy in mJ m^{-2}, in **air** for fibrinogen and the silicon oxide, titanium oxide and gold surfaces

	SiO_2-'OH'	SiO_2-'CH_3'	TiO_2	Au	Cr_xO_y	Fibrinogen
Fibrinogen	-106	-92	-95	-89	-92	-81

Table 3.7: Total interaction energy in mJ m^{-2} in **water** for fibrinogen and the silicon oxide, chromium oxide and titanium oxide surfaces

	SiO_2-'OH'	SiO_2-'CH_3'	Air	TiO_2	Au	Cr_xO_y	Fibrinogen
Fibrinogen	+27	-7.4	-11	+2.5	-11	-5.0	+42

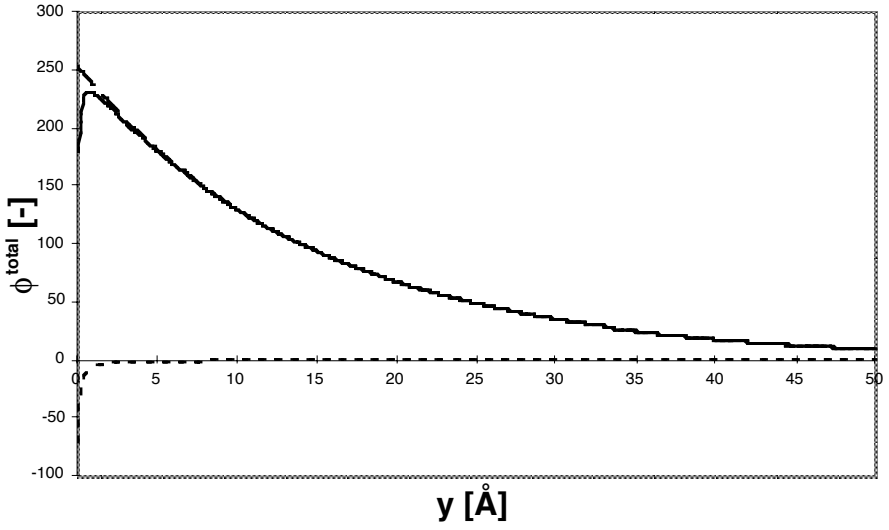

Figure 3.7: Total interaction energy (solid line), Acid-Base interaction energy (dashed line) and Lifshitz-Van der Waals interaction energy (dotted line) versus separation distance y. For the system Fibrinogen–Untreated Silicon Dioxide in water.

polar. The values of gold show in fact that its surface energy is almost completely determined by the apolar part.

3.4.5 Total Interaction Energy between Protein and Surface Material

In Tables 3.6 and 3.7 the results from Table 3.3, Table 3.5 and Table 3.4 have been used to calculate the total interaction energy of fibrinogen with the four surface materials and the air interface when

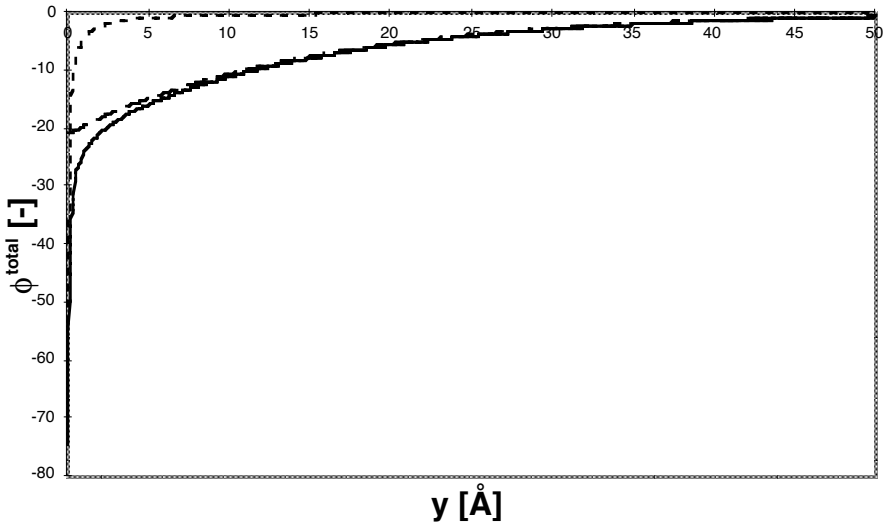

Figure 3.8: Total interaction energy (solid line), Acid-Base interaction energy (dashed line) and Lifshitz-Van der Waals interaction energy (dotted line) versus separation distance y. For the system Fibrinogen–Silanised Silicon Dioxide in water.

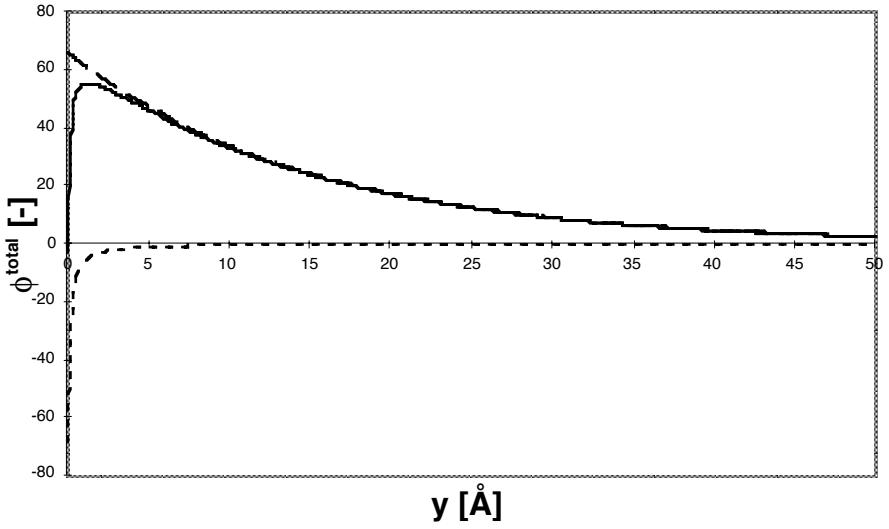

Figure 3.9: Total interaction energy (solid line), Acid-Base interaction energy (dashed line) and Lifshitz-Van der Waals interaction energy (dotted line) versus separation distance y. For the system Fibrinogen–Titanium Dioxide in water.

immersed in water. These tables should not be interpreted quantitatively because they represent the values of the total interaction energy when fibrinogen is in contact with a surface material in a geometry of semi-infinite parallel plates at a distance of y_0. What can be concluded from these tables is the relative strength of the interaction between fibrinogen and the four surface materials in air and water. A negative value of the total interaction represents attractive interaction, a positive value repulsive interaction. The total interaction energy in water is largest for gold and the air-water

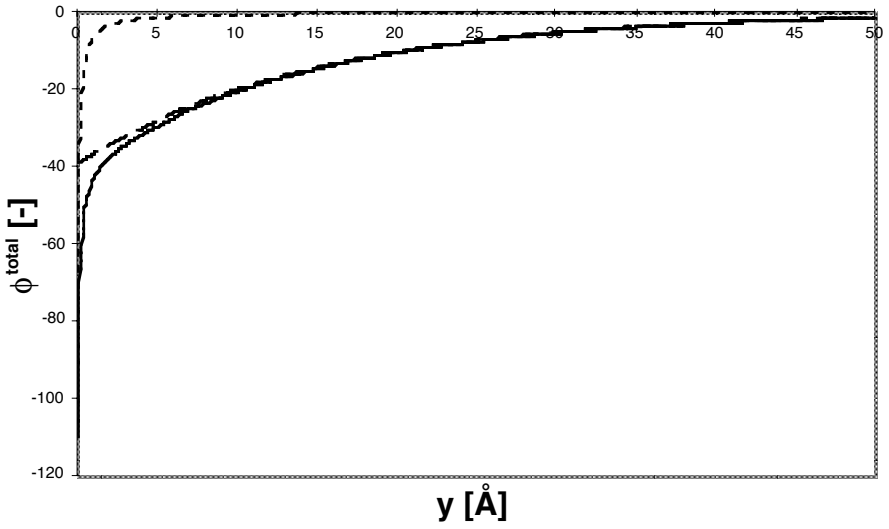

Figure 3.10: Total interaction energy (solid line), Acid-Base interaction energy (dashed line) and Lifshitz-Van der Waals interaction energy (dotted line) versus separation distance y. For the system Fibrinogen–Gold in water.

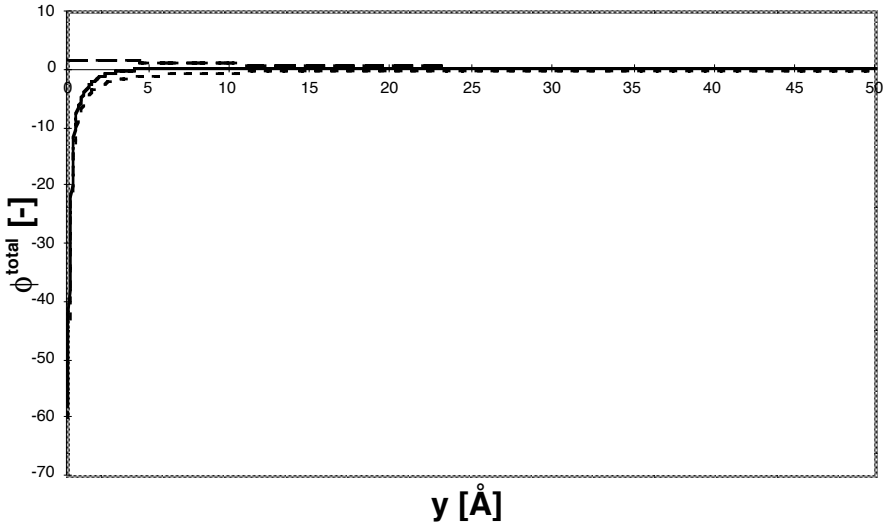

Figure 3.11: Total interaction energy (solid line), Acid-Base interaction energy (dashed line) and Lifshitz-Van der Waals interaction energy (dotted line) versus separation distance y. For the system Fibrinogen–Chromium Oxide in water.

interface followed by silanised silicon dioxide and chromium oxide, titanium dioxide, silicon dioxide and there is strong repulsion between two fibrinogen molecules in water.

The total interaction energy between fibrinogen and the surface materials in air is rather different. A comparison between Table 3.7 and Table 3.6 shows that for fibrinogen the interaction energy changes completely in air. The change is most pronounced for untreated silicon dioxide and chromium oxide. The results in Table 3.6 show that the interaction in air is almost identical and very large for

all surfaces.

3.5 Discussion

3.5.1 Decay with Distance of the Total Interaction Energy

In Figures 3.7-3.11 the total interaction energy versus distance curves show quantitative calculations using the sphere and plate geometry. The values used for y_0, a_p and λ were 1.57 Å, 3 nm and 0.6 nm respectively. The curves for silanised silicon dioxide, chromium oxide and gold show attraction at every distance, whereas the curves for silicon dioxide and titanium oxide show repulsive interaction except for very small distances. Comparing Figures 3.7-3.11 to Figure 3.1 shows that non of the extended-DLVO plots show a secondary minimium like in Figure 3.1b.

3.5.2 Rate Constant of Adsorption

Because of the repulsive interaction the curves for silicon dioxide and titanium dioxide can be used directly for determination of the rate constant of adsorption. Because titanium dioxide is used in this study as the surface material, it is interesting to calculate the rate constant of adsorption using Equation 3.31. Using a value of 100 nm for $\delta_{\text{diffusion}}$ and a diffusion coefficient of 2.0 $\cdot 10^{-11}$ m^2 s^{-1} for $\mathbb{D}_\infty$. A value of 7.6 $\cdot 10^{-7}$ m s^{-1}/16 mg m^{-2} = 4.8 $\cdot 10^{-8}$ m^3 mg^{-1} s^{-1} (1.6$\cdot 10^4$ ℓ mol^{-1} s^{-1}) is found for the adsorption rate constant.

3.6 Conclusions

The surface tension components determined using contact angle data using the VCG theory provide new information about the surface energy of, silicon dioxide both untreated and silanised, titanium dioxide and gold surfaces. It has revealed the polar character of all surfaces.

Calculations of the total interaction energy between protein and surface materials in two different media, water and air, showed that the interaction changes dramatically upon immersion or drying.

In the case of an repulsive interaction, i.e., when an energy barrier exists in the total interaction energy versus distance from the surface the IFBL approximation has been used to determine the rate constant of adsorption in the case of fibrinogen and titanium dioxide in water that has been used to model the kinetics of adsorption in Chapter 5. However, the IFBL approach could only be used in the case of titanium dioxide and is therefore not generally applicable.

Chapter 4

Adsorption of Fibrinogen onto TiO_2 in a Parallel Plate Flow Cell

Summary

In order to investigate the kinetics of adsorption of fibrinogen a parallel plate flow cell has been constructed and measurements under defined flow have been carried out using ellipsometry in attenuated total internal reflection mode. Also measurements in static solutions in a cuvette have been conducted. The surface material that has been used is titanium covered with a thin layer of native titanium dioxide. Experiments were carried out under static conditions (Renolds number zero) and laminar flow conditions with a Reynolds number of 1,000. The bulk concentrations of the model protein, fibrinogen, that have been used are 50, 100, 400 and 1,000 mg ℓ^{-1}. The time during which the experiments have been carried out was longer (up to 30 hours) than in most studies reported in the literature in which the experimental times are usually less then 1 hour.

In many studies phosphate buffer saline (PBS) has been used. However, in this study PBS buffer gave problems related to protein aggregates. Therefore, the experiments in this study were carried out using a sodium citrate HCl buffer that gave none of the problems mentioned before.

The experiments under laminar flow are very different from the static experiments in that all laminar flow experiments show overshoots in the adsorbed amount. The maximum and the 'plateau' values obtained do not directly correlate with the bulk concentration. However, the adsorbed amount was never higher than the amount calculated assuming a monolayer of end-on adsorbed fibrinogen and never lower than an side-on adsorbed monolayer (see Chapter 1). The overshoots are believed to result from the transition end-on to side-on adsorption of fibrinogen

The experimental results under laminar flow at a bulk concentration of 100 mg ℓ^{-1} carried out over 24 hours, show that over such long times the adsorbed amount determined by ellipsometry varies slowly between 0 and 2 mg m^{-2} until it rises sharply to 5-6 mg m^{-2} and then falls rapidly to 0 mg m^{-2}. This, however may be related to the special properties of fibrinogen.

Laminar flow experiments at a Reynolds number of 2,000 could not be interpreted, because the adsorbed protein layer starts absorbing light and could not be characterised.

4.1 Introduction

Although many studies have been devoted to protein adsorption at the liquid-solid interface, many questions remain unanswered and the process is still not well understood. Many previous studies have approached the problem of protein adsorption as an equilibrium adsorption problem. Adsorption 'isotherms' were measured and these isotherms mostly seemed to be in line with the Langmuir

isotherm. However, one of the basic assumption of the Langmuir isotherm, reversibility of adsorption has been questioned in the literature.

Many experiments reported in the literature have been performed for less than one hour. However, it has been argued that this is much to short to study these processes which take a long time compared to such experimental times. With more data becoming available it became clear that the process of protein adsorption can hardly be regarded reversible and that protein adsorption isotherms did in many cases show 'strange' behaviour, e.g., low plateau adsorption values at lower bulk concentrations and a kink in the adsorption isotherm at high bulk concentration values (Brash and Horbett 1995). It has also become clear that increasing the bulk concentration in steps to a final concentration gives different results compared to an increase in one step.

Studies of the dynamics of protein adsorption rather than 'equilibrium' studies are becoming more and more common in the literature. Unfortunately, these dynamic studies have mostly been carried out under conditions where mass transport limitations could be important, e.g., a stirred solution in a cuvette, and have raised questions about the rate determining step of the process, i.e., mass transfer or adsorption kinetics. Therefore, in this study we have performed measurements of protein adsorption onto the walls of a parallel plate flow cell, under laminar flow conditions that allows calculation of mass transport effects on the rate of adsorption, in order to determine the adsorption kinetics.

The technique that has been used to determine the amount of protein on the surface *in situ* was ellipsometry. This technique has been used in many other *in situ* studies of protein adsorption, see also Chapter 2 for details.

The protein selected for this study is fibrinogen. Fibrinogen is a blood protein that adsorbs readily onto almost any surface. It has been studied extensively because of its role in blood clotting. Fibrinogen is a large cigar shaped protein with a length to diameter ratio of eight, see also Chapter 1, Table 1.1.

4.2 Materials and Methods

4.2.1 Preparation of the Protein Solutions

The protein, human-fibrinogen (Enzyme Research, USA) was used as received. 1 gram of fibrinogen was dissolved in 30 ml of buffer. The buffer used was a 20 mM NaCitrate-HCl buffer prepared from NaCitrate and HCl with pH 7.4 prepared with water from a Milli-Qpak2 unit (Millipore, USA). This unit is fed with deionised water that passes a 0.5 μm prefilter before entering a macro reticular activated carbon and high purity mixed bed ion exchanger resin the final resistivity is 18.2 MΩcm. This solution was then transferred to ten small aquilots and stored at -21°C . Immediately before use the solutions were thawed in a water bath of 40°C and diluted with buffer to the desired concentration. The concentration was checked using UV absorption at 280 nm in a Uvikon 930 spectrophotometer (Uvikon, France). The total ionic strength of the buffer was 185 mM.

In the literature phosphate buffered saline (PBS) is often the buffer system of choice for many blood proteins. However, experiments using 100 mM PBS buffer at pH 7.4 gave problems related to protein aggregation. The prepared protein solutions were not always perfectly clear in PBS and sometimes showed the characteristic blue Tyndall light resulting from light scattering of particles in the hundred nanometer range. UV adsorption at 280 nm measurements at a range of concentrations showed a non-linear curve of the absorption versus concentration. Finally, AFM studies using PBS buffered protein solution showed large protein aggregates of approximately 200 nm when using PBS buffer.

4.2.2 Preparation of the Surfaces

For the measurements titanium layers were deposited on a glass slide by thermal evaporation in a Varian 3117 (Varian, USA). The slides (Menzel-Gläser, Germany). have dimensions 70 mm by 70 mm and have a thickness of ≈1 mm. The slides have a refractive index of $N = 1.515$ at a wavelength of 632.8 nm which matches the refractive index of the BK-7 glass prism used in the ellipsometer. The slides are cleaned and coated with a thin titanium layer of ≈ 40.0 nm.

Cleaning of the glass slides was performed using a standard wafer cleaning procedure. The standard wafer cleaning is a two step process that first removes contaminants such as oils and fingerprints and subsequently metallic contaminants such as K, Na and Ca by first dipping of the slides in two fuming HNO_3 bathes at 21°C for 5 minutes each. Then rinsing in quick dump rinser. A quick dump rinser is a bath containing demi-water, in which the glass slides are rinsed until the conductivity is less than 0.1 μS. Secondly, by dipping the glass slides in a bath of 70% HNO_3 at 95°C for 15 minutes. Then rinsing in the quick dump rinser and finally dry spinning on a spinner.

4.2.3 Static Adsorption Cuvette

The cuvette used for the static adsorption experiment consisted of a cylindrical glass piece with a diameter of 350 mm and a height of 350 mm. It was glued onto a slide with a low viscous UV-glue type 665 (Conloc, Germany). The slide was a 70 mm by 70 mm rectangular glass slide (Menzel GmbH, Germany), coated with a metal layer. Immersion oil (Merck, Germany) of matching refractive index is used to allow undisturbed passage of the laser beam through prism (Melles Griot, BK-7) immersion oil and glass plate to the metal–buffer solution interface, see also Figure 4.1.

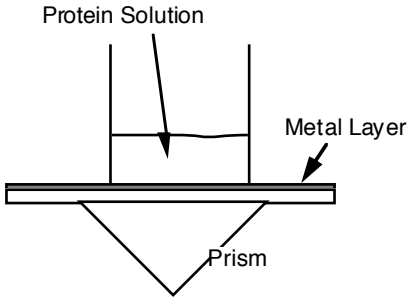

Figure 4.1: Schematic illustration of the cuvette for the static experiments.

4.2.4 Circulation System and Parallel Plate Flow Cell

The circulation system consists of a rotary gear circulation pump (Verder, Netherlands) capable of delivering 96 litres per hour at a maximum pressure of 10 bars. The general layout of the setup is given in Figure 4.2.

For the experiments under flow a parallel plate flow cell has been designed. In order to allow undisturbed flow, and be able to reflect a laser beam at the interfaces of interest, a glass slide coated with the surface material of interest forms the top wall of the channel. The cell has been constructed in a way similar to cells used for streaming potential measurements, see for example (Van Wagenen and Andrade 1980). To withstand high pressure the top and bottom parts of the cell were machined from aluminium. After construction both cell halves were anodised. Stainless steel spacer plates 0.1, 0.2, 0.5 and 1 mm in height provide a range of available channel heights. Figure 4.3 shows an expanded view of the flow cell. The actual flow channel side walls are formed by the spacer plate,

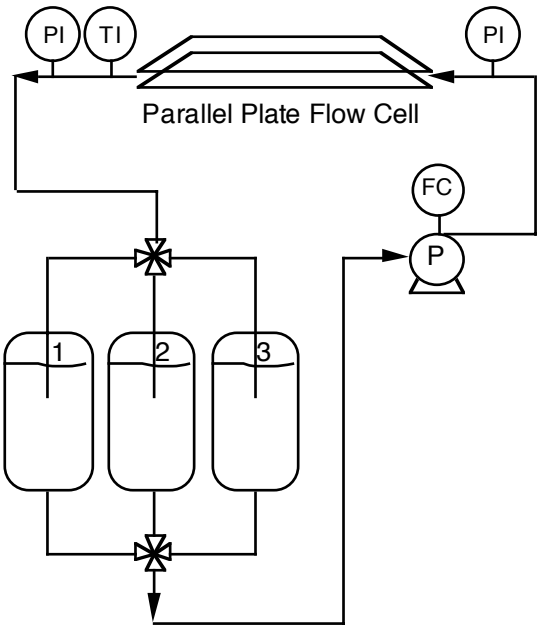

Figure 4.2: Schematic illustration of the experimental setup. P is a rotary gear pump, FC a flow controller, PI and TI are pressure and temperature indicators. The numbers 1 to 3 identify three storage flasks one with buffered protein solution, and two with pure buffer solution. The three flasks and inlet or outlet are connected to two four-way valves. The valves and fittings are made from Stainless steel 316 and all tubing was Teflon, with an inner diameter of 10 mm. Note that the protein solution is recirculated.

the upper wall by the metal layer that is studied, and the bottom wall by the bottom part of the flow cell. All three parts of the cell are connected using eight bolts. To prevent the glass slide from breaking and the prism from moving the prism is pressed from above onto a cylindrical glass piece, that fits into the upper part of the cell. Exact drawings can be found in Appendix C.

Figure 4.3: Expanded view of the parallel plate flow cell.

4.2.5 Measurement Protocol

Static Measurements

The measurements were carried out as follows. First, the glass–titanium plate was measured in air. Second, 5 mℓ of pure buffer solution was added to the cuvette and a measurement in buffer was performed. These two measurements enable the calculation of the thicknesses of both the titanium and titanium oxide layer. Next 5 mℓ of protein in buffer solution, at twice the final concentration, was added to the cuvette. The changes after the protein was added were recorded.

Laminar Flow Measurements

For the flow measurements, after the measurement in air, the pump was set for the desired flow strength with the four-way valve in the position that allowed flow of pure buffer solution through the flow cell. An adsorption measurement with protein solution was started after switching the four-way valve in the position that allowed flow of protein solution through the flow cell.

In this way a step response is obtained. By determination of the Péclet number for transverse dispersion in the tubing, the effect of dispersion of the ideal heaviside step function can be accounted for (Westerterp, van Swaaij, *et al.* 1987). The diameter of the tubing is 10 mm which leads to an average velocity of 0.1 m s^{-1}. The distance the fluid travels in the tubing from the valve to the flow cell is approximately 0.5 m. The Péclet number for transverse dispersion is given by:

$$\mathrm{Pe} \equiv \frac{\bar{v}2R}{\mathbb{D}} = 5.0 \cdot 10^7 \tag{4.1}$$

With $\bar{v}$ the average velocity, R the radius of the tubing and $\mathbb{D}$ the diffusion coefficient of fibrinogen ($2.0{\cdot}10^{-11}$ m^2 s^{-1}). At this high Péclet number the effect of dispersion in 5 seconds (the length to the cell divided by the average velocity) will be very small. In Table 4.1 an overview of the range of flow characteristics for the thinnest and thickest spacer plate that can be used is given.

Table 4.1: Overview of the flow characteristics, for different spacer plates, that can be used in the parallel plate flow cell. . With H the height, W = 15 mm the width and L = 87.4 mm the length of the rectangular channel, ϕ_v the volumetric flow rate, $\bar{v}$ the average velocity, $\dot{\gamma}$ the shear rate and Re the Reynolds number. The maximal attainable flow rates are limited by the fact that the flow cell can withstand a pressure drop of a maximum of 6 bars.

H [mm]	1.0	0.1
ϕ_v [m^3s^{-1}]	$8.0{\cdot}10^{-6}$	$5.5{\cdot}10^{-5}$
$\bar{v}$ [m s^{-1}]	$5.3{\cdot}10^{-1}$	$3.6{\cdot}10^{1}$
$\dot{\gamma}$ [s^{-1}]	$3.2{\cdot}10^{3}$	$2.2{\cdot}10^{6}$
Re [–]	$1{\cdot}10^{3}$	$7{\cdot}10^{3}$
L_e [m]	$2.3{\cdot}10^{-3}$	$2.2{\cdot}10^{-4}$

4.3 Results

4.3.1 Adsorption from Static Solutions

In Figures 4.4 and 4.5 adsorption experiments at a fibrinogen bulk concentration of 50 and 100 mg ℓ^{-1} on titanium oxide in the static cuvette are shown. In these two experiments the protein was not

dissolved in citrate buffer at pH 7.4, but in ultrapure water of pH 5.8. At pH 5.8 both the protein and the titanium dioxide surface are at their iso electric point and are therefore uncharged. In Figures 4.6 and 4.7 adsorption at a bulk concentration of 400 and 1000 mg ℓ^{-1} in citrate buffer pH 7.4 (Ionic strength 185 mM) are shown. By comparing the measurements at pH 5.8 and pH 7.4 the influence of a change of pH and ionic strength is shown.

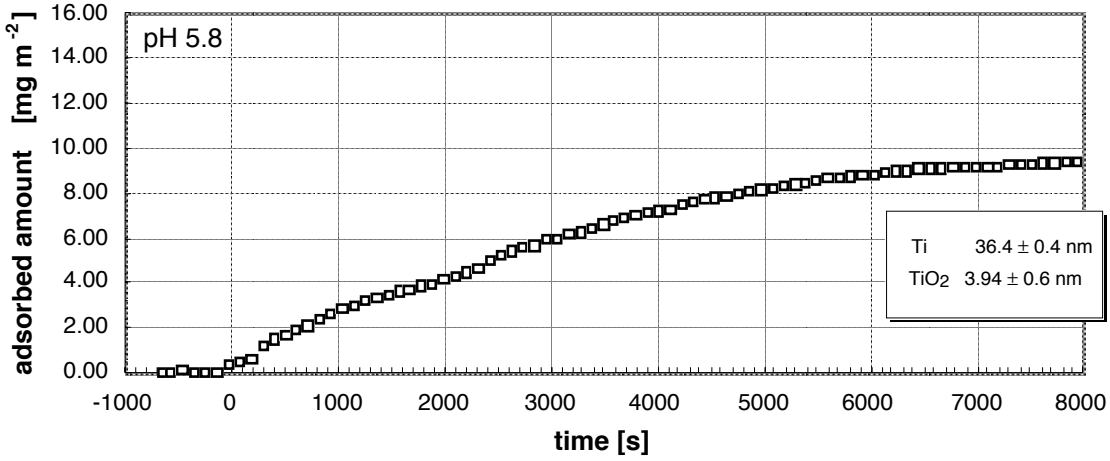

Figure 4.4: Static adsorption of fibrinogen 50 mg ℓ^{-1} on titanium oxide.

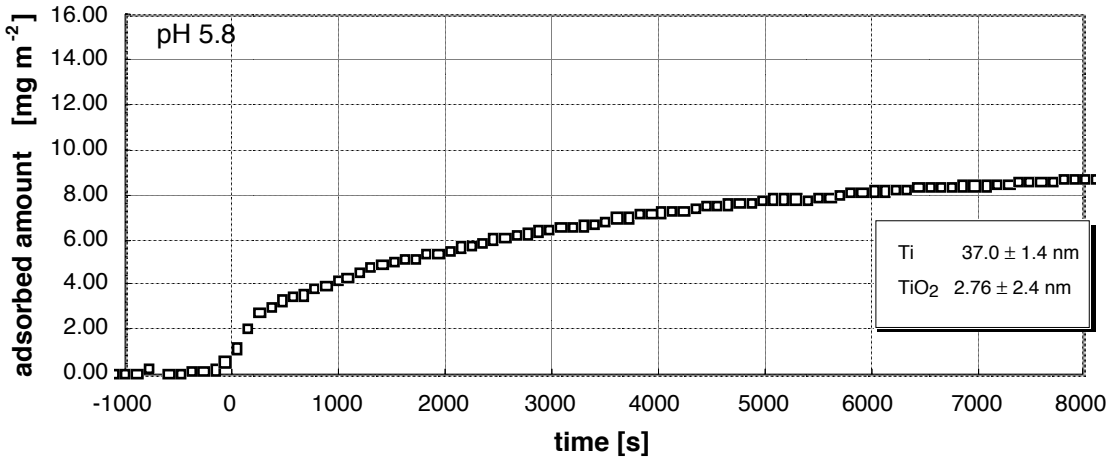

Figure 4.5: Static adsorption of fibrinogen 100 mg ℓ^{-1} on titanium oxide.

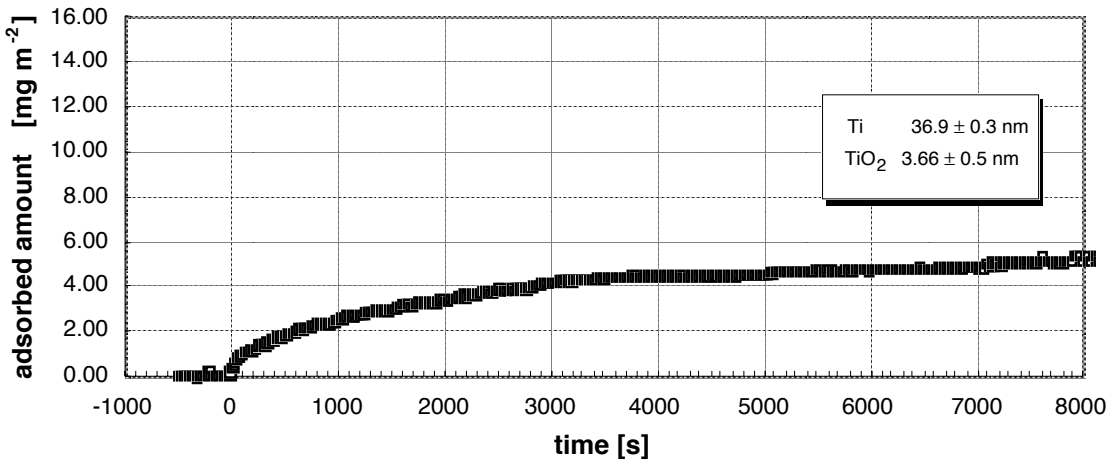

Figure 4.6: Static adsorption of fibrinogen 400 mg ℓ^{-1} on titanium oxide.

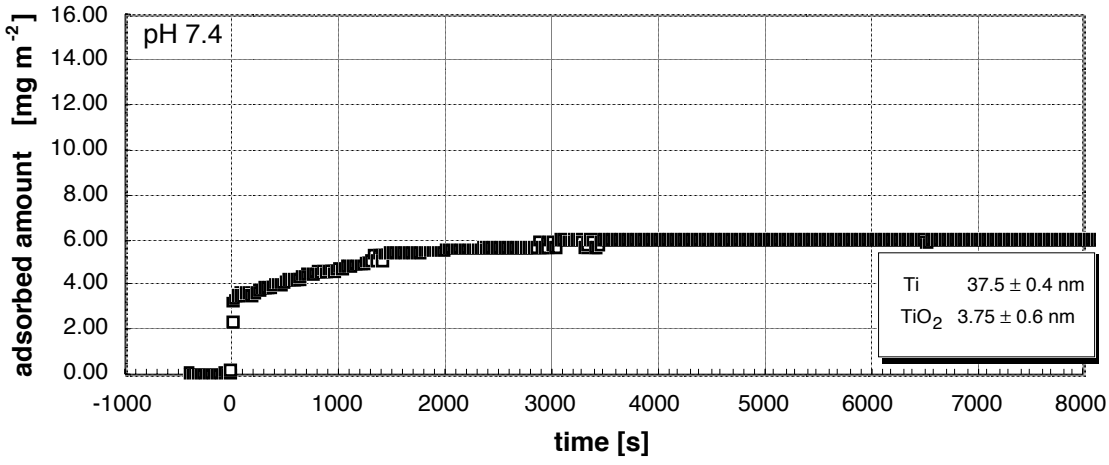

Figure 4.7: Static adsorption of fibrinogen 1000 mg ℓ^{-1} on titanium oxide.

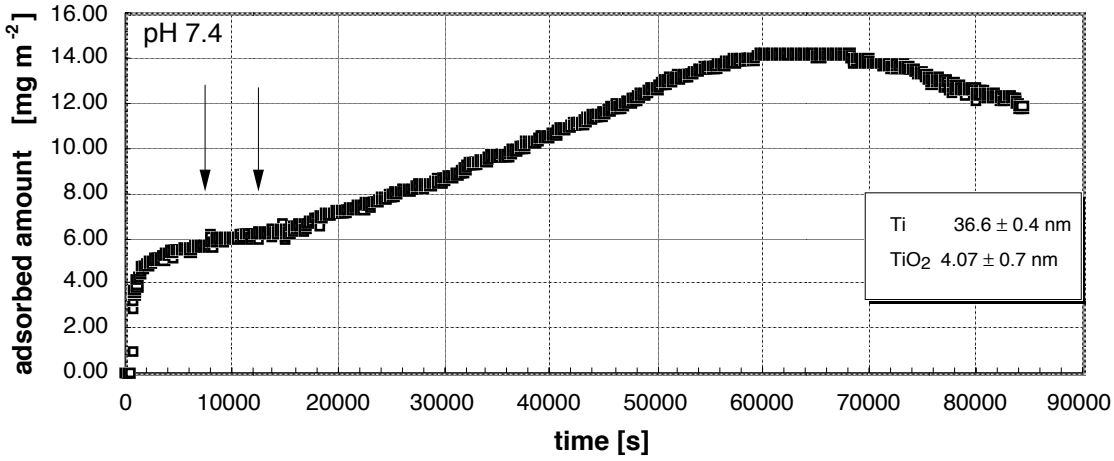

Figure 4.8: Static adsorption of fibrinogen 100-182-250 mg ℓ^{-1} on titanium oxide.

Figure 4.8 shows an experiment were the bulk concentration was increased in steps rather then in one step. The bulk concentration at the beginning of the experiment was 100 mg ℓ^{-1} (total volume 10 mℓ) and was increased to 182 mg ℓ^{-1} and 250 mℓ at t = 8,000 sec and t = 16,000 respectively by adding 1 mℓ of a 1,000 mg ℓ^{-1} solution. After the second addition of protein to a final bulk concentration of 250 mg ℓ^{-1} the slope of the adsorption curve increases sharply and a maximum of 14 mg m^{-2} is observed at approximately 62,000 seconds after which the adsorbed amount decreases again.

4.3.2 Adsorption During Laminar Flow

Table 4.2: Flow characteristics in the cell during the laminar flow experiment. With H the height, W the width and L the length of the rectangular channel, ϕ_v the volumetric flow rate, $\bar{v}$ the average velocity, $\dot{\gamma}$ the shear rate and Re the Reynolds number.

H×W×L [mm^3]	1×15×87.4
ϕ_v [m^{3}s^{-1}]	$8.0{\cdot}10^{-6}$
$\bar{v}$ [m s^{-1}]	$5.3{\cdot}10^{-1}$
$\dot{\gamma}$ [s^{-1}]	$3.2{\cdot}10^{3}$
Re [–]	$1{\cdot}10^{3}$
L_e [m]	$2.3{\cdot}10^{-3}$

Experiments at a Reynolds number of 1,000 have been performed in the parallel plate flow cell. The flow characteristics during these experiments are summarised in Table 4.2.

Shown are four experiments with a bulk concentration of 50, 100, 400 and 1,000 mg ℓ^{-1} in Figures 4.9-4.12 all in citrate buffer of pH 7.4 with an ionic strength of 185 mM.

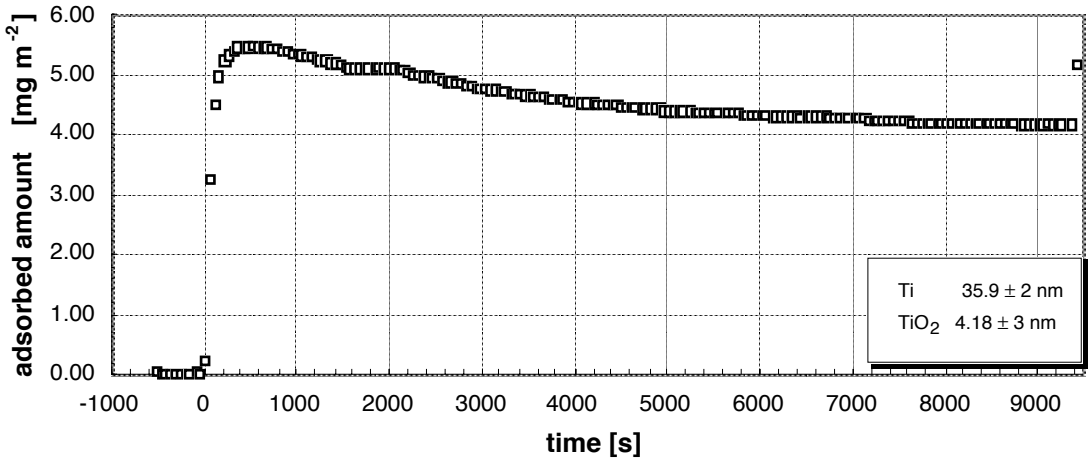

Figure 4.9: Adsorption during laminar flow of fibrinogen 50 mg ℓ^{-1} on titanium oxide.

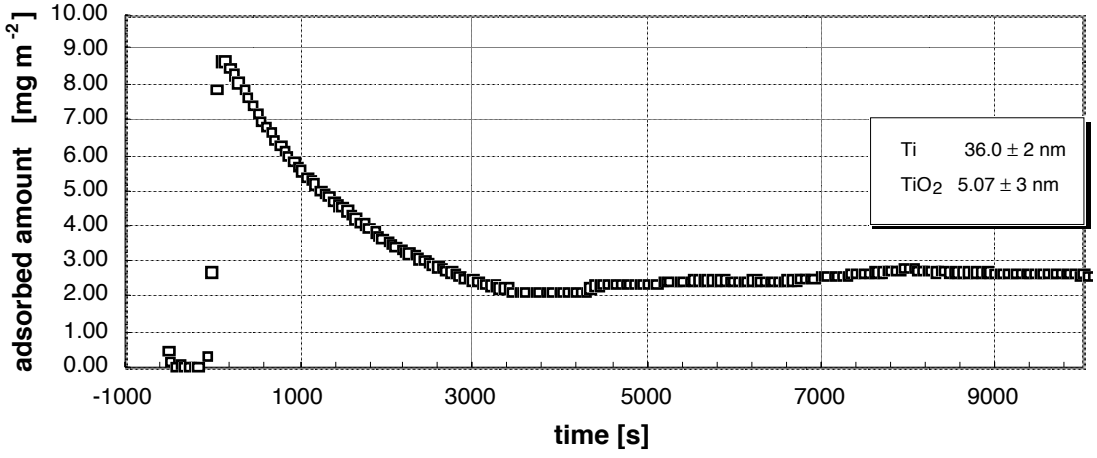

Figure 4.10: Adsorption during laminar flow of fibrinogen 100 mg ℓ^{-1} on titanium oxide.

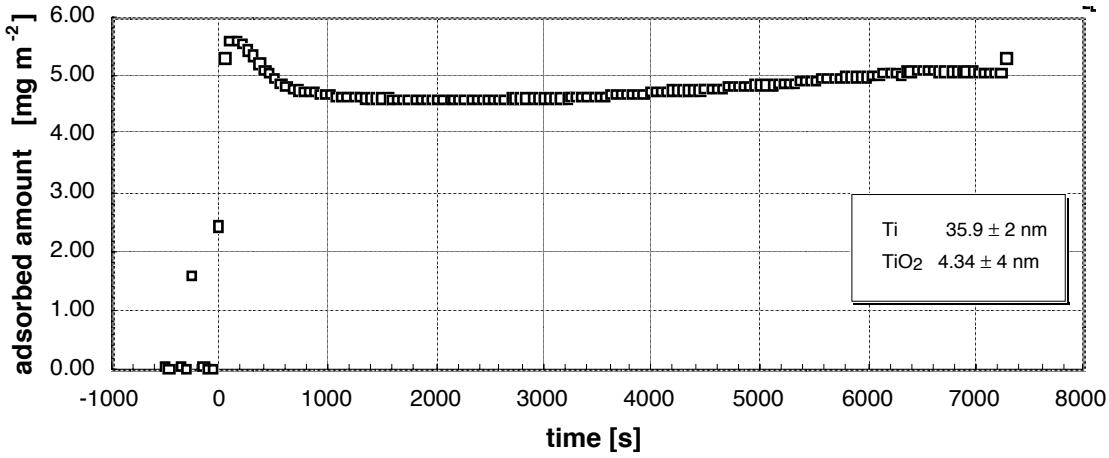

Figure 4.11: Adsorption during laminar flow of fibrinogen 400 mg ℓ^{-1} on titanium oxide.

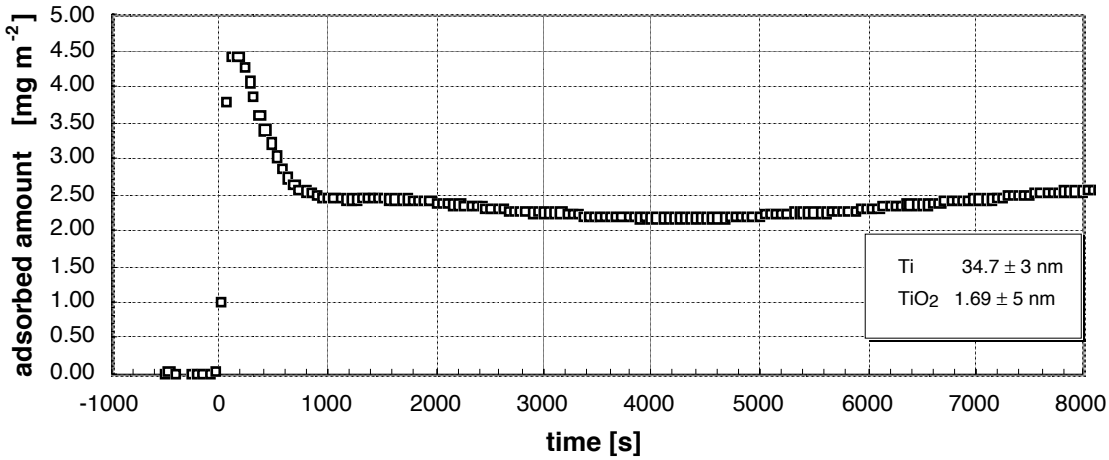

Figure 4.12: Adsorption during laminar flow of fibrinogen 1,000 mg ℓ^{-1} on titanium oxide.

In Figure 4.13 the adsorption of 100 mg ℓ^{-1} in citrate buffer of ionic strength 185 mM for more then 24 hours is show.

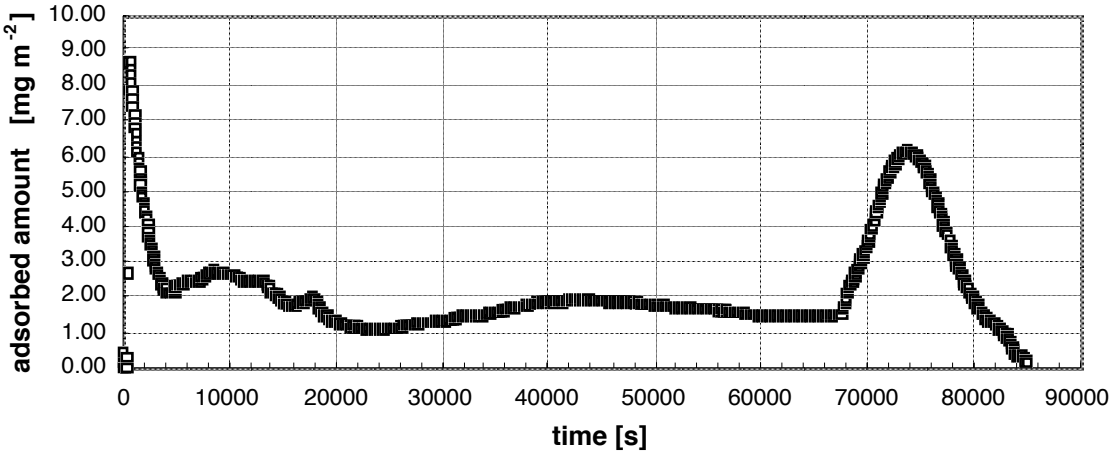

Figure 4.13: Adsorption during laminar flow of fibrinogen 100 mg ℓ^{-1} on titanium oxide.

4.4 Discussion

4.4.1 Static Measurements

The static measurements of fibrinogen on titanium dioxide at bulk concentrations of 50 and 100 mg ℓ^{-1} (Figures 4.4 and 4.5) show a monotonic increase in absorbed amount versus time. For both concentrations the absorbed amount is still increasing, even after 70,000 seconds in the case of a bulk concentration of 100 mg ℓ^{-1}. The high adsorbed amounts here are a result of the fact that the pH is at the iso-electric point of both fibrinogen and titanium dioxide.

The static measurements of fibrinogen on titanium at a higher bulk concentration of 400 mg ℓ^{-1} (Figure 4.6) and 1,000 mg ℓ^{-1} (Figure 4.7) in citrate buffer of ionic strength 185 mM, show a monotonic increase of the absorbed amount. Several authors have reported one of these values as plateau values, but it could be that these apparent plateau values are a function of the experimental adsorption time. Malmsten (Malmsten 1995) found plateau values of 2.5 and 4.5 mg m^{-2} in experiments lasting 8,000 seconds on silica and methylated silica from stirred PBS buffer.

In an other study Malmsten (Malmsten 1994) obtained adsorption isotherms from both individual measurements at a single bulk concentration and at successively increasing the concentration in the course of one experiment, which were similar. However, these experiments were carried out for less then 10,000 seconds. In Figure 4.8 an experiment is shown were the bulk concentration is increased during one experiment. The initial concentration of 100 mg ℓ^{-1} was increased to 182 and 250 mg ℓ^{-1} at the arrows in 8,000 second intervals.

4.4.2 Laminar Flow Experiments

The laminar flow experiments show a completely different picture compared to the static experiments. In all measurements the adsorbed amount increases rapidly and then decreases again. This kind of overshoot adsorption has been found before by a number of authors. Young *et al.* (Young, Pitt, *et al.* 1988) studied the adsorption of fibrinogen from PBS buffer onto polyvinyl chloride tubes with radiolabelling for 500 minutes. The concentration range they used was 5-4,600 mg ℓ^{-1}. Concentrations above 370 mg ℓ^{-1} showed overshoot adsorption. The maximum adsorbed concentration was 14 mg m^{-2}. Soderquist *et al.* (Soderquist and Walton 1980) studied the adsorption of fibrinogen from PBS buffer onto glass spheres coated with polymer in a column by UV adsorption at a wavelength of 280 nm. They found a pseudo plateau or kink in the adsorption isotherm at approximately 2 mg m^{-2}. Wahlgren (Wahlgren 1992) studied the adsorption of 400 mg ℓ^{-1} at methylated silica for 2,000 seconds with a maximum adsorbed concentration of approximately 7 mg m^{-2}.

4.5 Conclusions

In order to investigate the kinetics of adsorption of fibrinogen a parallel plate flow cell has been constructed and measurements under defined flow have been carried out using ellipsometry in total internal reflection mode. Also measurements in static solutions in a cuvette have been conducted. The surface material that has been used is titanium covered with a thin layer of native titanium dioxide. Experiments were carried out under laminar flow conditions with a Reynolds number of around 1000. The bulk concentrations of the model protein, fibrinogen, that have been used are 50, 100, 400 and 1,000 mg ℓ^{-1}. The time during which the experiments have been carried out was longer (up to 30 hours) than in most studies reported in the literature in which the adsorption times are usually less then 1 hour.

In many studies phosphate buffer saline (PBS) has been used. However, in this study PBS buffer gave problems. First, the prepared protein solutions in PBS were not always perfectly clear and sometimes showed the characteristic blue Tyndall light resulting from light scattering of particles in the hundred nanometer range. Second, UV adsorption at 280 nm measurements at a range of concentrations showed a strong non-linear curve of the absorption versus concentration. Finally, AFM studies using PBS buffered protein solution showed large protein aggregates when using PBS buffer. Therefore, the experiments in this study were carried out using a sodium citrate HCl buffer that gave no problems.

The experiments under laminar flow are very different from the static experiments in that all laminar flow experiments show overshoots in the adsorbed amount. The maximum and the 'plateau' values obtained do not directly correlate with the bulk concentration. However, the adsorbed amount was never higher than the amount calculated assuming a monolayer of end-on adsorbed fibrinogen and never lower than an side-on adsorbed monolayer. The overshoots are believed to result from the transition end-on to side-on.

The experimental results under laminar flow at a bulk concentration of 100 mg ℓ^{-1} carried out over 24 hours, show that over such long times the adsorbed amount determined by ellipsometry varies slowly between 0 and 2 mg m^{-2} until it rises sharply to 5-6 mg m^{-2} and then falls rapidly to 0 mg m^{-2}. This, however may be related to the special properties of fibrinogen.

Chapter 5

Modelling of Mass transfer and Kinetics of Protein Adsorption

Summary

In this study, the adsorption of the ellipsoidal protein fibrinogen onto titanium oxide has been studied in a parallel plate flow cell. Experiments under laminar flow at high shear rates have been used to minimise mass transport limitations. These experiments all show overshoot adsorption, which is modelled using a two-state kinetic model that allows for end-on side-on transition during adsorption. The values of the three kinetic parameters in the two-state kinetic model have been estimated for experiments using bulk concentrations of 50, 100, 400 and 1,000 mg ℓ^{-1} at a constant Reynolds number of 1,000. The value of k_a from Chapter 3 was used as starting value in the non-linear fit.

In the work described in the literature often mass transport plays an important role, and in many cases mass transport determines the rate of protein adsorption completely. In such cases it is impossible to find the underlaying end-on side-on transition kinetics even if mass transport limitation is taking into account correctly. This is caused by the fact that the transition from the end-on to the side-on state is fast.

To check that mass transport limitations were completely absent the complete non-stationary two-dimensional convection diffusion equation with the two-state kinetic model as boundary condition was solved numerically for a number of shear rates (Reynolds numbers) and compared to two-dimensional non-stationary mass transport limited solution and the kinetically limited solution.

With the kinetic two-state model the evolution of the adsorbed amount upto approximately 1,000 seconds can be modelled. However, the adsorption after approximately 1,000 seconds cannot be explained by the two-state model. The changes in the adsorbed amount beyond this stage are believed to be caused by the formation of aggregates of protein, crystallisation within the protein layer, or by multi-layer adsorption.

5.1 Introduction

In this chapter a model will be presented to explain the observed overshoot adsorption kinetics following a concentration step, as shown in Chapter 4. In protein adsorption studies reported in the literature (initial) adsorption has often been transport limited. The rate of protein adsorption is proportional to the amount of free surface. Because the free surface fills up the rate of protein adsorption will always become kinetically limited at longer times. It will be shown that the bulk concentration of protein and the flow conditions in the parallel plate flow cell in the experiments, are such that the kinetics are limiting throughout the entire experiment and hence the protein concentration available for adsorption does not change in time and is equal to the concentration at the inlet, allowing the immediate determination of the adsorption kinetics.

The adsorption kinetics are modelled using the concepts from reaction engineering, as in earlier studies reported in the literature. In these studies mass transfer in a parallel plate flow cell has been modelled with irreversible first order reaction kinetics at the wall (Dejardin, Le, *et al.* 1994; Dickinson and Cooper 1995; Lok, Cheng, *et al.* 1983a; Lok, Cheng, *et al.* 1983b). Other studies have modelled mass transfer with reversible first order kinetics (Cha and Beissinger 1996a; Cha and Beissinger 1996b; Shibata and Lenhoff 1992a; Shibata and Lenhoff 1992b). Therefore, the goal has been the extension of these models to include the non-linear kinetic phenomena encountered during the experiments in Chapter 4 in a general mass transfer and kinetic model and to determine the effect of mass transfer on the modelled kinetics.

5.2 Mathematical Formulation of Protein Adsorption in a Parallel Plate Channel

In order to model the adsorption of protein both the change in protein concentration in the bulk and on the surface, as a function of place and time have to be calculated. The three equations that are needed are:

1. a momentum balance that describes the hydrodynamics and describes the flow field in the parallel plate flow cell

2. a mass balance that describes the transport of protein molecules by convection and diffusion in the bulk as a function of place between the plates as a function of time

3. a kinetic equation for the heterogeneous pseudo chemical (surface) reaction between bulk molecules and the surface this equation forms the boundary condition of the mass balance at the wall.

In the next sections these three equation will be discussed.

5.3 Stationary Laminar Flow between Parallel Plates

In the parallel plates geometry the momentum balance that enables the calculation of the velocity profile can easily be found if the relation between shear forces and the velocity gradient is known (Beek and Muttzall 1975). For laminar flow of a non-compressible Newtonian fluid:

$$\tau_x = -\eta \frac{\mathrm{d}v_x}{\mathrm{d}y} \tag{5.1}$$

With τ_x the shear force, η the viscosity and v_x the velocity in the x-direction.

In order to determine the velocity profile it is assumed that the flow in the cell (that has a much larger width then height) can be approximated by the flow between two parallel plates of infinite width. If it is further assumed that the flow is fully developed and laminar, then the velocity profile is essentially two-dimensional and can be written as , see Figure 5.1, the analytical solution of the momentum balance in this system is as follows:

$$v_x = \frac{3}{2}\bar{v}\left[1 - \left(\frac{y}{a}\right)^2\right] \tag{5.2}$$

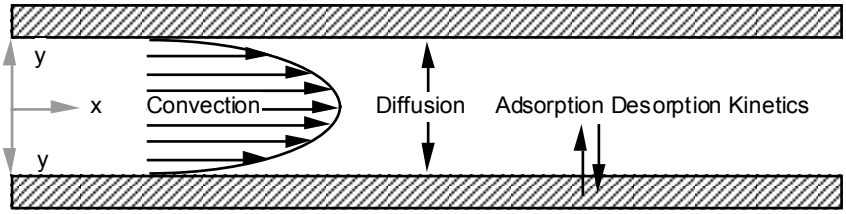

Figure 5.1: Schematic overview of the coordinate system used for the parallel plate flow. Only half of the flow is modelled. The x and y coordinate refer to the place variables.

with $\bar{v}$ the average velocity between the plates. Or by using, the shear rate $\dot{\gamma}$, defined as:

$$\dot{\gamma} \equiv \frac{\mathrm{d}v_x(y=a)}{\mathrm{d}y} = \frac{3\bar{v}}{a} \tag{5.3}$$

with $\bar{v}$ the average velocity and a the half height of the parallel plate flow channel:

$$v_x = \frac{\dot{\gamma}a}{2}\left[1 - \left(\frac{y}{a}\right)^2\right] \tag{5.4}$$

5.4 Mass Transport

To investigate the effect of mass transfer on the total rate of protein adsorption, the change in bulk concentration as a function of place and time should be calculated by using a mass balance.

Transport of protein to and from the surface is caused by fluid flow and by diffusion. The non-stationary mass balance for the bulk concentration, also called the convection (advection) diffusion equation, or transport equation, describes the mass balance of protein in the channel.

$$\frac{\partial c}{\partial t} = -v_x\frac{\partial c}{\partial x} - v_y\frac{\partial c}{\partial y} - v_z\frac{\partial c}{\partial z} + \mathbb{D}_x\frac{\partial^2 c}{\partial x^2} + \mathbb{D}_y\frac{\partial^2 c}{\partial y^2} + \mathbb{D}_z\frac{\partial^2 c}{\partial z^2} \tag{5.5}$$

Using the same assumptions under which Equation 5.2 was derived, three terms in Equation 5.5 can be dropped. $v_y = 0$ because during fully developed laminar flow there is no convection in the y-direction. Furthermore because there are no concentration gradients in the z-direction, the convection and diffusion terms in the z-direction (perpendicular to the xy-plane in Figure 5.1) are zero and Equation 5.5 reduces to a two dimensional convection diffusion equation. In this equation the diffusion term in the x-direction $\mathbb{D}_x\frac{\partial^2 c}{\partial x^2}$ has been neglected because it is small compared to the convective term in the x-direction (Pe $> 10^7$)*:

$$\frac{\partial c}{\partial t} = -v_x\frac{\partial c}{\partial x} + \mathbb{D}_y\frac{\partial^2 c}{\partial y^2} \tag{5.6}$$

Since Equation (5.6) is first order in t and x and second order in y, one initial condition and three boundary conditions are needed in order to solve this partial differential equation (PDE). The initial state of the system at $t = 0$, in the case of adsorption is:

$$c(x, y, t = 0) = 0 \tag{5.7}$$

*However, in numerically solving the equation this term is retained, see Appendix D.

The conditions chosen at the physical boundary's are as follows:

$$c\left(x=0,y,t\right) = c_0 \tag{5.8}$$

$$-\mathbb{D}\frac{\partial c\left(x,y=0,t\right)}{\partial y} = 0 \tag{5.9}$$

$$-\mathbb{D}\frac{\partial c\left(x,y=a,t\right)}{\partial y} = \frac{\partial \Gamma(x,t)}{\partial t} \tag{5.10}$$

The mass balance and the adsorption kinetics are coupled in boundary condition Equation 5.10.

5.5 Kinetics

To be able to model the adsorption kinetics, an expression for the change in surface concentration in time has to be used. However, much uncertainty about the exact form of such a kinetic equation exists. In the literature the most widely used model is that of Langmuir (Langmuir 1918).

$$\frac{\mathrm{d}\Gamma}{\mathrm{d}t} = k_{\mathrm{a1}}c_w\left(\Gamma_{\max}-\Gamma\right) - k_{\mathrm{d1}}\Gamma \tag{5.11}$$

With Γ the surface concentration. k_{a1} the rate constant of adsorption, c_w the bulk concentration at $y=a$, i.e., $c_w = c(x,y=a,t)$, $\Gamma_{\max}$ the maximal surface concentration and k_{d1} the rate constant of desorption.

The Langmuir model has the necessary phenomenology, in that both adsorption and desorption rate constants and a decreasing free area necessary to explain the kinetics of protein adsorption are present. It is therefore that the Langmuir model is often used as a starting point.

The results for fibrinogen adsorption onto titanium under laminar flow from Chapter 4 have shown overshoots in the adsorbed concentration that cannot be explained by the Langmuir model. Fibrinogen is a protein that is not spherical but has a more ellipsoidal form, see also Chapter 1 Table 1.1. Therefore, it is possible that fibrinogen molecules can be adsorbed in different orientations with respect to the surface.

Experimental studies reported in the literature have shown that adsorbed fibrinogen probably exists in two different populations on the surface, as determined by the difference in elutability between these populations (Retzinger, Cook, *et al.* 1994). Models that have been proposed for fibrinogen adsorption use two possible orientations at the surface, end-on and side-on (Schaaf and Dejardin 1988). Other authors have proposed a models in which the fibrinogen molecule changes its orientation with respect to the surface from end-on to side-on (Beissinger and Leonard 1982).

An extension of the Langmuir model to a general model that includes the possibility of two populations of molecules with different orientations with respect to the surface and hence a different occupied area per molecule and also the possibility of transformation from one state to another is the following system of equations:

$$\frac{\partial \Gamma_1}{\partial t} = \left(k_{\mathrm{a1}}c_w - k_{\mathrm{t12}}\Gamma_1 + k_{\mathrm{t21}}\Gamma_2\right)\left(\Gamma_{max}-\Gamma_1-\alpha\Gamma_2\right) - k_{\mathrm{d1}}\Gamma_1 \tag{5.12}$$

$$\frac{\partial \Gamma_2}{\partial t} = \left(k_{\mathrm{a2}}c_w - k_{\mathrm{t12}}\Gamma_1 - k_{\mathrm{t21}}\Gamma_2\right)\left(\Gamma_{max}-\Gamma_1-\alpha\Gamma_2\right) - k_{\mathrm{d2}}\Gamma_2 \tag{5.13}$$

$$\Gamma = \Gamma_1 + \Gamma_2 \tag{5.14}$$

In this general model state 1 is associated with end-on adsorption and state 2 with side-on adsorption and hence Γ_1 represents the adsorbed concentration of the fibrinogen molecules in state 1 and Γ_2 in

state 2. α is the ratio of the occupied area between state 2 and state 1. Γ_{max} is the maximum adsorbed concentration in state 1. c_w is the bulk concentration at the wall and $k_{\mathrm{a}1}, k_{\mathrm{a}2}, k_{\mathrm{d}1}, k_{\mathrm{d}2}, k_{\mathrm{t}12}$ and $k_{\mathrm{t}21}$ the rate constants of adsorption, desorption and transformation for the two states respectively.

By fitting the model to kinetically limited measurements, i.e., $c_w = c_0$, the six parameters in the system of Equations 5.12-5.14 may al be determined. Initial fits of this general model to experimental data showed that the effect of including the adsorption constant for end-on molecules $k_{\mathrm{a}2}$, the desorption constant of side-on molecules $k_{\mathrm{d}2}$ and the transformation constant from side-on to end-on $k_{\mathrm{t}21}$ did not have a significant effect on the goodness of fit and were very small. Therefore, we have adopted the above model in a way also used by Beissinger *et al.* (Beissinger and Leonard 1982) and Kulik *et al.* (Kulik and Sevast'yanov 1991).

$$\frac{\partial \Gamma_1}{\partial t} = (k_{\mathrm{a}1} c_w - k_{\mathrm{t}12}\Gamma_1)(\Gamma_{max} - \Gamma_1 - \alpha\Gamma_2) - k_{\mathrm{d}1}\Gamma_1 \tag{5.15}$$

$$\frac{\partial \Gamma_2}{\partial t} = k_{\mathrm{t}12}\Gamma_1 (\Gamma_{max} - \Gamma_1 - \alpha\Gamma_2) \tag{5.16}$$

$$\Gamma = \Gamma_1 + \Gamma_2 \tag{5.17}$$

In this model molecules are reversibly bound to the surface in state 1 in which they occupy little area per molecule and will transform into an irreversible bound state 2 that occupies more area per molecule.

Γ_{max} (the maximum monolayer amount in state 1) and α can then be found from the molecular dimensions to be 16 mg m^{-2} and 7.5 respectively assuming monolayer coverage.

For the initial adsorption kinetics Γ_1 and Γ_2 are zero and all models discussed reduce to:

$$\frac{\mathrm{d}\Gamma_1}{\mathrm{d}t} = k_{\mathrm{a}1} c_w \Gamma_{max} \tag{5.18}$$

Hence, the value of $k_{\mathrm{a}1}$ can be determined by using the value of k_{a} from Chapter 3 assuming first order irreversible kinetics, after dividing by Γ_{max}. This gives a value of $4.8 \cdot 10^{-8}$ m^3 mg^{-1} s^{-1}. This value was used as start value in the non-linear fit in Figures 5.10-5.13.

The kinetic scheme is shown in Figure 5.2

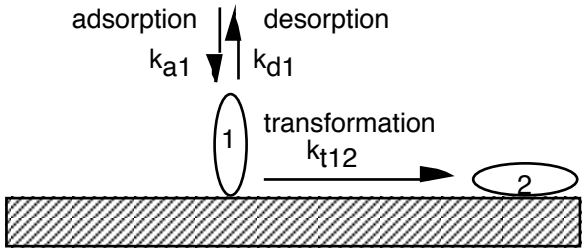

Figure 5.2: Schematic illustration of the proposed adsorption kinetics. In the end-on orientation desorption is possible, after transformation from end-on to side-on orientation no desorption is possible.

5.5.1 Mass transport and Kinetics

As discussed in the last two sections, the modelling protein adsorption from laminar flow involves solving the transport equation 5.6 and the kinetic Equations 5.15-5.17 that are coupled in boundary condition Equation 5.10. No analytical solutions exist for this general case and therefore numerical

solutions have to be obtained. The numerical technique and mathematical verification can be found in Appendix D.

For the general model two limiting cases can be identified. Firstly, when mass transport is limiting a kinetic equation is not necessary and boundary condition Equation 5.10 becomes:

$$c(x, y = a, t) = 0 \tag{5.19}$$

Secondly, when mass transport limitation is completely absent. Equation 5.6 reduces to:

$$c(x, y, t) = c_0 \tag{5.20}$$

In Figure 5.3 calculations are shown to illustrate the evolution of the total adsorbed amount in time assuming no mass transport limitation.

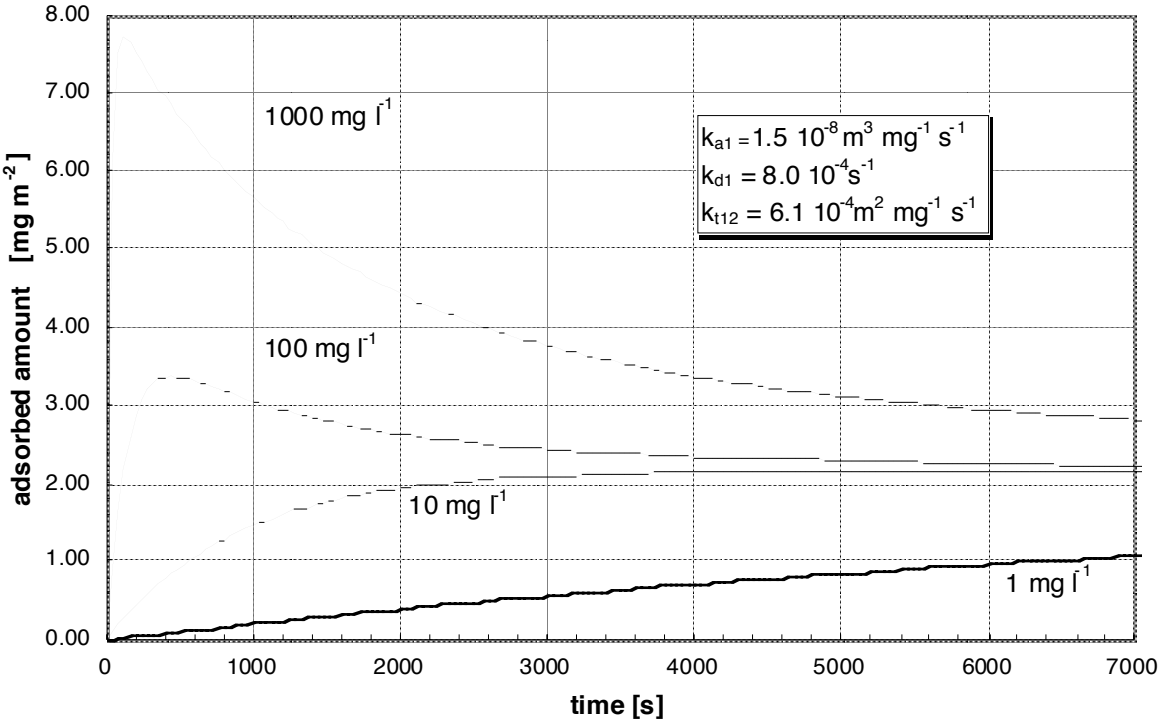

Figure 5.3: The adsorbed amount versus time from calculations using the end-on side-on transition model (Equations 5.15-5.17) to model protein adsorption kinetics. The calculations are for the kinetically limited situation with bulk concentrations $c_w = c_0$ of 1, 10, 100 and 1,000 mg ℓ^{-1} using the constants given in the graph and $\alpha = 7.5$ and $\Gamma_{max} = 16$ mg m^{-2}.

5.6 Approximations Assuming Complete Mass Transport Limitation

5.6.1 Introduction

In the next sections, analytical solutions are presented assuming complete mass transport limitation. These analytical solutions can be found by neglecting one or more terms in 5.6. The first two sections treat the problem of forced convection as occurring in the parallel plate flow cell. In the following sections diffusion models in absence of convection that can be used for static and stirred cuvettes are discussed. All mass transport models presented are often used to model initial adsorption rates.

Equation 5.6 with boundary conditions Equations 5.8-5.10 has to be solved numerically.

In the literature in order to be able to derive analytical solutions to the problem an often used approach is to solve the mass transport equation 5.6 with the following boundary condition:

$$c\left(x, y = a, t\right) = 0 \tag{5.21}$$

replacing Equation 5.10 and then to calculate the adsorbed concentration using:

$$\frac{\mathrm{d}\Gamma(x,t)}{\mathrm{d}t} = -\mathbb{D}\frac{\partial c\left(x, y = a, t\right)}{\partial y} \tag{5.22}$$

This transport limited model has been used in the literature to provide a number of analytical solutions to the problem of protein adsorption.

5.6.2 Non-Stationary Forced Convection During Laminar Flow

In this model all terms in Equation 5.6 are retained. The PDE that results is:

$$\frac{\partial c}{\partial t} = -v_x\frac{\partial c}{\partial x} + \mathbb{D}_y\frac{\partial^2 c}{\partial y^2} \tag{5.23}$$

The following boundary conditions are used:

$$c(x = 0, y, t) = c_0 \tag{5.24}$$

$$-\mathbb{D}\frac{\partial c\left(x, y = 0, t\right)}{\partial y} = 0 \tag{5.25}$$

$$c(x, y = a, t) = 0 \tag{5.26}$$

and Equation 5.4 for the velocity profile. This PDE is therefore equal to the original mass balance 5.6 only the boundary condition Equation 5.10 at the wall being replaced by Equation 5.26. It has to be solved numerically.

5.6.3 Stationary Forced Convection During Laminar Flow: Graetz Solution

In this stationary model the mass balance 5.6 reduces to:

$$0 = -v_x\frac{\partial c}{\partial x} + \mathbb{D}_y\frac{\partial^2 c}{\partial y^2} \tag{5.27}$$

With Equation 5.4 for the velocity profile and boundary conditions:

$$c(x=0,y) = c_0 \tag{5.28}$$
$$c(x,y=0) = c_0 \tag{5.29}$$
$$c(x,y=a) = 0 \tag{5.30}$$

an analytical approximation in the form a series expansion is available, which reduces asymptotically to a simpler form for high flow rates or small values of x (Bird, Stewart, *et al.* 1960; Jakob 1949):

$$\frac{\partial\Gamma(x)}{\partial t} = -\mathbb{D}\frac{\partial c\,(x,y=a)}{\partial y} = \frac{1}{9^{1/3}\int\limits_{r=0}^{r=\infty}\mathrm{e}^{-r}\;r^{\frac{4}{3}-1}\mathrm{d}r}\left(\frac{\dot\gamma}{\mathbb{D}x}\right)^{1/3}\mathbb{D}c_0 = 0.538\left(\frac{\dot\gamma}{\mathbb{D}x}\right)^{1/3}\mathbb{D}c_0 \tag{5.31}$$

after integration:

$$\Gamma(x,t) = 0.538\left(\frac{\dot\gamma}{\mathbb{D}x}\right)^{1/3}\mathbb{D}c_0 t \quad \text{for}\frac{\mathbb{D}x}{\bar v(2a)^2} = \frac{\mathbb{D}x3}{\dot\gamma 4a^3} < 0.05 \tag{5.32}$$

With $\int\limits_{r=0}^{r=\infty}\mathrm{e}^{-r}\;r^{p-1}\mathrm{d}s$ the complete gamma function that has p as parameter, and x the distance from the point where the adsorption starts, i.e., in this case the entrance of the parallel plate channel. The group $\frac{\mathbb{D}x}{\bar v(2a)^2}$ is the Graetz number. Equation 5.31 is referred to as the Lévêque equation. Hence, the rate of adsorption is dependent on the diffusion coefficient, the shear rate, the solution concentration, and the distance from the entrance of the flow channel.

In many reports described in the literature, the asymptotic solution of the Graetz problem for high flow rates or small$x$, i.e., the Lévêque solution has been used to model the total rate of adsorption of protein. In Figure 5.4 this Lévêque solution is compared to the numerical solution of the non-stationary mass transport limited model. Four different shear rates and a fixed bulk concentration of 100 mg ℓ^{-1} were used. For each shear rate the dashed line corresponds to the stationary solution, the lower concave solid line to the non-stationary solution. From Figure 5.4 it becomes clear that the difference in adsorbed amount calculated using the Lévêque solution and the non-stationary mass transport limited solution diminish as the shear rate increases.

When the non-stationary mass transport limited solution is compared to the complete non-stationary model including adsorption kinetics in Figure 5.5, conclusions can be drawn about the adsorption of fibrinogen onto titanium dioxide under flow. Even at the lowest shear rate shown, the overall kinetics cannot be described by the non stationary mass transport limited model. This means that c_w is not equal to zero, as assumed in the derivation of both the stationary and non-stationary solutions in Figure 5.4. Hence, at shear rates higher than 100 s^{-1} the adsorption rate is not determined by mass transport limitation but by adsorption kinetics only. Furthermore, at low shear rates the adsorbed amount changes almost monotonically and the overshoot from the curves at high shear rate the adsorbed amount shows overshoot adsorption.

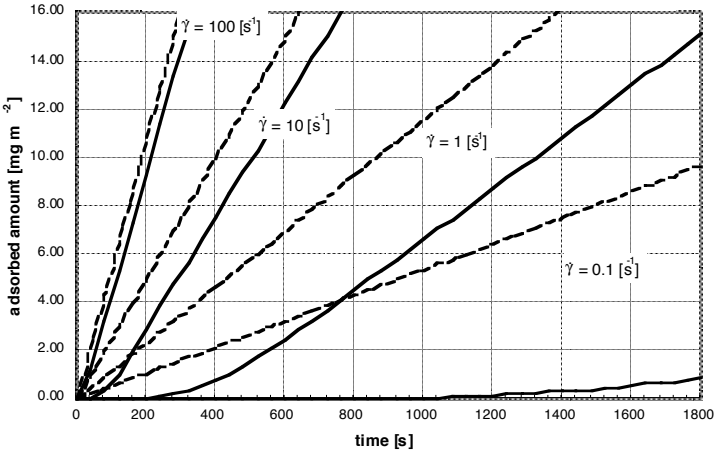

Figure 5.4: Graph of the stationary solution Equation 5.32 (dashed lines) and the non-stationary solution (solid lines) for a bulk concentration of 100 mg ℓ^{-1} for four shear rates 0.1 s^{-1} (Re = 0.0313), 1 s^{-1} (Re = 0.313), 10 s^{-1} (Re = 3.13) and 100 s^{-1} (Re = 31.3).

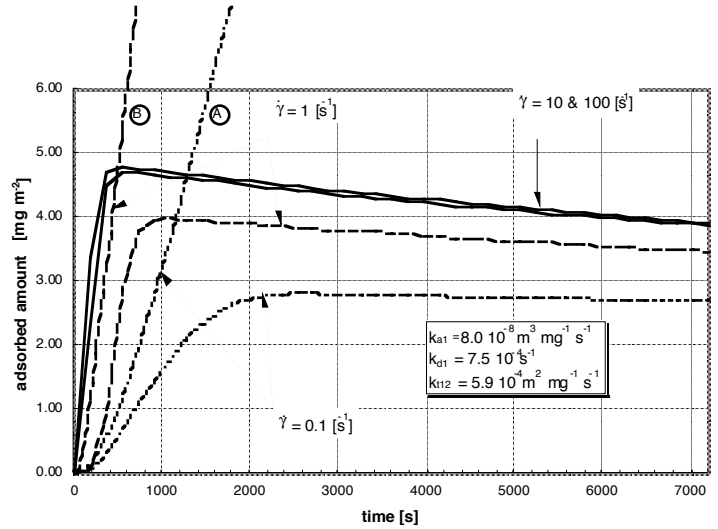

Figure 5.5: Calculated adsorbed amount as a function of time showing the influence of shear rate on the adsorption of protein during flow for a bulk concentration of 50 mg ℓ^{-1}. The different curves are for shear rates of 0.1 s^{-1} (dotted line), 1 s^{-1} (dashed line), 10 s^{-1} (solid line) and 100 (solid line) s^{-1} using the complete model Equation 5.6 with boundary conditions 5.8-5.10 and Equations 5.15-5.17. The values for the kinetic model that where used are shown in the graph. The value of the two other parameters Γ_{max} and α that were used are 16 mg m^{-2} and 7.5 respectively. Also the rate of adsorption as calculated by the non stationary mass transport limited solution has been plotted for shear rates of 0.1 s^{-1} (dotted line labelled Ⓐ) and 1 s^{-1} (dashed line labelled Ⓑ).

5.6.4 Non-stationary Diffusion: Penetration Model

if the convective term in the x-direction is dropped but the transient term is taken into account, the mass balance Equation 5.6 becomes:

$$\frac{\partial c}{\partial t} = \mathbb{D}_{\mathrm{y}} \frac{\partial^2 c}{\partial y^2} \tag{5.33}$$

The initial condition is:

$$c(y, t = 0) = c_0 \tag{5.34}$$

The boundary conditions are

$$c(y = a, t) = 0 \tag{5.35}$$
$$c(y = 0, t) = c_0 \tag{5.36}$$

The analytical solution of this PDE is the so-called penetration model, see for example (Beek and Muttzall 1975).

$$\frac{\mathrm{d}\Gamma(t)}{\mathrm{d}t} = -\mathbb{D} \frac{\partial c\,(y = a, t)}{\partial y} = \sqrt{\frac{\mathbb{D}}{\pi t}} c_0 \tag{5.37}$$

or

$$\Gamma(t) = 2\sqrt{\frac{\mathbb{D}}{\pi}} c_0 \sqrt{t} \tag{5.38}$$

if $\Gamma(t = 0) = 0$. In this case the surface concentration Γ varies with the square root of time. The rate determined by the bulk concentration, the diffusion constant and time.

5.6.5 Stationary Diffusion: Stagnant Film Model

If both the convection term in the x-direction and the transient term are neglected Equation 5.6 becomes one-dimensional and reduces to an equation for stationary diffusion:

$$0 = \mathbb{D}_{\mathrm{y}} \frac{\mathrm{d}^2 c}{\mathrm{d}y^2} \tag{5.39}$$

With boundary conditions

$$c(y = a) = 0 \tag{5.40}$$
$$c(y = a - \delta) = c_0 \tag{5.41}$$

The analytical solution of this ordinary differential equation (ODE) is called the stagnant film model.

$$\mathbb{D} \frac{\mathrm{d}c}{\mathrm{d}y} = \text{constant} = -\frac{\mathbb{D}}{\delta} c_0 \tag{5.42}$$

Substituting Equation 5.44 in Equation 5.22 gives:

$$-\mathbb{D} \frac{\partial c\,(y = a, t)}{\partial y} = \frac{\mathrm{d}\Gamma}{\mathrm{d}t} = \frac{\mathbb{D}}{\delta} c_0 \tag{5.43}$$

Hence, it follows that:

$$\Gamma = \frac{\mathbb{D}}{\delta} c_0 t \tag{5.44}$$

if $\Gamma(t = 0) = 0$. So in this case the surface concentration Γ varies linearly with time, with a rate determined by the concentration, the diffusion constant and the thickness of the diffusion boundary layer δ.

5.7 Results

5.7.1 Static Measurements

The penetration model for mass transport limited adsorption together with the static measurements from Chapter 4 can be used to determine whether mass transfer or kinetics is limiting the adsorption of fibrinogen on titanium oxide. To this end calculations using the penetration model Equation 5.38 have been plotted together with the measurements in Figures 5.6-5.9.

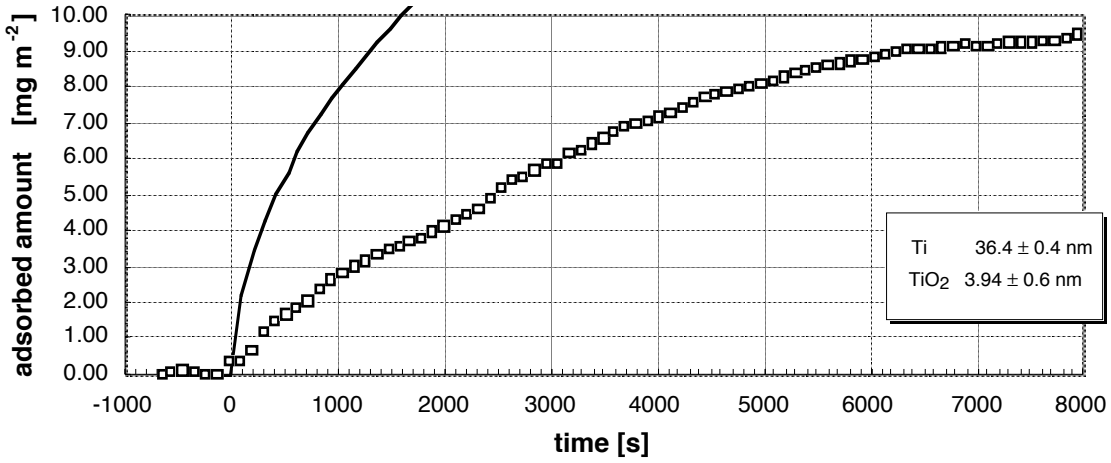

Figure 5.6: Static adsorption of fibrinogen 50 mg ℓ^{-1} on titanium oxide. Penetration model 5.38 (–) using a diffusion coefficient of 2.0 $\cdot 10^{-11}$ m^2 s^{-1}, measurements (□) from Figure 4.4.

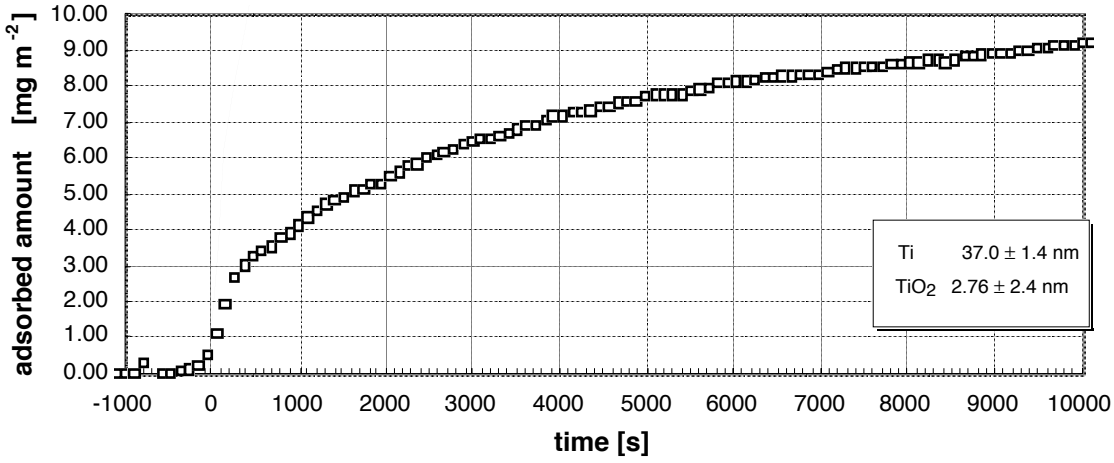

Figure 5.7: Static adsorption of fibrinogen 100 mg ℓ^{-1} on titanium oxide. Penetration model 5.38 (–), measurements (□) from Figure 4.5.

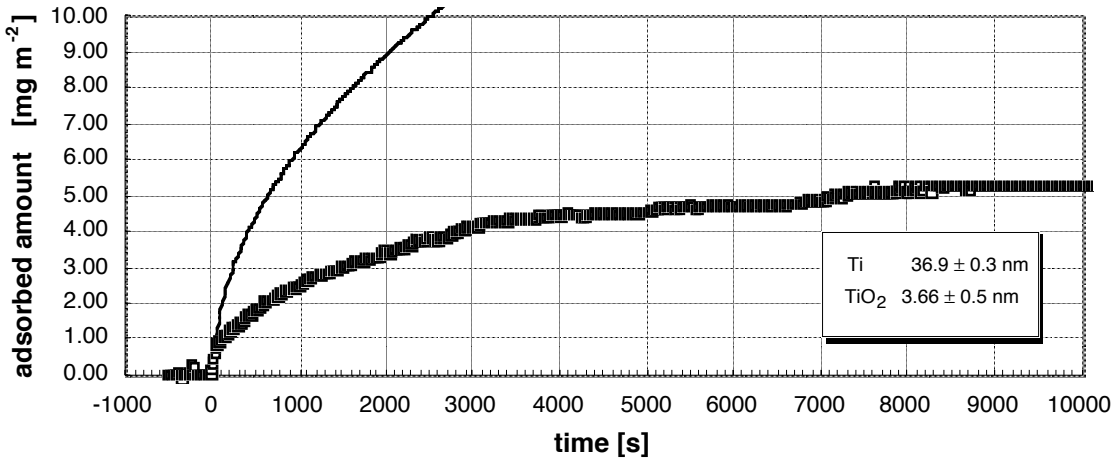

Figure 5.8: Static adsorption of fibrinogen 400 mg ℓ^{-1} on titanium oxide. Penetration model 5.38 (–), measurements (□) from Figure 4.6.

5.7.2 Laminar Flow Experiments

Assuming kinetic limited adsorption during the flow experiments the three rate constants $k_{\mathrm{a1}}, k_{\mathrm{d1}}$ and k_{t12} in the two-state kinetic model 5.15-5.17 were approximated by solving the the system of ODE's using a fourth order Runge Kutta and by fitting the rate constants using a non-linear least squares criterium on the experiments presented in Chapter 4. The two other parameters Γ_{max} and α were fixed at values of 16 mg m^{-2} and 7.5 respectively.

The results are given in Figures 5.10-5.13 and the parameters collected in Table 5.1.

To check whether or not the assumption of kinetic limitation was justified calculations using the complete model, i.e., Equation 5.6 with boundary conditions 5.8-5.10 and Equations 5.15-5.17 have

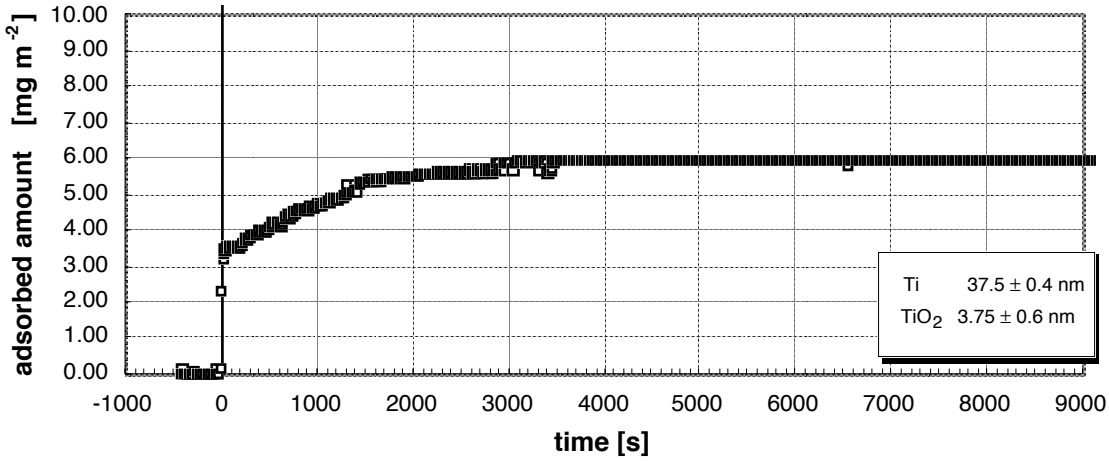

Figure 5.9: Static adsorption of fibrinogen 1000 mg ℓ^{-1} on titanium oxide. Penetration model 5.38 (–), measurements (□) from Figure 4.7.

been performed for different shear rates. The results are given in Figure 5.5.

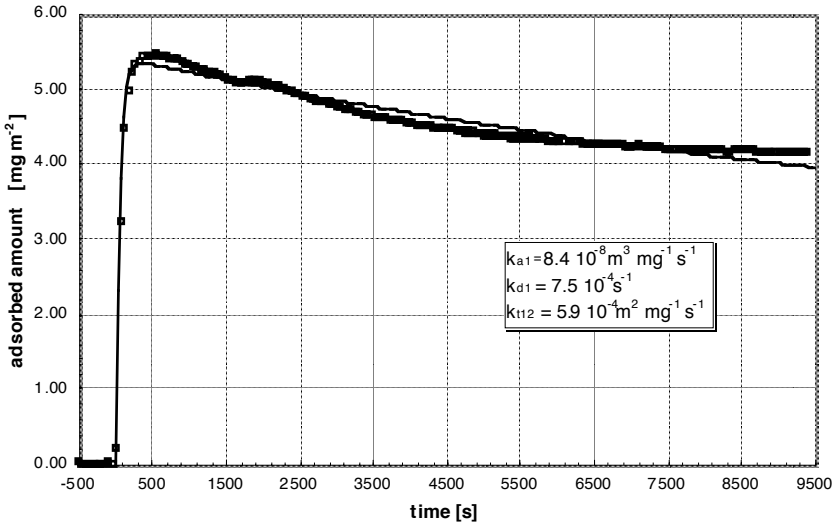

Figure 5.10: Non-linear parameter estimation using the two state model for the experimental adsorption of fibrinogen 50 mg ℓ^{-1} on titanium oxide during flow from Figure 4.9. fit (–), measurements (□).

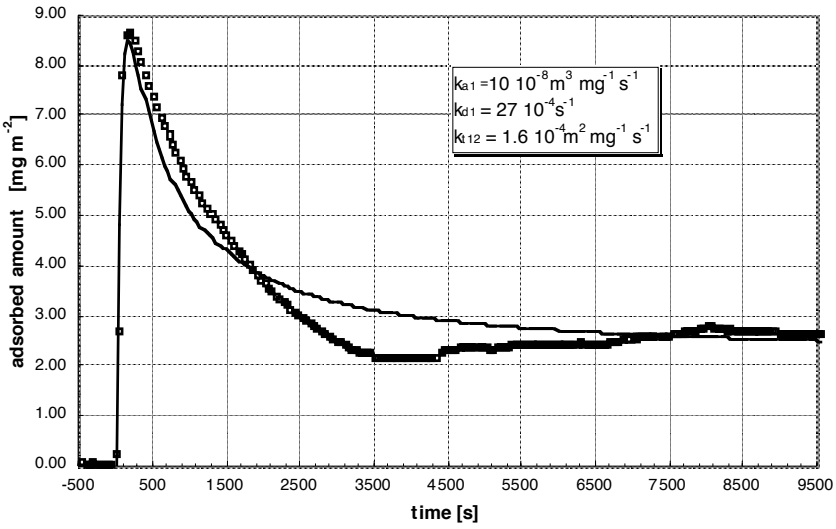

Figure 5.11: Non-linear parameter estimation using the two state model for the experimental adsorption of fibrinogen 100 mg ℓ^{-1} on titanium oxide during flow from Figure 4.10. fit (–), measurements (□).

5.8 Discussion

5.8.1 Static Measurements

Adsorption during static measurements is most likely to be completely mass transport limited for prolonged times. However, from Figures 5.6-5.9 it must be concluded that the rate of adsorption is less than calculated using the penetration model 5.38 using the literature value of $2.0{\cdot}10^{-11}$ m^2 s^{-1} for the diffusion coefficient of fibrinogen. At the higher concentrations in Figures 5.8-5.9 only the

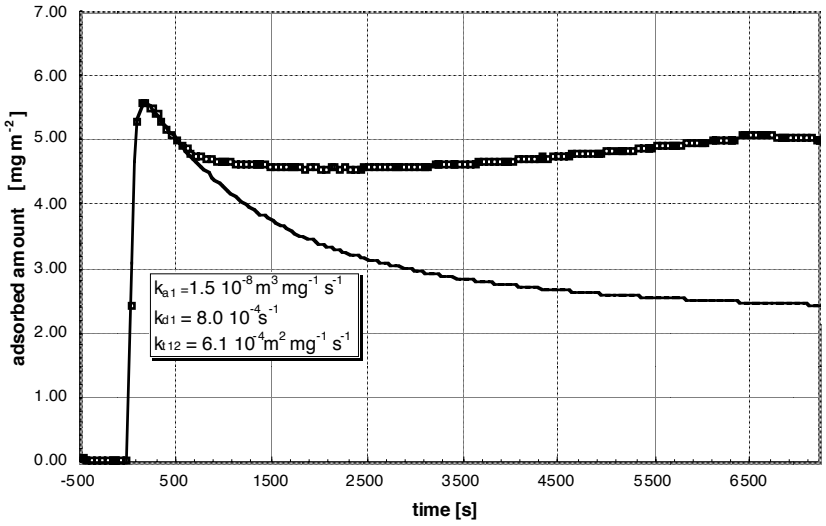

Figure 5.12: Non-linear parameter estimation using the two state model for the experimental adsorption of fibrinogen 400 mg ℓ^{-1} on titanium oxide during flow from Figure 4.11. fit (–), measurements (□).

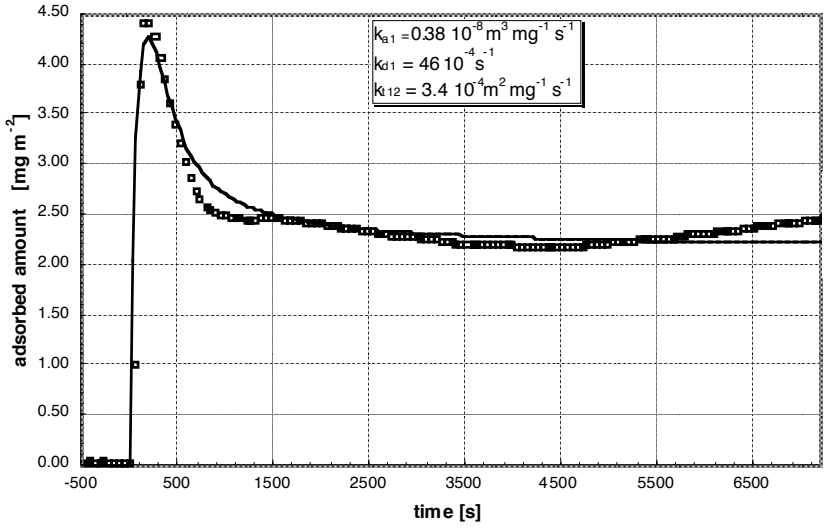

Figure 5.13: Non-linear parameter estimation using the two state model for the experimental adsorption of fibrinogen 1,000 mg ℓ^{-1} on titanium oxide during flow from Figure 4.12. fit (–), measurements (□).

Table 5.1: Overview of the fitted values of the parameters in the model 5.15-5.17 as shown in Figures 5.10-5.13. The start value in the non-linear fit for k_{a1} was 4.8 $\cdot 10^{-8}$ m^3 mg^{-1} s^{-1} (1.6$\cdot$10^4 ℓ mol^{-1} s^{-1}).

	50 [mg ℓ^{-1}]	100 [mg ℓ^{-1}]	400 [mg ℓ^{-1}]	1,000 [mg ℓ^{-1}]
k_{a1} [m^3 mg^{-1} s^{-1}]	8.4$\cdot$10^{-8}	10$\cdot$10^{-8}	1.5$\cdot$10^{-8}	0.38$\cdot$10^{-8}
k_{d1} [s^{-1}]	7.5$\cdot$10^{-4}	27$\cdot$10^{-4}	8.0$\cdot$10^{-4}	46$\cdot$10^{-4}
k_{t12} [m^2 mg^{-1} s^{-1}]	5.9$\cdot$10^{-4}	1.6$\cdot$10^{-4}	6.1$\cdot$10^{-4}	3.4$\cdot$10^{-4}

early stages can be described using the penetration theory. Hence, kinetic limitations are slowing down the rate of adsorption considerably even under static adsorption.

In studies reported in the literature the penetration model has also been used to model protein adsorption from a static, i.e., un stirred cuvette, see for example Van der Scheer (van der Scheer 1978). Van der Scheer used this model to describe the initial adsorption of fibrinogen onto polystyrene surfaces. The adsorption from a static solution of 32 mg ℓ^{-1} was followed and the penetration model was found applicable to about 900 seconds after adsorption if a diffusion coefficient of $0.8{\cdot}10^{-11}$ m^2 s^{-1} was assumed, i.e., much smaller than the actual value $2.0{\cdot}10^{-11}$ m^2 s^{-1}. This small diffusion coefficient could mean that kinetic limiation should be included.

The static measurements in this study show that even without convection, i.e., in case where one could expect complete mass transport limitation, kinetic limitations become apparent.

In Figure 5.14, Figure 4.6 is replotted against the square root of time minus the start time. Straight lines are giving that approximate slopes of linear parts of the adsorption curve.

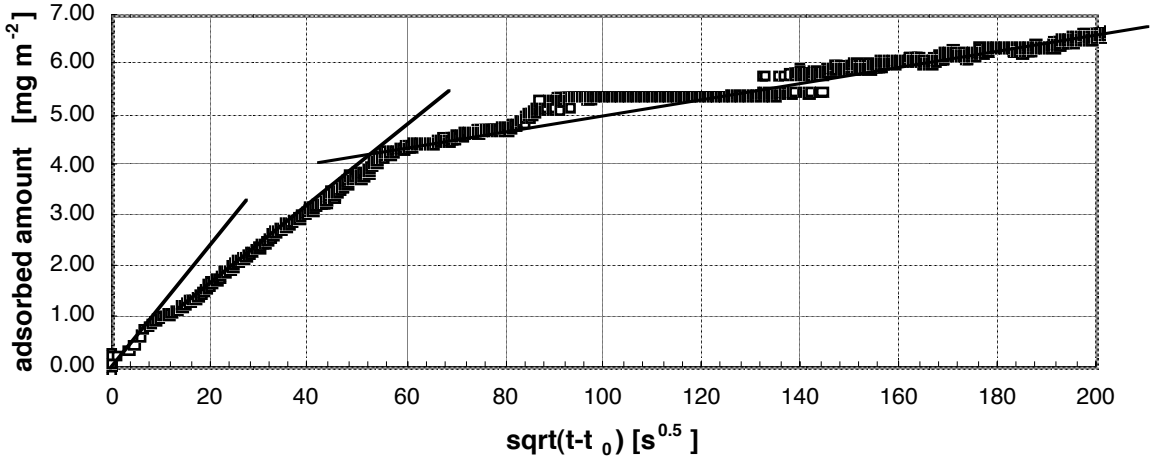

Figure 5.14: Static adsorption of fibrinogen 400 mg ℓ^{-1} on titanium oxide.

The same experiment is shown in Figure 5.15 but on a semi logarithmic scale that shows the differences even more pronounced. Experiments in the static cuvette can be mass transport limited upto several hundred seconds after the start of the experiment, depending on the bulk concentration chosen. Because the transition from end-on to side-on in the two state model is quite rapid, an overshoot in the adsorbed amount can be obscured in these mass transport limited experiments and the adsorption kinetics cannot be extracted, not even by taking into account the mass transport limitations correctly.

5.8.2 Laminar Flow Experiments

Protein adsorption in laminar flow experiments have often been modelled using the Lèvêque model 5.32 for stationary mass transport, e.g., (Dejardin, Le, *et al.* 1994; Ho and Hlay 1995; Lok, Cheng, *et al.* 1983a; Lok, Cheng, *et al.* 1983b; Shibata and Lenhoff 1992b). Furthermore, Lok *et al.* (Lok, Cheng, *et al.* 1983a) have shown that for fibrinogen and albumin adsorption onto crosslinked polydimethylsiloxane at a shear rate of 58 s^{-1} initial adsorption rates from solutions with concentrations higher than approximately 200 mg ℓ^{-1} the stationary solution was not applicable and the non-stationary solution had to be used.

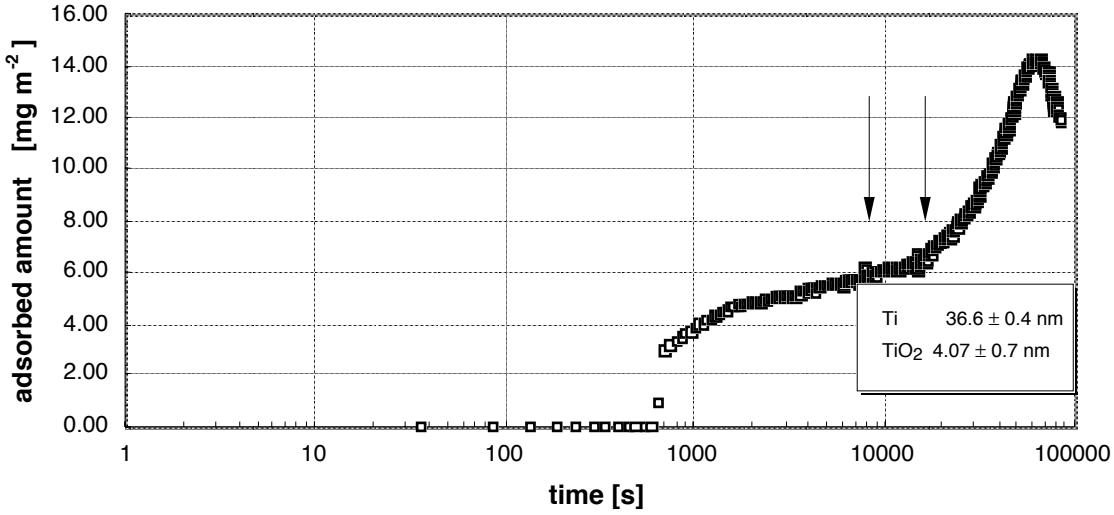

Figure 5.15: Static adsorption of fibrinogen 100-182-250 mg ℓ^{-1} on titanium oxide.

This study of fibrinogen adsorption onto titanium dioxide under laminar flow has shown that the adsorption rate was controlled by kinetics and not by mass transport.

By nonlinear parameter estimation the best values of the parameters in a two-state kinetic model Equations 5.15-5.17 have been estimated for four different concentrations tabulated in Table 5.1. From the table it can be concluded that the values are in higher at lower bulk concentration, which is a quite general phenomenon, see for example (Cuypers, Willems, *et al.* 1987; Van Regenmortel, Altschuh, *et al.* 1994). The value of the adsorption rate constant that was found in Chapter 3, therefore has to be compared to the value extrapolated to zero bulk concentration. The agreement between the extrapolated value in Table 5.1 and the value in Chapter 3 is reasonable.

Using high shear rate measurements and the two state kinetic model, approximately the first 1,000 seconds can be modelled. At longer times the change in adsorbed amount that occur cannot be explained by the two state kinetic model.

What can be seen from the experiments is that the adsorbed concentration never exceeds the value for an end-on monolayer of adsorbed fibrinogen of 16 mg m^{-2} and that a 'plateau' value of 2 mg m^{-2} corresponds to a side-on monolayer. Therefore, the overshoots are believed to arise from the transition end-on to side-on. Side-on multilayers might explain a 'plateau' value of 4.5 mg m^{-2} although not in the middle of an experiment, but in the literature multilayer adsorption of fibrinogen is usually found to be absent.

5.9 Conclusions

The adsorption of protein at different bulk concentrations under laminar flow conditions at the wall of a parallel plate flow cell were modelled and compared to measurements.

For complete mass transfer limited adsorption the complete model reduces to one non-stationary equation with a zero concentration boundary condition at the wall. For complete kinetic limitation the model reduces to a single non-stationary kinetic equation with the concentration at the wall constant and equal to the bulk concentration.

The experiments under laminar flow could not be modelled by using mass transport limited models, because the kinetics are limiting the adsorption process.

Fibrinogen is an ellipsoidal molecule and the kinetics of adsorption of fibrinogen are described by an end-on side-on transition model. This model is able to explain the observed overshoots in the adsorbed amount during adsorption. The values of the three kinetic parameters, one for adsorption, desorption and transformation, in the two-state kinetic model have been estimated for experiments using bulk concentrations of 50, 100, 400 and 1,000 mg ℓ^{-1}. The rate constants were found by non-linear parameter estimation. The value of k_a from Chapter 3 was used as start value in the non-linear fit.

In work described in the literature mass transport limitation is usually present and in many cases mass transport determines the rate of protein adsorption completely. In the experiments in this work mass transport limitations were absent and the adsorption rate in the experiments are kinetically limited.

With the kinetic two-state model the evolution of the adsorbed amount upto approximately 1,000 seconds can be modelled. The changes in the adsorbed amount at longer times may be caused by aggregation or crystallisation within a side-on protein monolayer. However, it is also possible that aggregation or crystallisation leads to structures in which the protein is at an angle with respect to the surface. Multi-layer adsorption of proteins, although unlikely initially may become important later during the adsorption process.

Appendix A

Determination of the Adsorbed Concentration Using Ellipsometry

A.1 Reflection and Refraction of a Polarised Light Beam

Fundamentals of reflection and refraction (transmission) and hence ellipsometry are already known for a long time. The technique was introduced as early as 1853 by among others Greven (Greven 1853) and Drude in 1889, and is treated in a number of books. The standard reference book is (Azzam and Bashara 1977), (Tompkins 1993) also gives a comprehensive overview of the technique with emphasis on the application, rather than the mathematics.

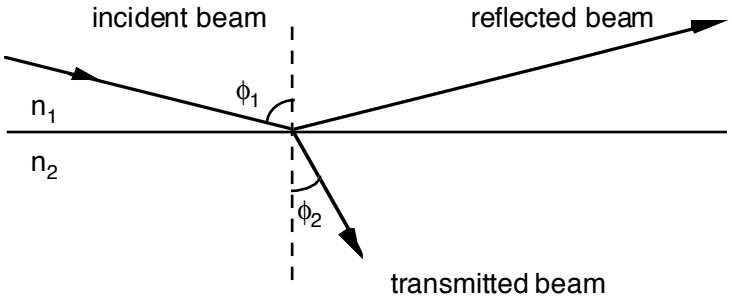

Figure A.1: Schematic drawing of reflection and transmission (refraction) in a single interface system. 1 denotes the ambient (usually air or water), 2 denotes the substrate. n is the index of refraction. The incident angle is ϕ_1 and ϕ_2 the angle of the transmitted beam, both with respect to the normal to the surface.

Consider a parallel beam of light with wavelength λ falling on a plane, homogeneous, isotropic surface, see Figure A.1. A part of the incident beam is reflected and an other part transmitted (refracted). The incident and reflected beams have the same angle with respect to the normal on the surface, and the angles of the refracted beam are found using Snell's law:

$$n_2 \sin(\phi_2) = n_1 \sin(\phi_1), \quad \text{or in a form used later} \tag{A.1}$$

$$\cos(\phi_2) = \sqrt{1 - \left(\frac{n_1}{n_2}\sin(\phi_1)\right)^2} \tag{A.2}$$

If the incident beam in Figure A.1 is a linearly polarised monochromatic, i.e., one wavelength only, light beam it can be described as a two-dimensional transversal wave characterised by its:

- amplitude

- phase
- incident angle relative to the interface

The incident angle is usually expressed with regard to the plane of incidence*. Furthermore, any linearly polarised light beam can be decomposed into two orthogonal components, one linearly polarised parallel to the plane of incidence and one linearly polarised perpendicular to the plane of incidence. For historic reasons the perpendicular component is denoted with a subscript s, the parallel component by a subscript p†.

Both components have different interaction with an interface. Hence, a linearly polarised light beam will in general not be linearly polarised anymore but will be elliptically polarised after interaction with the surface, see Figure A.2. With an ellipsometer this elliptically polarised light is

Figure A.2: Illustration of the ellipsometric parameters ψ and Δ. The p and s components of the incident linearly polarised beam of light in general change in amplitude and phase upon reflection. The relative phase change is denoted by Δ, while the amplitude ratio is denoted by $\tan(\psi)$. ϕ_0 is the incident angle. [From Jans, J.C. (1993), *Non-Destructive Analysis by Spectroscopic Ellipsometry*, Philips Journal of Research, **47**, p. 347-360].

analysed. This is how the technique received its name.

The reflection of both p and s components can be described by complex reflection coefficients r:

$$r_{\mathrm{p}} = |r_{\mathrm{p}}|\, \mathrm{e}^{\mathrm{i}\delta_{\mathrm{p}}} \tag{A.3}$$

$$r_{\mathrm{s}} = |r_{\mathrm{s}}|\, \mathrm{e}^{\mathrm{i}\delta_{\mathrm{s}}} \tag{A.4}$$

With $|r|$ the amplitude and δ the phase of the reflected wave and $\mathrm{i}^2 = -1$.

To this end it would be possible to determine r_{p} and r_{s} separately, but in order to eliminate the effect of intensity fluctuations in the incident light beam an ellipsometer determines the ratios of the amplitudes of the p and s components, and the phase difference between p and s components rather than the absolute values. Usually these two parameters are expressed as two angles, psi (ψ) and delta (Δ). Where ψ is the angle whose tangent is the absolute ratio of the complex amplitudes reflection coefficients of p and s polarisation, and Δ is defined as the change in phase difference between p and s component.

$$\tan(\psi) = \frac{\left|r_{\mathrm{p}}^r\right|}{\left|r_{\mathrm{s}}^r\right|} \tag{A.5}$$

$$\Delta = (\delta_p^r - \delta_s^r) \tag{A.6}$$

*The plane of incidence is the plane through the incident, reflected, and transmitted beam and through the normal of the surface.

†p for parallel and s for perpendicular from the German word *senkrecht*.

The superscript r denotes the reflected light beam. Hence, the total effect of reflection of light is characterised by

$$\tan(\psi)\mathrm{e}^{\mathrm{i}\Delta} = \frac{r_\mathrm{p}}{r_\mathrm{s}} = \left|\frac{r_\mathrm{p}}{r_\mathrm{s}}\right| \mathrm{e}^{\mathrm{i}(\delta_\mathrm{p}-\delta_\mathrm{s})} \tag{A.7}$$

in the case of a linearly polarised incident light beam.

The angle ψ can have any value between 0 and $\frac{\pi}{2}$ radians. The value of Δ can have any value between 0 and 2π radians. Furthermore, ρ is defined as:

$$\rho = \tan(\psi)\mathrm{e}^{\mathrm{i}\Delta} \tag{A.8}$$

ρ is called complex reflectance ratio. ρ depends on the wavelength of the light, λ, the angle of incidence, ϕ_1, and the optical properties of the surface material.

The polarisation state of a light beam can now be fully characterised by the amplitude ratio, $|r_p| / |r_s|$, and the phase difference $\delta_p - \delta_s$, between the two components of the electric vector parallel and normal to the plane of incidence.

By determining the change in amplitude ratio and phase difference between parallel and perpendicular components of a light beam, optical parameters of a surface material can be calculated (Drude 1889a; Drude 1889b; Drude 1890). Furthermore, when a beam of light is incident on a surface covered with a (thin) layer, or even a sparsely distributed sub-monolayers of atoms or molecules, the change in state of polarisation will be different compared to that of the uncovered surface. From this difference in polarisation, it is in turn possible to obtain information about the layer.

In ellipsometry the optical resolution normal to the surface for a layer on a surface is determined by the phase difference and is only a fraction of the wavelength used, i.e., Ångstroms rather then nanometers. The optical resolution parallel to the surface is limited by light diffraction to about half of the wavelength. For good lateral resolution a small diameter of the incident light beam has to be employed. Surface roughness and flatness must be considered but result in irregularities that are in general small compared to the dimensions of the light beam, i.e., 1 mm^2, and are averaged.

A.2 Complex Index of Refraction

Transparent surface materials only reflect and refract the light. Other surface materials may not only reflect and refract an incident beam but also absorb some of its energy. Light absorption is a phenomenon that is rather different from reflection and refraction of light, nevertheless one can mathematically incorporate absorption without affecting the validity of the formulae given before as follows:

$$N = n - \mathrm{i}k \tag{A.9}$$

N is then called the complex refractive index, and n the index of refraction. The extinction coefficient k accounts for the absorption of light and is related to α the absorption coefficient by:

$$k \equiv \frac{\lambda}{4\pi}\alpha \tag{A.10}$$

With λ the wavelength of the light in vacuum.

Using Equation A.9, Snell's law Equation A.1 becomes[‡]:

$$N_1 \sin(\phi_1) = N_2 \sin(\phi_2) \tag{A.11}$$

[‡]When either one or both media are absorbing the angle ϕ_2 becomes complex and is not simply the angle of refraction, nevertheless all formulae derived for non-absorbing, i.e., transparent materials, remain valid.

A.3 Determining the Complex Index of Refraction of a Substrate

In the case of a clean surface material the reflection or transmission of both p and s components of a light beam at a single interface like in Figure A.1, are found by using the Fresnel equations.

$$r_{\mathrm{p12}} = \frac{N_2\cos(\phi_1) - N_1\cos(\phi_2)}{N_2\cos(\phi_1) + N_1\cos(\phi_2)} \tag{A.12}$$

$$r_{\mathrm{s12}} = \frac{N_1\cos(\phi_1) - N_2\cos(\phi_2)}{N_1\cos(\phi_1) + N_2\cos(\phi_2)} \tag{A.13}$$

$$t_{\mathrm{p12}} = \frac{2N_1\cos(\phi_1)}{N_2\cos(\phi_1) + N_1\cos(\phi_2)} \tag{A.14}$$

$$t_{\mathrm{s12}} = \frac{2N_1\cos(\phi_1)}{N_1\cos(\phi_1) + N_2\cos(\phi_2)} \tag{A.15}$$

r_{p}, r_{s}, t_{p} and t_{s} are respectively called the reflection and transmission coefficients. The angles ϕ_1 and ϕ_2 between the directions of propagation in media 1 and 2 and the normal to the film boundaries are found by using Snell's law.

Because ρ can be calculated from the measured values of ψ and Δ, using Equation A.8 the complex index of refraction of medium 2, N_2, can be determined, requiring only the index of refraction N_1 and ϕ_1 as follows:

$$N_2 = N_1\sin(\phi_1)\sqrt{1 + \left(\frac{1-\rho}{1+\rho}\right)^2\tan^2(\phi_1)} \tag{A.16}$$

Assuming that the instrument is operating correctly, ψ and Δ (ρ) can be measured very precise. Whether the calculated sample refractive index is correct depends on if the assumed model is correct, i.e., negligible surface roughness and no additional contamination layers. The Fresnel equations itself A.12-A.13 are valid only for semi-infinite homogeneous and optically isotropic media with negligible surface roughness.

A.4 Determining the Real Index of Refraction and Thickness of a Layer

If a surface is covered with a layer like in Figure A.3, the two interfaces do not only cause reflection and transmission of an incident light beam, but also multiple reflections and transmissions will combine either constructively or destructively due to interference. The result of summation of all reflections and transmissions occurring between the two interfaces result in equations that are a combination of the Fresnel reflection coefficients Equation A.12-A.13. Furthermore, Fresnel reflection coefficients are a function of the refractive index and incident angle only. β the phase difference is also dependent on the distance d between the two interfaces and the wavelength λ.

$$\beta_{\mathrm{f}} = \frac{4\pi d_{\mathrm{f}} N_{\mathrm{f}}\cos(\phi_{\mathrm{f}})}{\lambda_1} \tag{A.17}$$

The total reflection coefficients then become:

$$r_{\mathrm{p1f2}} = \frac{r_{\mathrm{p1f}} + r_{\mathrm{pf2}}\mathrm{e}^{-2\mathrm{i}\beta_{\mathrm{f}}}}{1 + r_{\mathrm{p1f}}r_{\mathrm{pf2}}\mathrm{e}^{-2\mathrm{i}\beta_{\mathrm{f}}}} \tag{A.18}$$

$$r_{\mathrm{s1f2}} = \frac{r_{\mathrm{s1f}} + r_{\mathrm{sf2}}\mathrm{e}^{-2\mathrm{i}\beta_{\mathrm{f}}}}{1 + r_{\mathrm{s1f}}r_{\mathrm{sf2}}\mathrm{e}^{-2\mathrm{i}\beta_{\mathrm{f}}}} \tag{A.19}$$

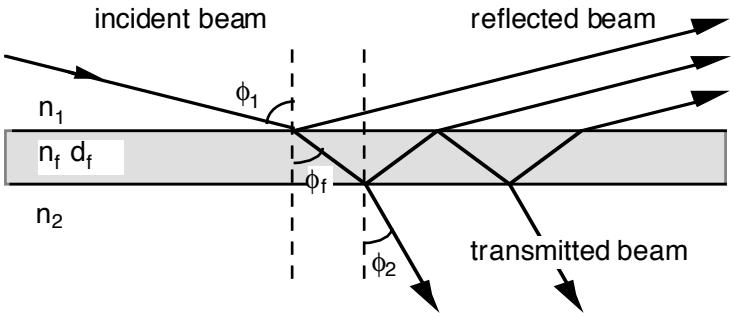

Figure A.3: Schematic drawing of reflection and transmission in a two interface system. 1 denotes the ambient (usually air or water), 2 denotes the substrate and f denotes the protein film. d is the thickness of the film. n is the index of refraction. The incident angle is ϕ_1, ϕ_f the angle in the film and ϕ_2 the angle of the transmitted beam, all three with respect to the normal to the surface.

The angles of incidence can be calculated using Snell's law:

$$N_1 \sin(\phi_1) = N_\mathrm{f} \sin(\phi_\mathrm{f}) = N_2 \sin(\phi_2) \tag{A.20}$$

For a transparent film n_f and d_f can be calculated from a single measurement if the refractive index of the ambient, the refractive index of the clean substrate, the angle of incidence and the wave length of the light are known. It is assumed that the interfaces have parallel-plane boundaries and are sandwiched between semi-infinite ambient and the substrate media. The media are assumed to be homogeneous and optically isotropic. Surface roughness, inhomogeneity and anisotropy are therefore not accounted for in these equations. The calculation requires an iterative solution of the equations, since no explicit expression for the refractive index and thickness as a function of ψ and Δ exists.

A.5 Determining the Adsorbed Amount of a Layer

To determine the adsorbed amount of a layer from the refractive index n and optical thickness d, the model that is mainly used is that of De Feijter *et al.* (De Feijter, Benjamins, *et al.* 1978). De Feijter argues that if the refractive index n_b of a protein solution is a linear function of the concentration in solution, the adsorbed amount can be determined unambiguously. For proteins the linearity of a graph of the refractive index versus bulk concentration has been verified by a number of authors (van der Scheer 1978; Welin-Klintström 1992). The slope of the aforementioned graph is called the refractive index increment ($\frac{dn}{dc}$). For the refractive index of a protein solution n_b one can then write:

$$n_\mathrm{b} = n_1 + \frac{dn}{dc} \cdot c_\mathrm{b} \tag{A.21}$$

With n_1 the refractive index of the solution without protein. They continue by writing:

$$c_\mathrm{f} = c_\mathrm{b} = \frac{\Gamma}{d_\mathrm{f}} \tag{A.22}$$

$$n_\mathrm{f} = n_\mathrm{b} \tag{A.23}$$

for c_f and n_f the concentration and refractive index in the adsorbed layer. By using Equations A.21 and A.23 the expression for the Γ then becomes:

$$\Gamma = \frac{d_\mathrm{f}\,(n_\mathrm{f} - n_1)}{\frac{dn}{dc}} \tag{A.24}$$

With $\frac{dn}{dc}$ the refractive index increment, i.e., the change in refractive index with concentration. Hence, the values of the refractive index and the thickness of a layer obtained from an ellipsometric measurement can be used to calculate the adsorbed amount per unit area, i.e., the surface concentration Γ.

The validity of the calculated amounts using Equation A.24 have been verified using radio labelling (Engström and Backström 1987; Jönsson, Malmqvist, *et al.* 1985; Wahlgren 1992), with differences between ellipsometry and radio labelling not exceeding 15 %.

A.6 Illustrative Example of the Calculation of the Adsorbed Amount from Ellipsometric Measurements

The study of fibrinogen at a bulk concentration of 10 mg ℓ^{-1} from 100 mM Tris HCl buffer at pH 7.0 onto 'hydrophobic' chromium oxide surfaces (treated with hot chromic acid), as reported in the literature by Cuypers *et al.* (Cuypers 1976; Cuypers, Hermens, *et al.* 1977) will be used as an illustrative example of ellipsometric calculations. The experiment was carried out in a stirred cuvette.

In Cuypers' setup the situation of incident beam (ϕ_1), protein solution (N_1), protein film (n_f) and chromium (n_2) can be modelled as shown in Figure A.3. The values of the parameters was as follows: $\phi_1 = 68$ °, $\lambda = 632.8$ nm and $N_1 = 1.3338$

The refractive index of the chromium oxide can be determined using Equation A.16 this gives $N_2 = 2.5803 - 2.5821i$ for the measurement at 500 seconds. After 500 seconds protein was added and the resulting film refractive index and thickness can be found using Equation A.17-A.19. Finally the adsorbed amount Γ can be determined using Equation A.24 using for fibrinogen dn/dc = 0.188 mℓ g^{-1}. The values of the different parameters are shown in Table A.1.

A few remarks about this example should be made. The value of chromium oxide is in fact a combined or pseudo refractive index, because the surface consists of bulk chromium with a thin layer of chromium oxide. Neglecting this fact introduces errors in the calculation of the refractive index and thickness of the protein film. The values of the refractive index and thickness of the protein film reported in Cuypers' article are different from the values calculated here. However, similar adsorbed amounts are obtained when using Equation A.24. Malmsten (Malmsten 1994) studying adsorption of a 100 mg ℓ^{-1} fibrinogen solution in PBS buffer of pH 7.4 onto hydrophobic silica obtained similar refractive indices and thicknesses as in Table A.1 taking into account both the silicon bulk and silicon dioxide layer separately.

To obtain reliable results for the refractive index and thickness of a protein film one should correctly take into account the bulk surface material with it's oxide layers separately. Furthermore, the original calculations of refractive index and thickness by Cuypers are believed to be erroneous.

A.7 Absorption, Inhomogeneity and Anisotropy of Layers

While the thickness of an inorganic layer obtained from an ellipsometric measurement matches the actual physical thickness, for organic layers caution must be observed when interpreting results. Adsorbed macromolecules do not form a homogeneous adsorbed layer. Hence, when using the model of flat isotropic layers the refractive index and thickness obtained, represent an optical average of the layer.

Models to interpret ellipsometric measurements of small spheroids, e.g., The Maxwell Garnet theory, can be found in the literature (Azzam and Bashara 1977). The protein molecule used in

Table A.1: ψ and Δ values as a function of time taken from (Cuypers 1977). N_f, d_f and Γ recalculated.

t [s]	ψ [°]	Δ [°]	N_f [–]	d_f [nm]	Γ [mg m^{-2}]
0	24.56	103.64	–	–	–
500	24.55	103.60	–	–	–
1000	25.35	101.12	1.434	9.405	5.01
1500	25.49	100.64	1.464	8.806	6.13
2000	25.52	100.42	1.5215	6.797	6.80
2500	25.54	100.38	1.5119	7.225	6.86

this study is not a spherical molecule but is more cigar like with large length over diameter ratio and is therefore better described as a prolate ellipsoid. Because of their shape, ellipsoids introduce anisotropy, i.e., the polarisability is not equal in all three space directions. When the molecules are randomly oriented on the surface this anisotropy will disappear and the layer will optically behave like an effectively isotropic layer. However, when adsorbed protein molecules are orientated either parallel or perpendicular to the surface this can be taken into account either by using optical models that allow for anisotropy (Azzam and Bashara 1977; Engelsen 1971; Engelsen 1974; Engelsen 1976) or by rigorously incorporating the shape of the molecules in the optical model.

Appendix B

Attenuated Total Internal Reflection Ellipsometry

B.1 Ellipsometric Setup Used In This Study

Figure B.1 schematically shows the essentials of how the measurement technique is used. Attenuated

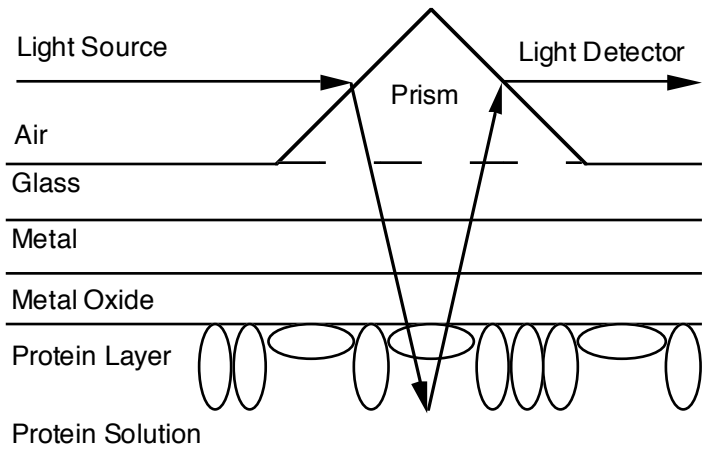

Figure B.1: Schematic illustration showing enlarged the essentials of the measurement technique. The pathway of the light beam is drawn only to show how the light enters and exits the prism, the path in between is simply drawn as two straight lines.

total internal reflection is used. Under conditions of total internal reflection (when $\sin(\theta_1) > \frac{n_2}{n_1}$) only a wave with an amplitude that decreases exponentially penetrates the less dense medium. The field propagates as a so-called evanescent wave. This field is the reason why the reflected light is sensitive to optical changes within a distance of the order of the wavelength from the interface under conditions of total internal reflection. In this study we are interested in the adsorption of proteins at the metal oxide–solution interface. When the refractive index of the glass prism, the glass, the metal, the metal oxide and the protein solution together with the thickness of the metal and metal oxide are known, it is possible to determine the refractive index and the thickness of the protein layer from a single ellipsometric measurement, see Appendix A. Each layer is assumed to be flat and parallel to the other, and each layer is assumed to be homogeneous and isotropic*. If all these assumptions

*An isotropic material has the same refractive index for every polarisation. The opposite, anisotropy is encountered when a material has two or more different refractive indices, for different optical axes.

are correct then only Snell's law and the laws of Fresnel have to be used in order to fully describe the changes in the light beam from the passage through the multiple interfaces shown in Figure B.1.

B.2 Total Internal Reflection

All equations derived for reflection at interfaces remain valid if an arbitrarily optical plane wave is incident on an interface from the side of high index of refraction at an incident angle greater than the critical angle. However, because $\sin(\phi_1) > \frac{n_1}{n_2}$ Equation A.2 should be replaced by:

$$\cos(\phi_2) = \pm \mathrm{i} \sqrt{\left(\frac{n_1}{n_2}\sin(\phi_1)\right)^2 - 1} \tag{B.1}$$

Although there is no net energy transfer into the medium of lower refractive index there still are non-zero electromagnetic fields in the second medium that have an exponential decay (the evanescent field). Furthermore, because light penetrating the second medium is attenuated not amplified in Equation B.1 the minus sign should be used. Since this evanescent field in fact probes the refractive index in the second medium the reflection coefficient will be sensitive to a film of non-equal refractive index in this second medium.

B.3 Change in Polarisation by Oblique Transmission Through a Prism

Because a prism is used the total ρ should be divided by a factor that takes into account the different transmission of the p and s-component through the prisms entrance and exit interface.

$$\rho^{\text{total}} = \rho_{\text{t01}}\ \rho^{\text{measurement}}\ \rho_{\text{t10}} \tag{B.2}$$

With

$$\rho_{\text{t01}}\ \rho_{\text{t10}} = \frac{t_{\text{p01}}}{t_{\text{s01}}}\ \frac{t_{\text{p10}}}{t_{\text{s10}}} \tag{B.3}$$

using

$$t_{\text{p01}} = \frac{2n_0\cos(\phi_0)}{n_1\cos(\phi_0) + n_0\cos(\phi_1)} \tag{B.4}$$

$$t_{\text{s01}} = \frac{2n_0\cos(\phi_0)}{n_0\cos(\phi_0) + n_1\cos(\phi_1)} \tag{B.5}$$

and

$$t_{\text{p10}} = \frac{2n_1\cos(\phi_1)}{n_0\cos(\phi_1) + n_1\cos(\phi_0)} \tag{B.6}$$

$$t_{\text{s10}} = \frac{2n_1\cos(\phi_1)}{n_1\cos(\phi_1) + n_0\cos(\phi_0)} \tag{B.7}$$

$$\rho_{\text{t01}}\ \rho_{\text{t10}} = \left[\frac{n_0\cos(\phi_0) + n_1\cos(\phi_1)}{n_1\cos(\phi_0) + n_0\cos(\phi_1)}\right]^2 \tag{B.8}$$

Using Snell's law and for our case $\phi_0 = \frac{1}{3}\pi$, $n_1 = 1.515$ for BK-7 at λ =632.8 nm, and $n_0 = 1.000$ for Air gives:

$$\rho_{t01}\ \rho_{t10} = \left[\frac{n_0\,\frac{1}{2} + n_1\sqrt{1-\frac{3}{4}\,\frac{n_0^2}{n_1^2}}}{n_1\,\frac{1}{2} + n_0\sqrt{1-\frac{3}{4}\,\frac{n_0^2}{n_1^2}}}\right]^2 = 1.220144382 \tag{B.9}$$

B.4 Selection of the Optimal Angle of Incidence

As can be seen from Figure B.2 the changes in ψ and Δ by adsorption of a protein layer depend to a large extent on the chosen angle of incidence. If the model of flat isotropic layers is used in the case of total internal reflection, it is not possible to distinguish between refractive index and thickness, i.e., only a change in the product of refractive index and thickness can be determined.

While this is a disadvantage of using choosing an angle greater than the critical angle, it can be seen in Figure B.2 that the increase in sensitivity is significantly increased. From Figure B.2

we can further inver that if the incident angle is chosen to be 65° the change in Δ is large while the change in ψ is almost zero, see also Figure B.3 for the changes in ψ and Δ during a typical adsorption experiment.

The fact that the change in ψ is almost zero also results in a simple relation between the change in Δ and the adsorbed amount.

Martensson *et al.* (Martensson, Arwin, *et al.* 1995) argue that in their case of adsorption of ferritin onto gold a gold-protein layer is formed that is adsorbing resulting in a non zero imaginary part of the refractive index. The advantage of choosing the incident angle in this way is that any change in ψ must be the result of a non-dielectric, i.e., absorbing layer. So by choosing the incident angle to be 65° we know immediately whether or not the protein layer shows light absorption.

B.5 Optical properties of Thin Metal Films

Thickness

Because we used total internal reflection to determine the adsorption of protein at the surface of a material, thin layers of metal (in the order of 40 nm) had to be used. The upper limit of the layer thickness is determined by the absorption of light in the layer. For layers thicker than approximately 40 nm light will not penetrate through the layer anymore. To increase the sensitivity it would be advantageous to use even thinner layers of metal. However, the lower limit of the layer thickness is limited by the fact that very thin layers are not continuous and isotropic, and therefore the description of the optical properties of the metal layer would become a difficult task. An excellent article about the minimal thickness necessary in order to tread the metal film as a continuous isotropic layer is (Yamamoto and Namioka 1992). In this article Yamamoto *et al.* also give an interesting method to determine the refractive index and layer thickness from ellipsometric measurements[†].

Oxide Layer

On most metals a layer of oxide is formed spontaneously. This native oxide is approximately 2-4 nm thick. For titanium the oxide layer can be described using the real (bulk) refractive index n of TiO_2. This is also the case for silicon and a number of other metals. However, the oxide layer on chromium cannot be described using a single refractive index. The oxide layer of chromium cannot

[†]Unfortunately there is an error in equation (A5) in the article. The denominator on the left hand side of Equation (A5) should be squared

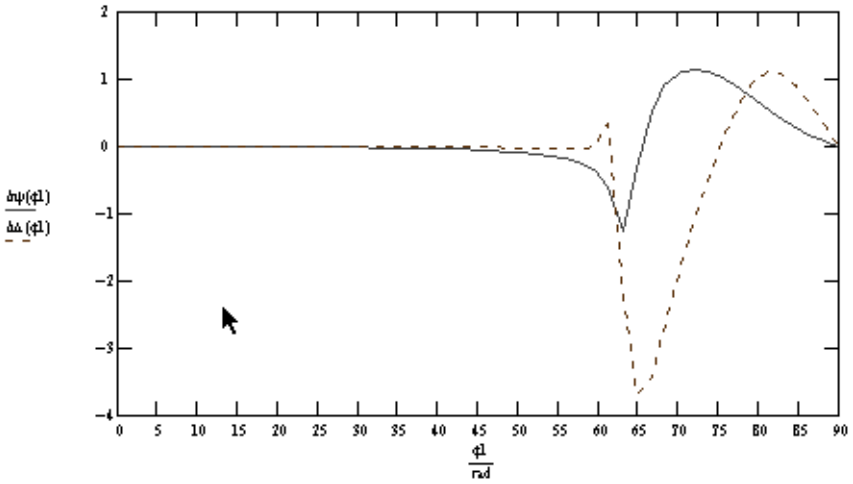

Figure B.2: Variation of ψ (solid line) and Δ (dashed line) upon adsorption of a protein layer of n=1.37 and thickness of 50 nm onto a 37 nm Ti layer with 4 nm of TiO_2 as function of the incident angle on the Ti layer from a BK-7 prism. Note that the variation of ψ almost zero at 65°.

be described by a real refractive index because it is absorbing, also the fraction of oxide varies within the oxide layer and this makes a correct optical description of the chromium-chromium oxide layer difficult.

Adsorbed Water

On some metals water adsorbs more than on others. McCrackin *et al.* (McCrackin, Passaglia, *et al.* 1963) show that the water layer adsorbed onto chromium can be as thick as 2.5 nm, whereas on gold a layer of 0.4 nm was determined. On silicon the water layer can safely be neglected (Landgren and Jönsson 1993).

B.6 Ellipsometric Setup

The experimental configuration for ellipsometric measurements is a rotating analyser ellipsometer (RAE arrangement). To allow the laser beam to be reflected at the surface of interest a prism and total internal reflection is used in the sample cell as shown schematically in Figure B.4. The top angle of the prism in the cell has been chosen in order to have an angle of incidence on the interface that will give total reflection. Total reflection has at least two distinct advantages, first the resulting evanescent wave penetrates the solution only a few microns deep and therefore air bubbles will not deteriorate measurements[‡], second the instrument can be constructed to operate in straight through configuration. This has the advantage that the instrument does not need two (expensive) goniometers and that it contains less moving parts making it easier to line-out.

The ellipsometer that is used in this study is a photometric rotating analyser ellipsometer (RAE). It uses a synchronously rotating-analyser to detect the state of polarisation of the light beam after reflection from the sample, by recording the light intensity after the rotating analyser.

The apparatus consists of a linearly polarised HeNe laser (Spectra Physics, USA) as the light source, with a wavelength of 632.8 nm. A diaphragm limits the beam diameter to 2 mm, before it

[‡]Measurements using reflection ellipsometry on silicon wafer strips placed inside a cuvette, shows substantial noise due to air bubbles present in the buffer solution in the cuvette, even after deaerating the buffer and filtering through a hydrophobic filter.

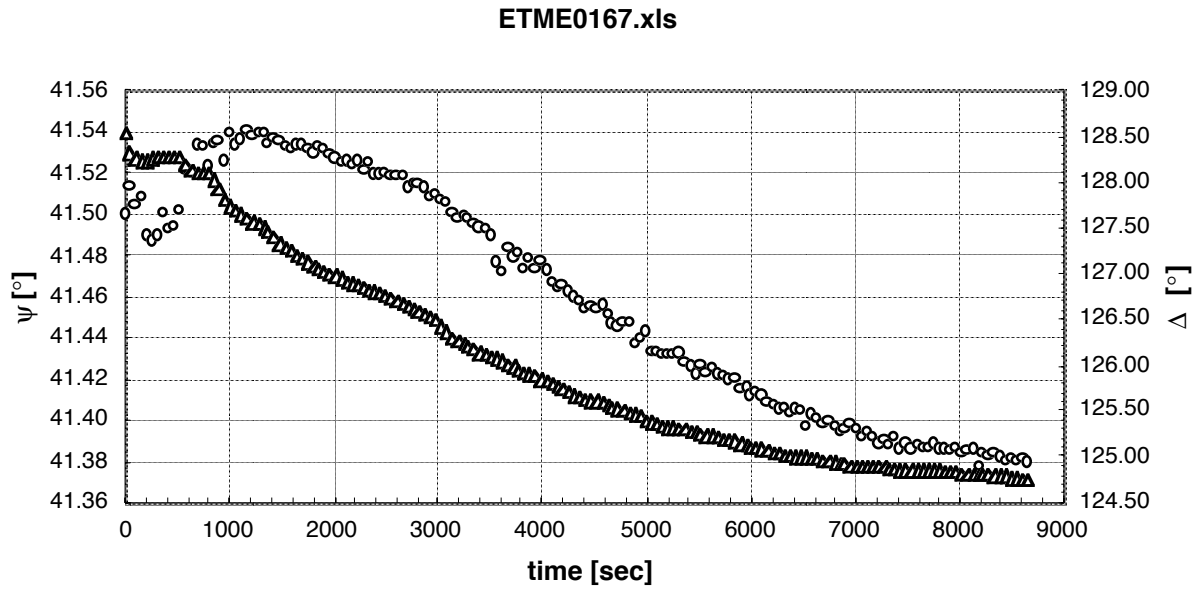

Figure B.3: Static adsorption of fibrinogen 50 mg ℓ^{-1} on titanium oxide. Raw ψ and Δ values are shown. Note that the change in ψ (triangles) is very small.

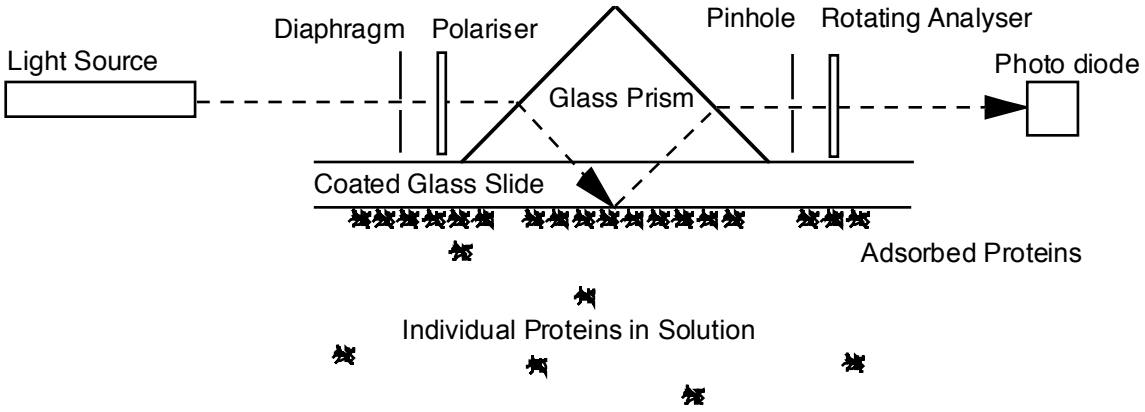

Figure B.4: Schematic illustration of the pathway of the laser beam

passes a Glan-Taylor polariser. The polariser is fixed during a measurement at an angle of ± 45°. After reflection at the sample, the polarisation state of the light is analysed with a second polariser. This is the analyser and it rotates at a frequency of 57 Hz. The light is detected with a 13DSI009 silicon photo diode (Melles Griot, USA) and amplified using a 13AMP003 dynamic range amplifier (Melles Griot, USA). Due to the rotation of the analyser a sinusoidal signal with a double frequency is recorded. This signal is digitised with an AD-converter which measures the signal at 180 equidistant points in one mechanical revolution. A shutter provides a dark signal measurement.

The line out of the instrument is done by evaluating the frequency components in the signal. Non-parallel transmission through the polarisers induces components at the single, triple, fourth, fifth and higher frequencies next to the fundamental double frequency. A good line out is considered to be achieved if all frequency components are 30 dB or less with respect to the double frequency component for two angles of the polariser.

The actual angles of the polariser and analyser with respect to the plane of incidence are found with a calibration method. This method also calibrates the signal for different amplification of DC

and AC components. Depending on the values of ψ and Δ, a calibration on the residue or a phase calibration was chosen.

Appendix C

Drawings of the Different Parts of the Parallel Plate Flow Cell

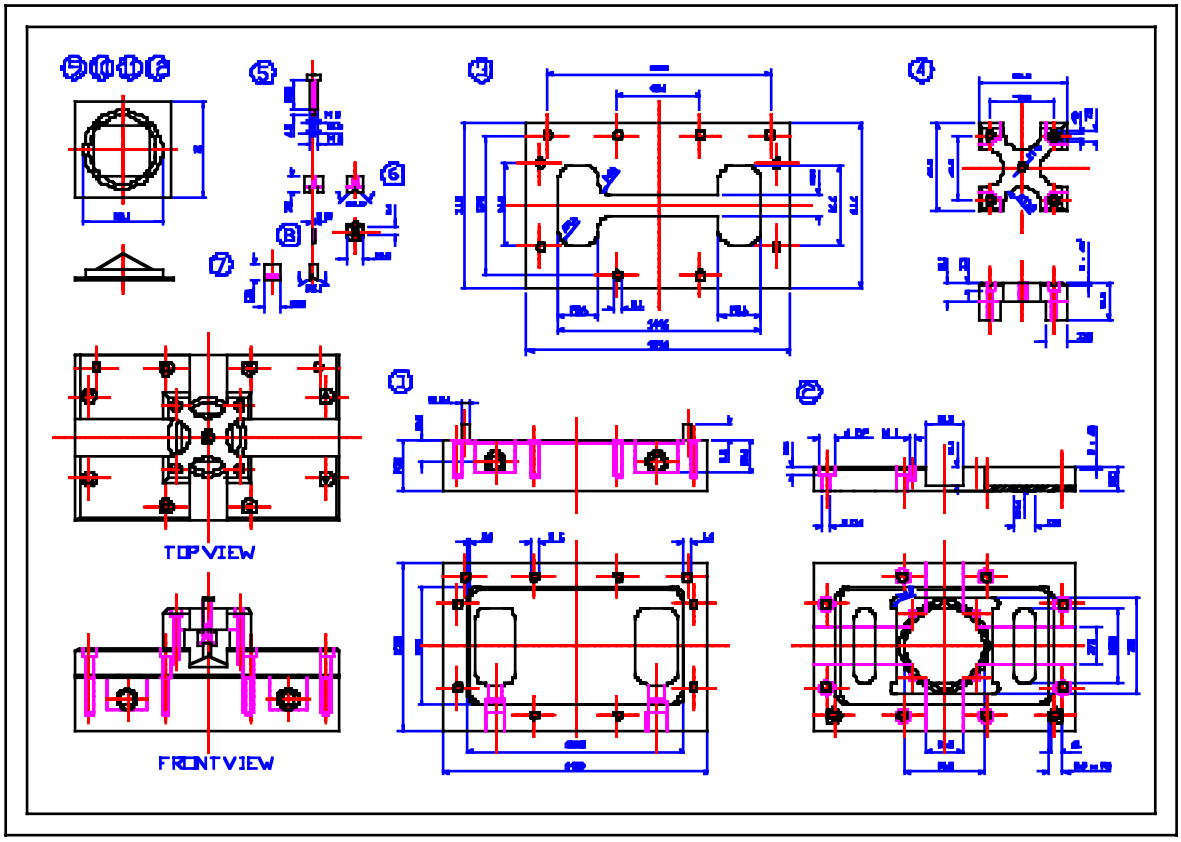

Figure C.1: All the different parts of the parallel plate flow cell combined.

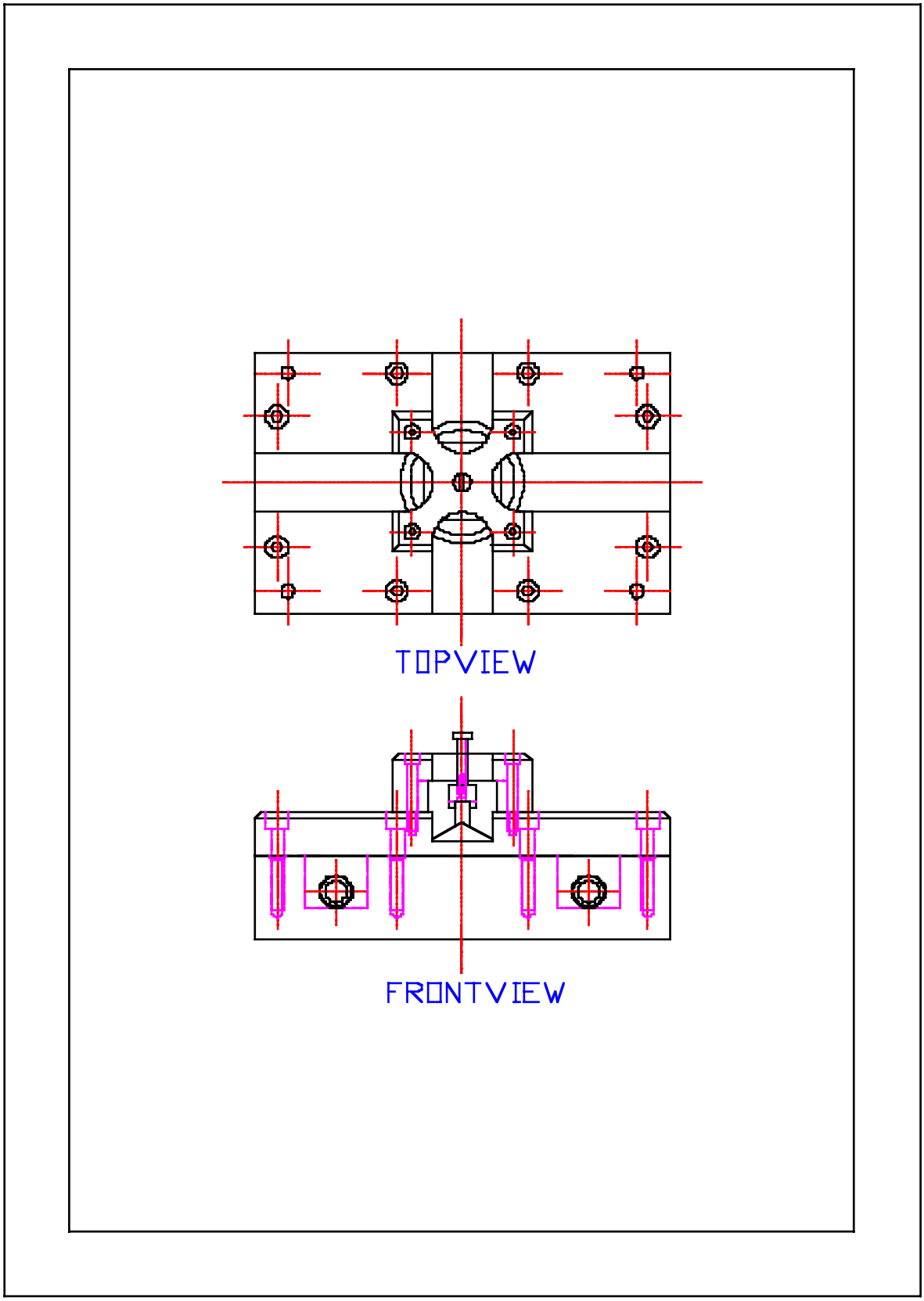

Figure C.2: Assembled top and front view of the parallel plate flow cell.

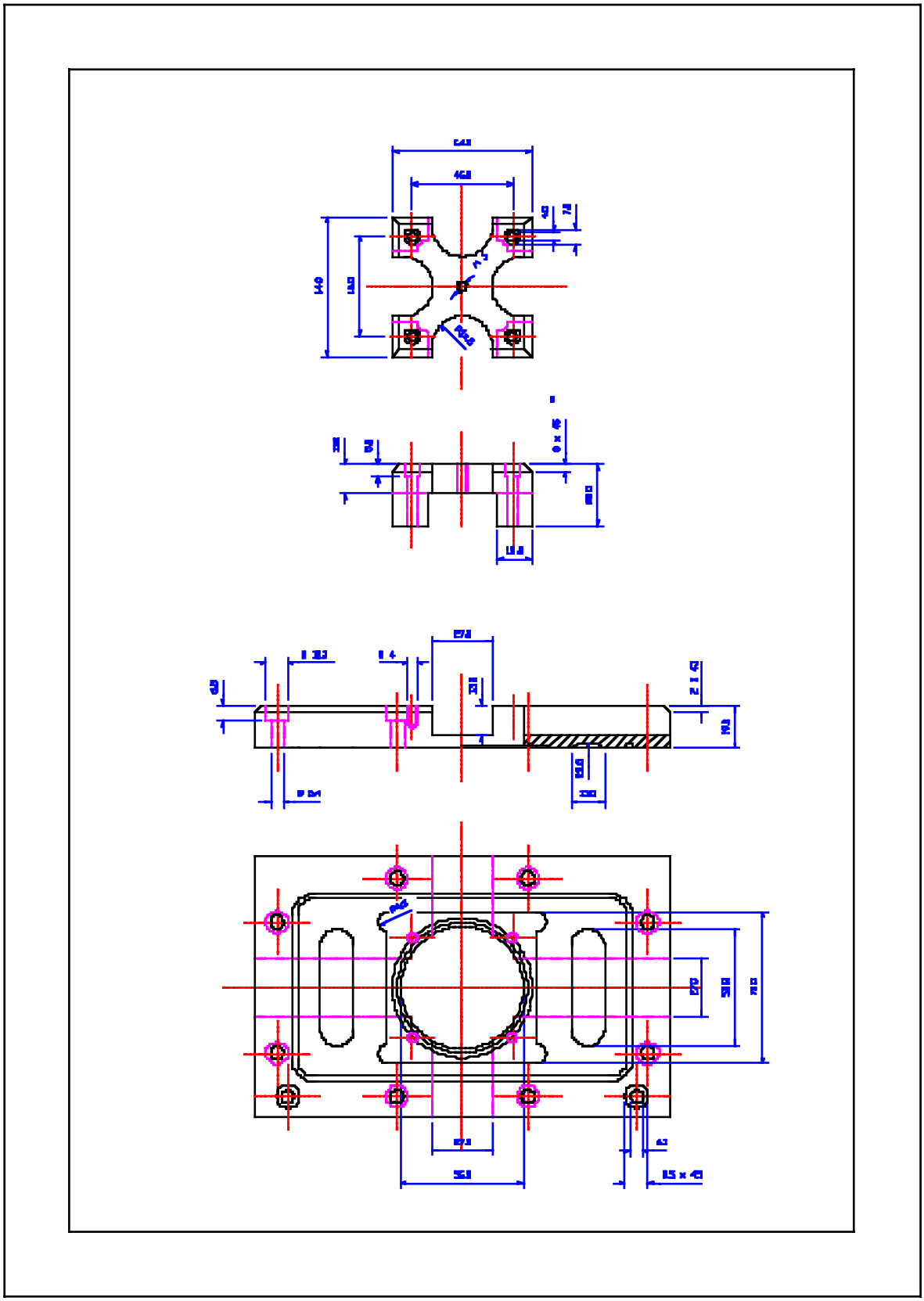

Figure C.3: Top part of flow cell with prism housing (dimensions in mm).

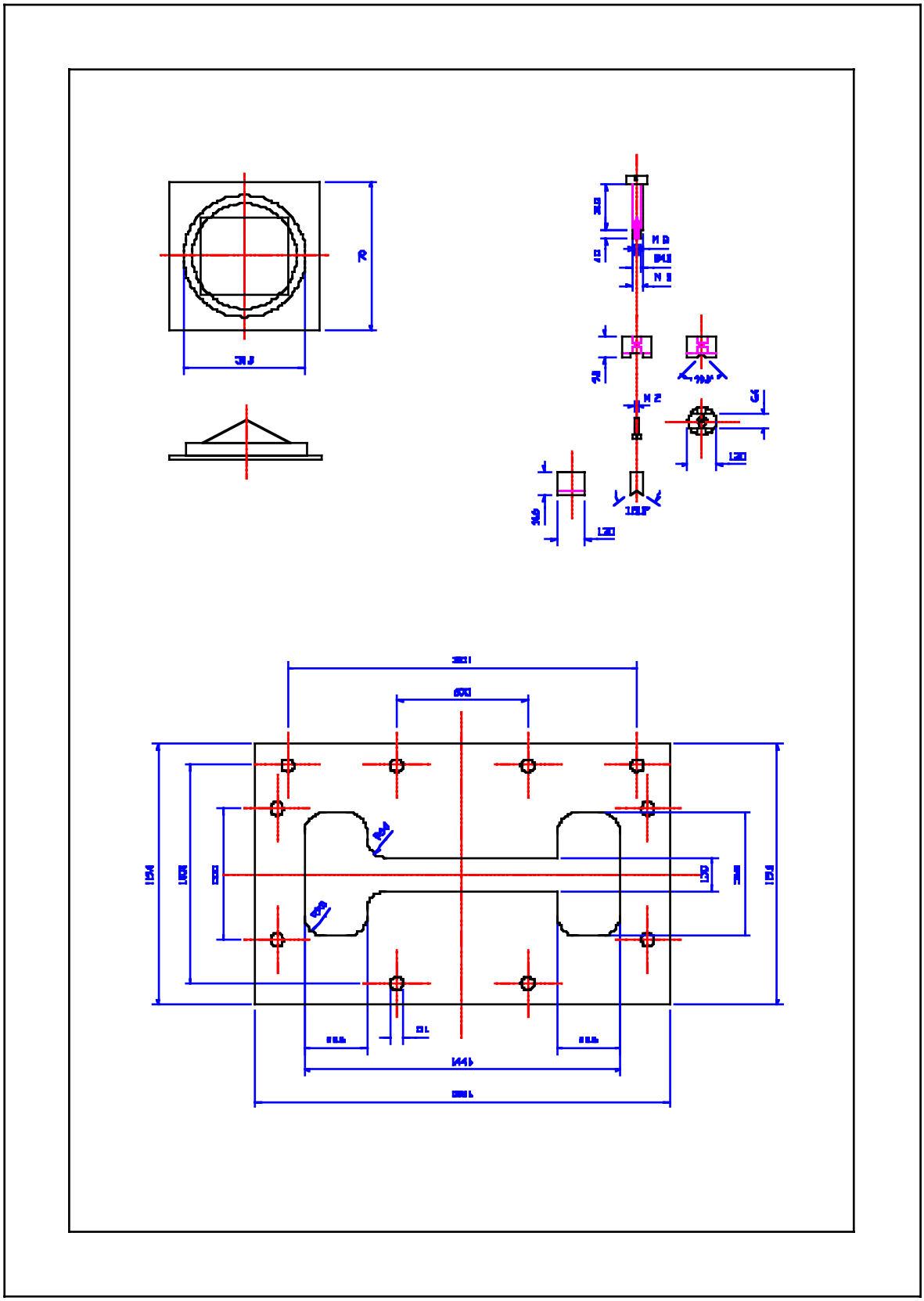

Figure C.4: Glass slide + prism, prism clamp and spacer plate (dimensions in mm).

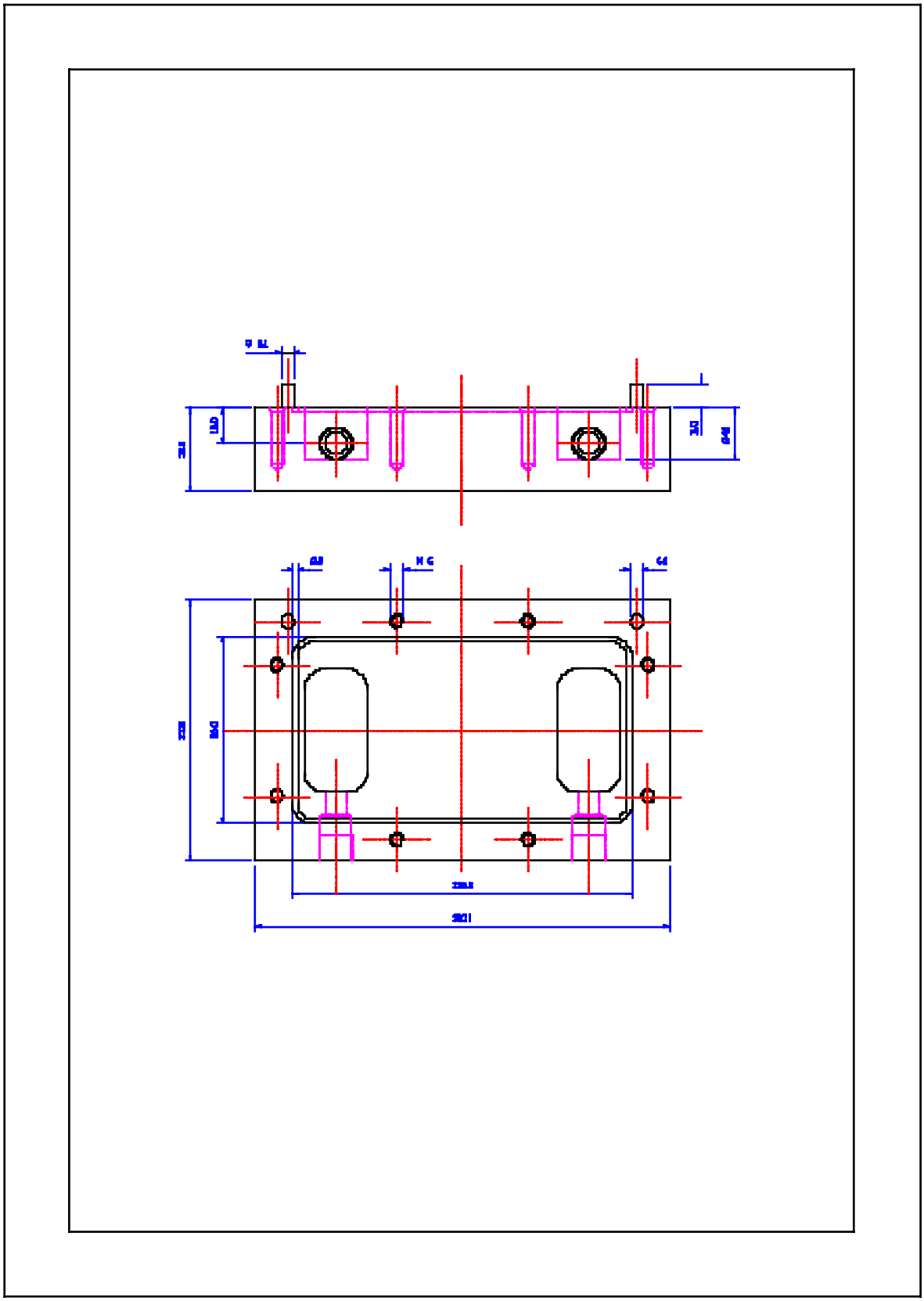

Figure C.5: Bottom part of flow cell with entrance and exit chambers side and top view (dimensions in mm).

Appendix D

Numerical Solution of the Two-Dimensional Convection-Diffusion Equation with Non-Linear Reversible Adsorption Kinetics as Boundary Condition

D.1 Introduction

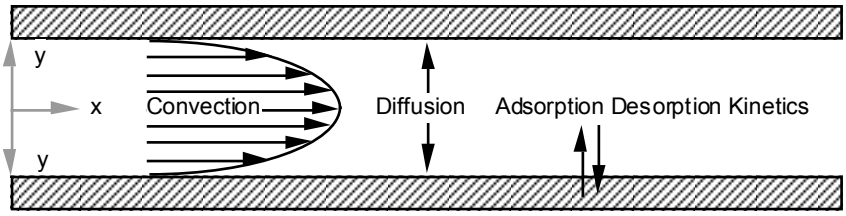

Figure D.1: Schematic overview of the coordinate system used for the parallel plate flow. Only half of the flow is modelled. The x and y coordinate refer to the place variables.

To solve the two-dimensional convection–diffusion equation with non-linear boundary reversible adsorption kinetics, numerical techniques have to be used, as no analytical solutions are available. The equation that has been solved are:

$$\frac{\partial c}{\partial t} = -\frac{3}{2}\bar{v}\left[1-\left(\frac{y}{a}\right)^2\right]\frac{\partial c}{\partial x} + \mathbb{D}\frac{\partial^2 c}{\partial x^2} + \mathbb{D}\frac{\partial^2 c}{\partial y^2} \tag{D.1}$$

Subject to the following initial and boundary conditions

$$c\left(x,y,t=0\right) = 0 \tag{D.2}$$
$$\Gamma\left(x,y,t=0\right) = 0 \tag{D.3}$$

$$c\left(x=0,y,t\right) = c_0 \tag{D.4}$$
$$-\mathbb{D}\frac{\partial c\left(x=L,y,t\right)}{\partial x} = 0 \tag{D.5}$$

$$-\mathbb{D}\frac{\partial c\,(x, y = 0, t)}{\partial y} = 0 \tag{D.6}$$

$$-\mathbb{D}\frac{\partial c\,(x, y = a, t)}{\partial y} = \frac{\partial \Gamma}{\partial t} \tag{D.7}$$

It should be noted that in Equation D.1 the diffusion term in the x-direction will *not* be neglected. As a consequence a boundary condition at $x = L$ is needed. The reason for keeping the diffusion term in the x-direction is that near and at the surface the velocity in the x-direction is small or zero. Without diffusion in the x-direction, there would be no means of transportation of protein in the x-direction.

Analytical solutions that exist with simpler boundary conditions or analytical solutions that are obtained by sequentially (as opposed to simultaneously) solving the equations — and thereby completely separating mass transfer from adsorption and desorption steps — are not correct.

The equation becomes stiffer with increasing flow rates as the convection diffusion equations shifts from being mainly parabolic to mainly hyperbolic, making it more difficult to find accurate stable numerical solutions. This limits the available techniques by ruling out essentially all explicit numerical techniques.

Implicit methods, although giving good stability, require a large computational effort, especially in more dimensions.

D.2 Alternating–Direction–Implicit method

Alternating-direction implicit (ADI) method was developed by Peaceman and Rachford in the late 1950s. ADI was the first of an entire class of methods now known as *splitting methods*. ADI has the stability benefits of an implicit method without the penalty in computation time that arises in two-dimensional problems. It treats the x-directions implicitly and the y-direction explicitly in the first half time step and in the second half time step this is reversed. Hence, it treats the directions alternatingly implicit. The computational costs are proportional to twice the number of mesh points. The ADI method reduces banded matrices from pentadiagonal matrices to two systems of tridiagonal matrices, that can be solved very effectively by a linear systems solver (Hoffman 1993). In this case LU-decomposition according to Crout is used. Ferziger (Ferziger 1981) shows that the ADI method is unconditionally stable and is second order accurate.

The convective first order derivative is implemented as a two point upwind first order Finite Difference Approximation (FDA). The diffusive second order derivative is implemented as a three point second order central FDA. The first order derivative in the boundary conditions are implemented as a three point second order backward FDA.

D.3 Non Uniform Grid Using a Transformation Function

To implement a narrower grid approaching y=a the following transformation function is used:

$$a\,[1 - ((1 - p)(1 - y)^m + p(1 - y))] \tag{D.8}$$

This function is also shown in Figure D.2.

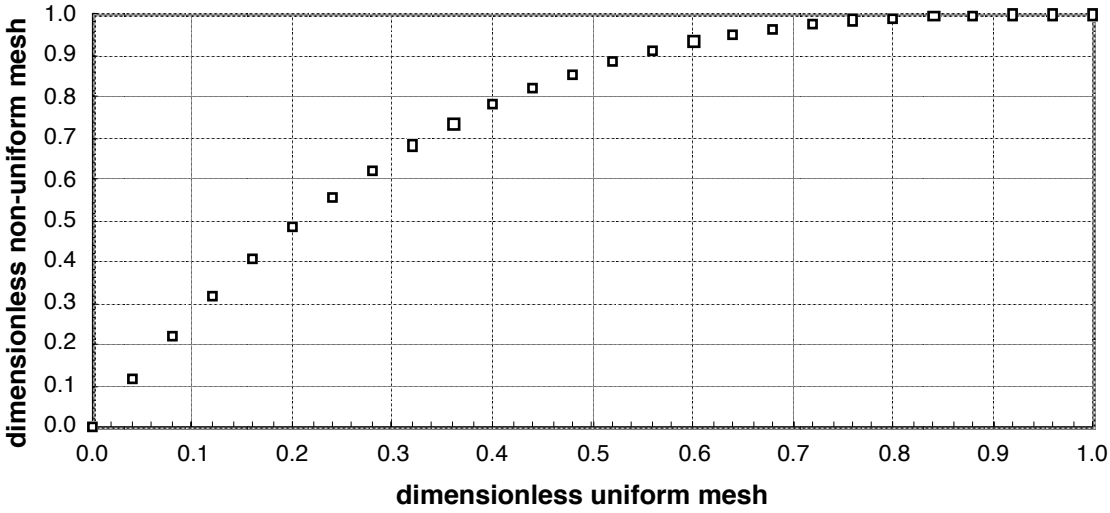

Figure D.2: Graphical illustration of the transformation function with $p = 0.01$ and $m = 3$ on a mesh of 25 points on the x-axis the original uniform mesh on the y-axis the transformed non-uniform mesh after transformation.

D.4 Testing of numerical solutions

The numerical solutions were tested by reducing the time step by a factor two, and by increasing the number of mesh points by a factor two. The analytical solution of the Graetz-Nusselt problem, i.e., the two-dimensional stationary forced convection equation with constant boundary conditions, was compared to its numerical solution. The analytical solution of the Langmuir kinetics were compared to the numerical solution at high flow rates. Typical Values that are used are: Number of mesh points: 49×49, time step 0.1 second. Computational time (on an Intel Pentium 200 MHz system): 10 minutes.

The Graetz number is defined as follows:

$$\mathrm{Gz} = \frac{\mathbb{D}L}{\bar{v}(2a)^2} \tag{D.9}$$

With $\mathbb{D}$ the diffusion coefficient, L the length of the channel, $\bar{v}$ the average velocity and $2a$ the distance between the plates.

The cup-mixing dimensionless concentration is defined as:

$$< Y > \;=\; \frac{\int_{y=-a}^{y=a} Y v_x(y)\mathrm{d}y}{\int_{y=-a}^{y=a} v_x(y)\mathrm{d}y} \tag{D.10}$$

$$Y \;=\; \frac{c_w - c(x,y,t)}{c_w - c_0} \tag{D.11}$$

With a the halve distance between the plates, v_x the local velocity in the x-direction, c_w the concentration at the wall, c_0 the initial concentration, and $c(x,y,t)$ the local concentration.

A graph of the dimensionless cup-mixing concentration against the Graetz number is shown in Figure D.3.

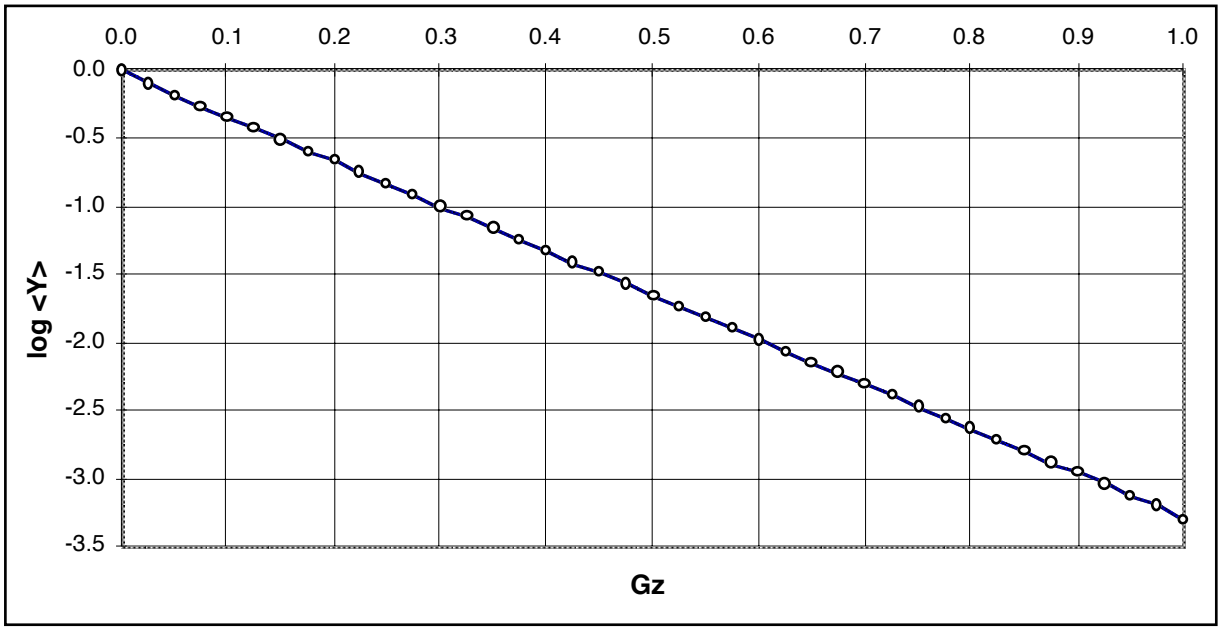

Figure D.3: Dimensionless flow-averaged or cup-mixing concentration $< Y >$ as a function of the Graetz number for laminar flow between flat plates with a separation distance of 2a. Theoretical value (–), Calculation (○).

References

Arnebrant, T. (1987), *Proteins at the metal/water interface*, Lund University, Sweden.

Azzam, R. M. and N. M. Bashara (1977), *Ellipsometry and Polarized Light*. New York, USA: North-Holland publishing company. 529.

Baeckström, K. (1987), *Removal of triglyceride and protein films from hard surfaces by aqueous surfactant solutions; an ellipsometry study*, Lund University, Sweden.

Beek, W. J. and K. M. K. Muttzall (1975), *Transport Phenomena*. London: Wiley.

Beissinger, R. L. and E. F. Leonard (1982), *Sorption Kinetics of Binary Protein Solutions: General Approach to Multicomponent Systems*. Journal of Colloid and Interface Science. **85**(2): p. 521-533.

Bhattacharjee, S., A. Sharma and P. K. Bhattacharya (1994), *Surface Interactions in Osmotic Pressure Controlled Flux Decline during Ultrafiltration*. Langmuir. **10**: p. 4710-4720.

Bird, R. B., W. E. Stewart and E. N. Lightfoot (1960), *Transport Phenomena*. New York: Wiley.

Brash, J. L. and T. A. Horbett (1995), *Proteins at Interfaces; an Overview*, in *Proteins at Interfaces II; Fundamentals and Applications*, T. A. Horbett and J. L. Brash, Editors. American Chemical Society: Washington, DC.

Brash, J. L. and Q. M. Samak (1978), *Dynamics of Interactions between Human Albumin and Polyethylene*. Journal of Colloid and Interface Science. **65**(3): p. 495-504.

Brenner, H. (1961), *The slow motion of a sphere through a viscous fluid towards a plane surface*. Chemical Engineering Science. **16**: p. 242-251.

Cha, W. and R. Beissinger (1996a), *Macromolecular Mass Transport to a Surface: Effects of Shear Rate, pH, and Ionic Strength*. Journal of Colloid and Interface Science. **177**: p. 666-674.

Cha, W. and R. L. Beissinger (1996b), *Augmented Mass Transport of Macromolecules in Sheared Suspensions to Surfaces*. Journal of Colloid and Interface Science. **178**: p. 1-9.

Cheng, Y.-L., S. A. Darst and C. R. Robertson (1987), *Bovine Serum Albumin Adsorption and Desorption Rates on Solid Surfaces with Varying Surface Properties*. Journal of Colloid and Interface Science. **118**(1): p. 212-223.

Cuypers, P. A. (1976), *Dynamic Ellipsometry; Biochemical and Biomedical Applications*, Rijksuniversiteit Limburg, Netherlands.

Cuypers, P. A., W. T. Hermens and H. C. Hemker (1977), *Ellipsometric Study of Protein Film on Chromium*. Annals New York Academy of Sciences. **283**: p. 77-86.

Cuypers, P. A., G. M. Willems, J. M. M. Kop, J. W. Corsel, M. P. Janssen and W. T. Hermens (1987), *Kinetics of Protein Sorption on Phospholipid Membranes Measured by Ellipsometry*, in *ACS Symposium Series 343; Proteins at Interfaces; Physicochemical and Biochemical Studies*, J. L. Brash and T. A. Horbett, Editors. American Chemical Society; Division of Colloid and Surface Chemistry: Washington, DC. p. Chapter 14.

Dabros, T. and T. G. M. van de Ven (1983), *A direct method for studying particle deposition onto solid surfaces*. Colloid and Polymer Science. **261**: p. 694-707.

De Feijter, J. A., J. Benjamins and F. A. Veer (1978), *Ellipsometry as a Tool to Study the Adsorption Behavior of Synthetic and Biopolymers at the Air-Water Interface*. Biopolymers. **17**: p. 1759-1772.

Dejardin, P., M. T. Le, J. Wittmer and A. Johner (1994), *Adsorption Rate in the Convection-Diffusion Model*. Langmuir. **10**: p. 3898-3901.

Derjaguin, B. V. and L. D. Landau (1941), *Theory of the stability of strongly charged lyophobic solids and of the adhesion of strongly charged particles in solutions of electrolytes*. Acta Physicochimica URSS. **14**: p. 733-762.

Dickinson, R. and S. L. Cooper (1995), *Analysis of Shear-Dependent Bacterial Adhesion Kinetics to Biomaterial Surfaces*. AIChE Journal. **41**(9): p. 2160-2174.

Dijt, J. C., M. A. Cohen Stuart, J. E. Hofman and G. J. Fleer (1990), *Kinetics of Polymer Adsorption in Stagnation Point Flow*. Colloids and Surfaces. **51**: p. 141-158.

Doolittle, R. F. (1980), *Fibrinogen*, in *Section I: Hematology*, R. M. Schmidt, Editor. CRC Press: Cleveland. p. 324.

Drude, P. (1889a), *Ueber Oberflaechenschichten I*. Ann. Phys. Chem. **36**: p. 532-560.

Drude, P. (1889b), *Ueber Oberflaechenschichten II*. Ann. Phys. Chem. **36**: p. 865-897.

Drude, P. (1890), *Bestimmung der optischen Konstanten der Metalle*. Ann. Phys. Chem. **39**: p. 481-554.

Elimelech, M. (1994), *Particle deposition on ideal collectors from dilute flowing suspensions: Mathematical formulation, numerical solution, and simulations*. Sep. Technol. **4**: p. 186-212.

Elimelech, M., J. Gregory, X. Jia and R. A. Williams (1995), *Particle deposition and aggregation: measurement, modelling, and simulation*. First Edition ed. Colloid and Surface Engineering: Applications in the process industries Controlled Particle, Droplet and Bubble Formation, ed. R. A. Williams. Oxford: Butterworth-Heinemann, Ltd. 441.

Den Engelsen, D. (1971), *Ellipsometry of Anisotropic Films*. Journal of the Optical Society of America. **61**(11): p. 1460-1466.

Den Engelsen, D. (1974), *Ellipsometric Study of Organic Monolayers*. Journal of The Chemical Society, Faraday Transactions I. **70**: p. 1603-1614.

Den Engelsen, D. (1976), *Optical anisotropy in ordered systems of lipids*. Surface Science. **56**: p. 272-280.

Engström, S. and K. Backström (1987), *Ellipsometry as a Tool to study Detergency at Hard Surfaces*. Langmuir. **3**: p. 568-574.

Ferziger, J. H. (1981), *Numerical Methods for Engineering Application*. New York: John Wiley & Sons.

Gourley, L., M. Britten, S. F. Gauthier and Y. Pouliot (1994), *Characterization of adsorptive fouling on ultrafiltration membranes by peptides mixtures using contact angle measurements*. Journal of Membrane Science. **97**: p. 283-289.

Greven, G. (1853), *Over de elliptische polarisatie van het licht*, University of Utrecht.

Hammes, G. G. (1978), *Principles of Chemical Kinetics*. New York: Academic Press.

Haynes, C. A. and W. Norde (1994), *Globular proteins at solid/liquid interfaces*. Colloids and Surfaces B: Biointerfaces. **2**: p. 517-566.

Ho, C.-H. and V. Hlay (1995), *Adsorption of Human Low-Density Lipoprotein onto a Silica-Octadecyldimethlysilyl (C_{18}) Gradient Surface*, in *Proteins at Interfaces II; Fundamentals and Applications*, T. A. Horbett and J. L. Brash, Editors. American Chemical Society: Washington, DC. p. 371-384.

Hoffman, J. D. (1993), *Numerical Methods for Engineers and Scientists*. McGraw-Hill international Editions; Mechanical Engineering Series, Singapore: McGraw-Hill, Inc. 825.

Israelachvili, J. (1992), *Intermolecular & Surface Forces*. Second Edition ed. London: Academic Press Limited. 450.

Ivarsson, B. and I. Lundström (1986), *Physical Chararization of Protein Adsorption on Metal and Metal Oxide Surfaces*, in *Critical Reviews in Biocompatibility*. p. 1-95.

Ivarsson, B. A., P.-O. Hegg, K. Ingemar Lundström and U. Jönsson (1985), *Adsorption of Proteins on Metal Surfaces Studied by Ellipsometric and Capacitance Measurements*. Colloids and Surfaces. **13**: p. 169-192.

Jacobs, L. (1995), *Characterisation of the passive film on iron-chromium alloys by ellipsometry and electrochemical impedance spectroscopy*, Technical University Delft.

Jakob, M. (1949), *Heat Transfer*. Vol. I. New York: Wiley. pp. 451-464.

Jönsson, U., B. Ivarsson, I. Lundström and L. Berghem (1982), *Adsorption Behavior of Fibronectin on Well-Characterized Silica Surfaces*. Journal of Colloid and Interface Science. **90**(1): p. 148-163.

Jönsson, U., M. Malmqvist and I. Rönnerberg (1985), *Adsorption of Immunoglobuling G, Protein A, and Fibronectin in the Submonolayer Region Evaluated by a Combined Study of Ellipsometry and Radiotracer Techniques*. Journal of Colloid and Interface Science. **103**(2): p. 360-372.

Kulik, E. A. and V. I. Sevast'yanov (1991), *Differences between the protein/surface interaction energies and structural changes in adsorbed proteins*. Russian Journal of Physical Chemistry. **65**(8): p. 1181-1184.

Lacour, F., R. Torresi, C. Gabrielli and A. Caprani (1992), *Comparison of the Quartz-Crystal Microbalance and the Double Layer Capacitans Methods of Measuring the Kinetics of the Adsorption of Bovine Serum Albumin onto a Gold Electrode*. Journal of the Electrochemical Society. **139**(6): p. 1619-1622.

Landgren, M. and B. Jönsson (1993), .. Journal of Physical Chemistry. **97**: p. 1656.

Langmuir, I. (1918), .. Journal of the American Chemical Society. **40**: p. 1361.

Lassen, B. and M. Malmsten (1996), *Competitive Protein Adsorption Studied with TIRF and Ellipsometry*. Journal of Colloida and Interface Science. **179**: p. 470-477.

Lee, R. G. and S. W. Kim (1974), *Adsorption of Proteins onto Hydrophobic Polymer Surfaces: Adsorption Isotherms and Kinetics*. J. Biomed. Mater. Res. **8**: p. 251-259.

Levich, V. G. (1962), *Physicochemical Hydrodynamics*. Prentice-Hall international series in the physical and chemical engineering sciences, Vol. XVI. Prentice-Hall. 700.

Lok, B. K., Y.-L. Cheng and C. R. Robertson (1983a), *Protein Adsorption on Crosslinked Polydimethylsiloxane Using Total Internal Reflection Fluorescence*. Journal of Colloid and Interface Science. **91**(1): p. 104-116.

Lok, B. K., Y.-L. Cheng and C. R. Robertson (1983b), *Total Internal Reflection Fluorescence: A Technique for Examining Interactions of Macromolecules with Solid Surfaces*. Journal of Colloid and Interface Science. **91**(1): p. 87-103.

Malmsten, M. (1994), *Ellipsometry Studies of Protein Layers Adsorbed at Hydrophobic Surfaces*. Journal of Colloid and Interface Science. **166**: p. 333-342.

Malmsten, M. (1995), *Ellipsometry studies of the effects of surface hydrophobicity on protein adsorption*. Colloids and Surfaces B: Biointerfaces. **3**: p. 297-308.

Martensson, J., H. Arwin, H. Nygren and I. Lundstrom (1995), *Adsorption and Optical Properties of Ferritin Layers on Gold Studied with Spectroscopic Ellipsometry*. Journal of Colloid and Interface Science. **174**: p. 79-85.

McCrackin, F. L., E. Passaglia, R. R. Stromberg and H. L. Steinberg (1963), *Measurement of the Tickness and Refractive Index of Very Thin Films and the Optical Properties of Surfaces by Ellipsometry*. Journal of Research of the National Bureau of Standards: A. Physics and Chemistry. **67A**(4): p. 363-377.

Norde, W. and A. C. I. Anusiem (1992), *Adsorption, desorption and re-adsorption of proteins on soild surfaces*. Colloid and Surfaces. **66**: p. 73-80.

Norde, W., T. Arai and H. Schirahama (1991), *Protein adsorption in model systems*. Biofouling. **4**: p. 37-51.

Nygren, H., M. Stenberg and C. Karlsson (1992), *Kinetics supramolecular structure and equilibrium properties of fibrinogen adsorption at liquid-solid interfaces*. Journal of Biomedical Materials Research. **26**: p. 77-91.

Probstein, R. F. (1989), *Physicochemical hydrodynamics : an introduction*. Vol. XIII. Boston: Butterworths. 353.

Ramsden, J. J. (1993), *Experimental methods for investigating protein adsorption kinetics at surfaces*. Quarterly Reviews of Biophysics. **27**(1): p. 41-105.

Ramsden, J. J. (1995), *Puzzles and Paradoxes in Protein Adsorption*. Chemical Society Reviews. **24**(1): p. 73-78.

Retzinger, G. S., B. C. Cook and A. P. DeAnglis (1994), *The Binding of Fibrinogen to Surfaces and the Identification of Two Distinct Surface-Bound Species of the Protein*. Journal of Colloid and Interface Science. **168**: p. 514-521.

Ruckenstein, E. and D. C. Prieve (1973), *Rate of Deposition of Brownian Particles under the Action of London and Double-layer Forces*. Journal of the Chemical Society Faraday Transactions II. **69**: p. 1522-1536.

Schaaf, P. and P. Dejardin (1988), *Structural Changes within an Adsorbed Fibrinogen Layer during the Adsorption Process: a study by Scanning Angle Reflectometry*. Colloids and Surfaces. **31**: p. 89-103.

Schlichting, H. (1979), *Boundary-layer theory*. 7th ed. McGraw-Hill series in mechanical engineering, New York, USA originally Karlsruhe, FRG: McGraw-Hill. 817.

Shibata, C. T. and A. M. Lenhoff (1992a), *TIRF of Salt and Surface Effects on Protein Adsorption; I Equilibrium*. Journal of Colloid and Interface Science. **148**(2): p. 469-484.

Shibata, C. T. and A. M. Lenhoff (1992b), *TIRF of Salt and Surface Effects on Protein Adsorption; II Kinetics*. Journal of Colloid and Interface Science. **148**(2): p. 485-507.

Soderquist, M. E. and A. G. Walton (1980), *Structural Changes in Proteins Adsorbed on Polymer Surfaces*. Journal of Colloid and Interface Science. **75**(2): p. 386-397.

Spielman, L. A. and S. K. Friedlander (1974), *Role of the Electrican Double Layer in Particle Deposition by Convective Diffusion*. Journal of Colloid and Interface Science. **46**(1): p. 22-31.

Swanton, S. W. (1995), *Modelling Colloid Transport in Groundwater; the Prediction of Colloid Stability and Retention Behanviour*. Advances in Colloid and Interface Science. **54**: p. 129-208.

Tompkins, H. G. (1993), *A user's guide to ellipsometry*. Boston: Academic Press, cop. 260.

Van de Ven, T. G. M. (1989), *Colloidal Hydrodynamics*. first ed. Colloid Science, A Series of Monographs, ed. R. H. O. a. R. L. Rowell. Vol. 4. London: Academic Press Limited. 582.

Van der Scheer, A. (1978), *Adsorption of Plasma Proteins; Adsorption Behaviour on Apolar Surfaces and Effect on Colloid Stability*, PhD, Technische Hogeschool Twente.

Van der Vegt, W., W. Norde, H. C. van der Mei and H. J. Busscher (1996), *Kinetics of Interfacial Tension Changes during Protein-Adsorption form Sessile Droplets on FEP-Teflon*. Journal of Colloid and Interface Science. **179**: p. 57-65.

Van Oss, C. J. (1990), *Surface Properties of Fibrinogen and Fibrin*. Journal of Protein Chemistry. **9**(4): p. 487-491.

Van Oss, C. J. (1993), *Acid-base interfacial interactions in aqueous media*. Colloids and Surfaces A: Physicochemical and Engineering Aspects. **78**: p. 1-49.

Van Oss, C. J. (1994), *Interfacial Interactions in Aqueous Media*. 1 ed. New York: Marcel Dekker, Inc. 440.

Van Oss, C. J. (1997), *On the Predominant Electron-Donicity of Polar Solid Surfaces*. Journal of Adhesion. **63**: p. 71-88.

Van Oss, C. J. (accepted for publication 26 June, 1997), *Kinetics and Energetics of Specific Intermolecular Interactions*. Journal of Molecular Recognition. **X**: p. X.

Van Regenmortel, M. H. V., D. Altschuh, J.-L. Pellequer, P. Richalet-Sécordel, H. Saunal, J. A. Wiley and G. Zeder-Lutz (1994), *Analysis of Viral Antigens Using Biosensor Technology*. METHODS: A Companion to Methods in Enzymology. **6**: p. 177-187.

Van Wagenen, R. A. and J. D. Andrade (1980), *Flat Plate Streaming Potential Investigations: Hydrodynamics and Electrokinetic Equivalency*. Journal of Colloid and Interface Science. **76**(2): p. 305-314.

Van Wagenen, R. A., D. L. Coleman, R. N. King, P. Triolo, L. Brostrom, L. M. Smith, D. E. Gregonis and J. D. Andrade (1981), *Streaming Potential Investigations: Polymer Thin Films*. Journal of Colloid and Interface Science. **84**(1): p. 155-162.

Verwey, E. J. G. and J. T. G. Overbeek (1948), *Theory of the Stability of Lyophobic Colloids*. Amsterdam: Elsevier.

Von Smoluchowski, M. (1917), *Versuch einer mathematischen Theorie der Koagulationskinetik kolloider Lösungen*. Z. phys. Chem. **92**: p. 129-168.

Vroman, L. (1994), *Warm, rood, nat en lief*. Amsterdam: Uitgeverij Contact. 303.

Wahlgren, M. (1992), *Adsorption of Proteins and Interactions with Surfactants at the Solid/Liquid Interface*, University of Lund, Sweden.

Wahlgren, M., S. Welin-Klintström, T. Arnebrant, A. Askendal and H. Elwing (1995), *Competition between fibrinogen and a non-ionic surfactant in adsorption to a wettability gradient surface*. Colloids and Surfaces B: Biointerfaces. **4**: p. 23-31.

Wahlgren, M. C., T. Arnebrant, A. Askendal and S. Welin-Klintröm (1993), *The elutability of fibrinogen by sodium dodecyl sulphate and alkyltrimethylammonium bromides*. Colloids and Surfaces A: Physicochemical and Engineering Aspects. **70**: p. 151-158.

Wahlgren, M. C., M. A. Paulsson and T. Arnebrant (1993), *Adsorption of globular model proteins to silica and methylated silica surfaces and their elutability by dodecyltrimethylammonium bromide*. Colloids and Surfaces A: Physicochemical and Engineering Aspects. **70**: p. 139-149.

Welin-Klintström, S. (1992), *Ellipsometry and Wettability Gradient Surfaces*, Linköping University, Sweden.

Westerterp, K. R., W. P. M. van Swaaij and A. A. C. M. Beenackers (1987), *Chemical Reactor Design and Operation*. Student Edition ed. Chichester: John Wiley and Sons. 767.

Yamamoto, M. and T. Namioka (1992), *In situ ellipsometric study of optical properties of ultrathin films*. Applied Optics. **31**(10): p. 1612-1621.

Young, B. R., W. G. Pitt and S. L. Cooper (1988), *Protein Adsorption on Polymeric Biomaterials; II. Adsorption Kinetics*. Journal of Colloid and Interface Science. **125**(1): p. 246-260.

Summary

The subject of the work described in this thesis has been the adsorption of proteins from laminar flow onto flat, solid, impermeable surfaces.

The adsorption of soluble proteins at solid-liquid interfaces is of fundamental importance in nature. An example that is common to everyday life is the role played by proteins in blood clotting. Understanding of protein adsorption is also important in many industrial applications. Fouling by protein adsorption, or by bacterial adhesion to a precursor layer of protein, presents a major problem in, e.g., membrane separations and the design of biocompatible implants in the human body.

Protein adsorption is a spontaneous process highly influenced by interfacial forces between surface material and protein. Diffusion and convection must bring the protein to the surface before adsorption can take place. Because the rate of adsorption is a function of the bulk concentration of protein near the surface, the rate of mass transport to the surface directly influences the overall rate of adsorption. Hence, it is necessary to study the rate of adsorption under well defined hydrodynamic conditions. Only then it is possible to calculate the rate of mass transport and to be able to identify and eliminate mass transport limitation.

The aim of the study was to gain more insight into the processes that determine rate of adsorption of proteins onto a protein free surface, after a step in bulk concentration by:

- determining the adsorbed amount in time under defined hydrodynamic conditions
- formulating and verifying mathematical models of protein adsorption
- relating the results of contact angle measurements on surfaces and proteins to the measured adsorption kinetics

Throughout this thesis human fibrinogen, an ellipsoidal blood protein, and titanium dioxide have been used as the protein and surface material respectively. Sodiumcitrate, HCl and ultra pure water have been used to prepare the buffered protein solutions. Measurements have been performed in a parallel plate flow cell, of which the upper wall was formed by the surface material of interest. The optical technique ellipsometry was used to determine the adsorbed amount as a function of time.

In *chapter one* a general introduction is given.

In *chapter two* the selection of the type of flow cell and the experimental technique is presented. The advantages and disadvantages of a number of flow cells that provide defined hydrodynamic conditions are discussed, together with experimental techniques that are used in studies in the literature. The parallel plate flow cell was selected. Firstly because of the high flow strengths that can be obtained and secondly because of the relative mathematical simplicity of the flow pattern and mass transport equations in this case. Optical techniques, more specifically ellipsometry, were identified as the most promising because of the non-perturbing character of the technique and the variety of surface materials that can be used. In Appendices A and B to chapter two the technique of ellipsometry is discussed in detail.

Chapter three deals with the physico-chemical characterisation of surface materials using contact angle measurements and the VCG theory. The surface properties of oxidised silicon wafers both

untreated and silanised, gold, chromium oxide and titanium dioxide surfaces are determined. The interactions between fibrinogen and the four surfaces are calculated in water and air as the medium.

The medium has a large influence on the interaction energy. In air fibrinogen has a large interaction with all surface materials and with other fibrinogen molecules. In water the interaction changes dramatically, and becomes repulsive for two of the five surface materials. By using the surface properties of fibrinogen and the surface materials, interaction energy versus distance curves in water are calculated.

The adsorption constant for fibrinogen onto titanium dioxide is derived using the IFBL approximation. This adsorption constant is obtained by treating the interfacial interactions as a boundary condition to the convection diffusion equation as is also common in reaction engineering models. The value of the adsorption constant is used in the non linear fitting of chapter five.

In *chapter four* measurements of adsorption of fibrinogen in the parallel plate flow cell are described. Measurements under defined flow have been carried out using ellipsometry in attenuated total internal reflection mode. Also measurements in static solutions in a cuvette have been performed. Experiments were carried out under laminar flow conditions with a Reynolds number of 1,000. The bulk concentrations of fibrinogen, that have been used are 50, 100, 400 and 1,000 mg ℓ^{-1}. The time during which the experiments have been carried out was longer (up to 30 hours) than in most other studies.

In many studies phosphate buffer saline (PBS) has been used. However, in this study PBS buffer gave problems related to aggregation of protein causing the prepared protein solutions in PBS to not always being perfectly clear and to show the characteristic blue Tyndall scattering. Also, UV absorption at 280 nm measurements at a range of concentrations showed a strong non-linear curve of the absorption versus concentration. AFM studies using PBS buffered protein solution showed large protein aggregates when using PBS buffer. Therefore, the experiments in this study were carried out using a sodiumcitrate HCl buffer that gave none of the problems mentioned before.

The results of the experiments under laminar flow are very different from the static experiments in that all laminar flow experiments show overshoots in the adsorbed amount. The maximum and the 'plateau' values obtained do not directly correlate with the bulk concentration. However, the adsorbed amount was never higher than the amount calculated assuming a monolayer of end-on adsorbed fibrinogen and never lower than an side-on adsorbed monolayer. The overshoots are believed to result from the transition end-on to side-on.

In *chapter five* the experiments of the adsorption of the ellipsoidal protein fibrinogen onto titanium dioxide in the parallel plate flow cell of chapter four are modelled. The non stationary two-dimensional convection diffusion equation with a non-linear kinetics model as boundary condition was solved numerically for a number of shear rates (Reynolds numbers) and compared to the two-dimensional stationary and non stationary mass transport limited solution and the kinetically limited solution. From the model calculation it became evident that the laminar flow experiments were kinetically limited.

The overshoot adsorption measured in chapter four are modelled using a two-state kinetic model that allows for end-on adsorption and desorption and transition from end-on to side-on adsorption during adsorption. The values of the three kinetic parameters in this two-state kinetic model have been estimated for experiments using bulk concentrations of 50, 100, 400 and 1,000 mg ℓ^{-1} at a constant Reynolds number of 1,000. The value of the adsorption constant from chapter three has been used as start value in the non linear fit procedure.

With the kinetic two-state model the evolution of the adsorbed amount upto approximately 1000 seconds can be modelled. However, the adsorption after approximately 1,000 seconds cannot be explained by the two-state model. The changes in the adsorbed amount beyond this stage could be caused by the formation of aggregates of protein, crystallisation within the protein layer, or by

multi-layer adsorption.

The experimental results under laminar flow at a bulk concentration of 100 mg ℓ^{-1} carried out over 24 hours, show that over such long times the adsorbed amount determined by ellipsometry varies slowly until it suddenly increases rapidly and then decreases rapidly.

Samenvatting

Het onderzoek dat in dit proefschrift wordt beschreven heeft als onderwerp de adsorptie van eiwitten vanuit laminaire stroming aan vlakke, niet doordringbare vaste oppervlakken.

De adsorptie van oplosbare eiwitten aan vast-vloeistof grensvlakken is van fundamenteel belang in de natuur. Een voorbeeld uit het dagelijks leven is de rol die eiwitten spelen bij het stollen van bloed. Een goed begrip van eiwitadsorptie is ook belangrijk in veel industriële toepassingen. Vervuiling door eiwitadsorptie, of door bacteriële adsorptie aan een precursor laag van eiwitten, is een groot probleem in bijvoorbeeld membraanscheidingsprocessen en bij het ontwerpen van biocompatibele implantaten in het menselijk lichaam.

Eiwitadsorptie is een spontaan proces dat sterk beïnvloed wordt door grensvlakinteracties tussen het oppervlaktemateriaal en het eiwit. Diffussie en convectie moeten er voor zorgen dat eiwit naar het oppervlak wordt getransporteerd voordat adsorptie plaats kan vinden. Omdat de adsorptiesnelheid een functie is van de bulk concentratie van eiwit in de buurt van het oppervlak, wordt de totale adsorptiesnelheid direct beïnvloed door de snelheid van massatransport naar het oppervlak. Daarom is het nodig om de adsorptiesnelheid onder goed gedefinieerde hydrodynamische omstandigheden. Alleen dan is het mogelijk om de massatransportsnelheid te berekenen en massatransportlimiteringen te identificeren en te elimineren.

Het doel van dit onderzoek was een beter inzicht te verkrijgen in de processen die de adsorptiesnelheid van eiwitten aan oppervlakken bepalen, na een stapvormige verandering in bulkconcentratie door:

- de geadsorbeerde hoeveelheid te bepalen als functie van de tijd onder gedefinieerde hydrodynamische omstandigheden
- het formuleren en verifiëren van wiskundige modellen voor eiwitadsorptie
- de resultaten van randhoekmetingen op oppervlakken en eiwitten te relateren aan de gemeten adsorptiekinetiek

In het gehele proefschrift is gebruik gemaakt van respectievelijk menselijk fibrinogeen, een ellipsoïdaal bloedeiwit, en titaandioxide als eiwit en oppervlaktemateriaal. Natriumcitraat, HCl en ultrapuur water zijn gebruikt om gebufferde eiwitoplossingen te bereiden. De metingen werden uitgevoerd in een parallelle plaat stroomcel, waarvan de bovenste wand gevormd werd door het te onderzoeken oppervlaktemateriaal. De optische techniek ellipsometrie is gebruikt om de geadsorbeerde hoeveelheid als functie van de tijd te bepalen.

In *hoofdstuk een* wordt een algemene introductie gegeven.

In *hoofdstuk twee* wordt de selectie van het type stroomcel en de experimentele techniek besproken. De voor- en nadelen van een aantal stroomcellen die gedefinieerde hydrodynamische condities mogelijk maken worden gegeven, samen met experimentele technieken die gebruikt zijn in studies in de literatuur. De parallelle plaat stroomcel is geselecteerd. Ten eerste, omdat hoge stroomsnelheden mogelijk zijn en ten tweede omdat het stromingsprofiel en de vergelijkingen voor massatransport relatief eenvoudig zijn. Optische technieken, ellipsometrie in het bijzonder, bleken het meest

veelbelovend omdat deze technieken geen effect hebben op het proces zelf en omdat een keur aan oppervlaktematerialen kan worden gebruikt. In Appendices A en B behorende bij hoofdstuk twee wordt de techiek ellipsometrie in detail besproken.

Het onderwerp van *hoofdstuk drie* is de fysisch-chemische karakterisering van oppervlaktematerialen met behulp van randhoekmetingen en de VCG theorie. De oppervlakte-eigenschappen van geoxideerd silicium wafers zowel onbehandeld en gesilaniseerd, goud, chroomoxide en titaandioxide oppervlakken zijn bepaald. De interacties tussen fibrinogeen en vijf oppervlakken zijn berekend in water en lucht als medium.

Het medium heeft een grote invloed op de interactie-energie. In lucht heeft fibrinogeen sterke interactie met alle oppervlaktematerialen en met andere fibrinogeenmoleculen. In water veranderd de interactie-energie dramatisch en wordt afstotend in twee van de vijf oppervlaktematerialen. Grafieken van de interactie-energie tegen afstand werden berekend met behulp van de oppervlakte-eigenschappen van fibrinogeen en de oppervlaktematerialen.

De adsorptieconstante voor fibrinogeen aan titaan dioxide is bepaald met behulp van de IFBL benadering. Deze adsorptieconstante wordt gevonden als de grensvlakinteracties als randvoorwaarde voor de convectie-diffusievergelijking worden meegenomen zoals ook gebruikelijk is in de chemische reactorkunde. De waarde van de adsorptieconstante is gebruikt tijdens de niet-lineaire fitprocedure in hoofdstuk vijf.

In *hoofdstuk vier* worden de adsorptiemetingen met fibrinogeen in de parallelle plaat stroomcel beschreven. De metingen zijn uitgevoerd onder gedefinieerde stroomcondities waarbij gebruik gemaakt werd van ellipsometrie onder condities van afgezwakte totale interne reflectie. Ook werden metingen in statische oplossingen uitgevoerd in een cuvet. De experimenten zijn uitgevoerd onder laminaire stromingscondities met een Reynoldsgetal van 1000. De bulkconcentraties fibrinogeen die werden gebruikt zijn 50, 100, 400 en 1000 mg ℓ^{-1}. De tijdsduur van de experimenten was langer (tot 30 uur) dan in de meeste andere onderzoeken.

In veel studies worden fosfaatbuffers (PBS) gebruikt. Tijdens dit onderzoek gaf het gebruik van PBS buffer veel problemen die te maken hadden met aggregatie van het eiwit; dit zorgde ervoor dat oplossingen in PBS niet altijd perfect helder waren en de karakteristieke blauwe Tyndall verstrooiing vertoonden. Verder vertoonde UV absorptie bij 280 nm metingen over een reeks van concentraties een sterk niet-lineaire curve van absorptie tegen concentratie. Bestudering van PBS gebufferde eiwitoplossingen met AFM liet duidelijk zien dat eiwitaggregaten waren gevormd in PBS buffer. Daarom zijn de experimenten in dit onderzoek uitgevoerd in natriumcitraat HCl buffer waarin de bovengenoemde problemen niet optraden.

De resultaten van de experimenten onder laminaire stroming verschillen erg van de statische experimenten inzoverre dat alle laminaire stromingsexperimenten overshoots in de geadsorbeerde hoeveelheid vertonen. De maximale en de 'plateau'-waarden die zijn verkregen correleren niet direct met de bulkconcentratie. Echter de geadsorbeerde hoeveelheid was nooit hoger dan de hoeveelheid die berekend wordt uitgaande van een *end-on* geadsorbeerde monolaag en nooit lager dan een *side-on* geadsorbeerde monolaag.

In *hoofdstuk vijf* zijn de adsorptie-experimenten met het ellipsoïdale eiwit fibrinogeen aan titaandioxide in de parallelle plaat stroomcel uit hoofdstuk vier gemodelleerd. De niet-stationaire tweedimensionale convectie-diffusie-vergelijking met een niet-lineair kinetiek model als randvoorwaarde werd nummeriek opgelost voor een aantal afschuifsnelheiden (Reynolds getallen) en vergeleken met de twee-dimensionale stationaire en niet-stationaire massatransport gelimiteerde en kinetisch gelimiteerde oplossing. Uit de modelberekeningen bleek dat de laminaire experimenten kinetisch gelimiteerd waren.

De overshoot adsorptie gemeten in hoofdstuk vier zijn gemodelleerd met behulp van een tweetoestanden kinetisch model waarin zowel end-on adsorptie en desorptie en overgang van end-on naar

side-on adsorptie tijdens adsorptie mogelijk zijn. De waarden van de drie kinetische parameters in dit twee-toestanden kinetisch model zijn bepaald voor de experimenten voor bulkconcentraties van 50, 100, 400 en 1000 mg ℓ^{-1} bij een constant Reynoldsgetal van 1000. De waarde van de adsorptieconstante uit hoofdstuk drie is daarvoor gebruikt als startwaarde in de niet-lineaire fitprocedure.

Met het kinetische twee-toestanden model is het mogelijk om de veranderingen in de geadsorbeerde hoeveelheid tot ongeveer 1000 seconden te modelleren. Echter de adsorptie na ongeveer 1000 seconden kan niet verklaard worden door het twee-toestanden model. De veranderingen in de geadsorbeerde hoeveelheid na deze tijd zouden veroorzaakt kunnen worden door vorming van eiwitaggregaten, kristallisatie in de eiwitlaag of door multilaagadsorptie.

De experimentele resultaten onder laminaire stroming bij een bulk-concentratie van 100 mg ℓ^{-1} die uitgevoerd werden gedurende 24 uur laten zien dat in zo'n lange tijd de geadsorbeerde hoeveelheid zoals die met ellipsometrie wordt bepaald langzaam varieert totdat op een gegeven moment een abrupte stijging en daarna daling optreedt.

Curriculum Vitae

Sander Rekveld werd geboren op 12 oktober 1967 te Emmen. Aan het Katholiek Drenths College te Emmen behaalde hij in 1986 het Atheneum-B diploma. In dat zelfde jaar begon hij met de studie Chemische Technologie aan de toenmalige Technische Hogeschool Twente.

In september 1992 werd het diploma Scheikundige Technologie Vrij Doctoraal Informatica behaald na een stage bij ICI Chemicals & Polymers getiteld 'Developing a Model to predict Glass Transition Temperatures in Multi Copolymers used in Coatings' en een afstudeeropdracht in de onderzoekgroep Membraantechnologie bij Prof.dr. C.A. Smolders getiteld 'Development of a Pulse Induced Critical Scattering Nucleation and Nucleus Growth Setup'.

Op 1 oktober 1992 trad hij in dienst als Assistent In Opleiding voor een periode van vier jaar bij de Universiteit Twente, faculteit der Chemische Technologie, onderzoekgroep Fysische Scheidingen met als promotoren Prof.dr.ir. T. Reith en Prof.dr.ing. H. Strathmann, met een promotieopdracht, gesponsored door Unilever, met de titel 'Ellipsometric studies of protein adsorption onto hard surfaces in a flow cell'.

Vanaf 1 juli 1997 is hij werkzaam als universitair docent aan de universiteit Twente faculteit der Chemische Technologie bij de leerstoel TGM (Textieltechnologie) van Prof.dr.ir. M.M.C.G. Warmoeskerken.